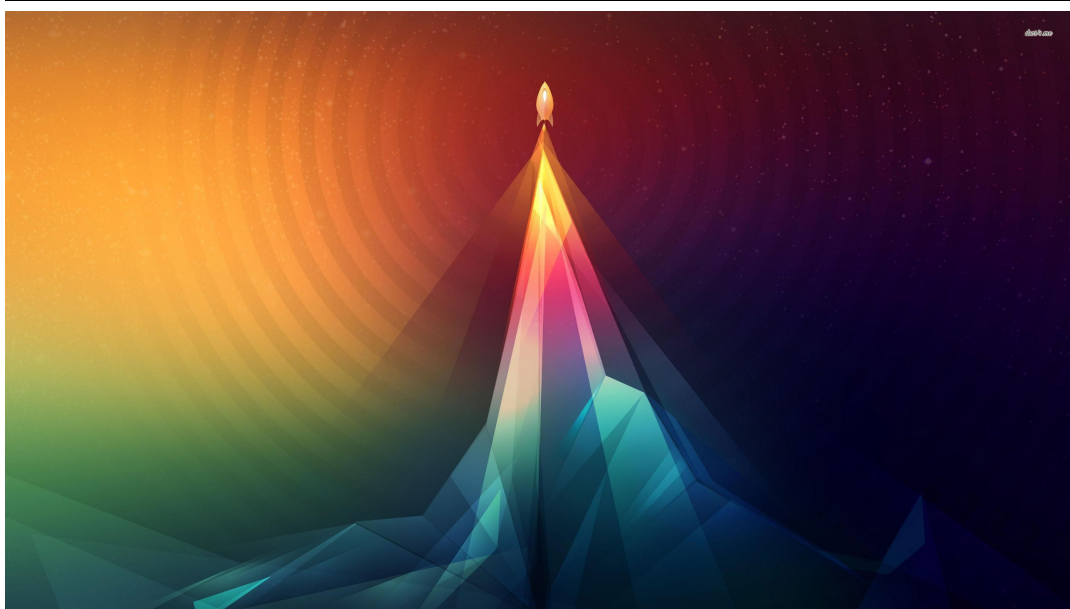

Rocket Trajectory Stability and Inverted Pendulum Balance

- Compare and Control -



Project Report
Group CE6-633
Aalborg University
Electronic Engineering and IT

Copyright © Group CE6-633, Electronic Engineering and IT, Aalborg University 2017

This report is compiled in L^AT_EX.



AALBORG UNIVERSITY
STUDENT REPORT

Electronic Engineering and IT

Aalborg University

<http://www.aau.dk>

Title:

Rocket Trajectory Stability
and
Inverted Pendulum Balance

Theme:

Control Engineering

Project Period:

Spring Semester 2017

Project Group:

Group CE6-633

Participants:

Geoffroy Sion
Jacob Lassen
Mathias Nielsen
Maxime Remy
Raphaël Casimir
Romain Dieleman

Supervisor:

Kirsten Nielsen
Tom Pedersen

Page Numbers: 140

Date of Completion:

?? June 2017

Abstract:

This report aims to investigate the inverted pendulum and rocket launches as balancing an inverted pendulum and following a flight path with a rocket are both unstable systems that are controlled by moving the bottom part of a long and narrow cylinder.

First a brief overview is given as to why the two systems have similar stability problems before a mathematical model is derived. Both models are nonlinear and are linearized and reduced to two simple models. It's found that the simple mathematical models for the two systems aren't identical. A single controller that can control both systems therefore can't be made. A controller for each system is thus made and implemented on the respective setup.

The controller designed for the inverted pendulum was implemented on an Arduino and uses two potentiometers and a tachometer as sensors. It's found that the controller balances the pendulum satisfactorily to the specifications made.

The controller designed for the rocket showed that it could follow the trajectory in a linear simulation based on the model. The rocket setup was built in its entirety by the group but the rocket controller wasn't successfully implemented due to time constraints.

In conclusion, while a rocket during flight and an inverted pendulum share similarities with instability, the models aren't identical and a controller cannot be made to work with both systems. A controller was made that showed satisfactory balancing of the inverted pendulum but the rocket controller ultimately wasn't tested.

The content of this report is freely available, but publication may only be pursued with reference.

Preface

This report is composed by group CE6-633 during the 6th semester of Electronic Engineering and IT at Aalborg University, 2017. The study of rocket stabilization and inverted pendulum balancing described in this report is part of the theme *Control Engineering*.

For citation the report employs IEEE style referencing. If citations are not present by figures or tables, these have been made by the authors of the report. Units are indicated according to the SI system.

The natural logarithm is denominated by \ln and \log_{10} is the base 10 logarithm.

A period is used as a decimal mark. Half a space is used as a 100 0 separator.

Aalborg University, May 26, 2017

Geoffroy Sion
<gsion16@student.aau.dk>

Jacob Lassen
<jlass14@student.aau.dk>

Mathias Nielsen
<mathni14@student.aau.dk>

Maxime Remy
<mremy16@student.aau.dk>

Raphaël Casimir
<rcasim16@student.aau.dk>

Romain Dieleman
<rdiele16@student.aau.dk>

Contents

I	Pre-analysis & requirements	1
1	Introduction	3
2	Initial Problem Statement	5
3	Preliminary Analysis of a Rocket	7
3.1	Controlling a Rocket's Stability	10
3.2	Systems with Similar Instability Problems	11
4	Delimitation	13
5	Inverted Pendulum Analysis	15
5.1	Inverted Pendulum Description	15
5.2	Modelling of the Arm and Stick	20
5.3	Modeling of the Gear System	24
5.4	Modeling of the DC-Motor	28
5.5	Combining the Models for the Inverted Pendulum	32
6	Rocket Analysis	33
6.1	Modeling of the angle	33
6.2	Comparison of the Inverted Pendulum and Rocket Models	35
7	Requirements and Specifications	37
7.1	Acceptance Test Specification	40
II	Design	41
8	Design of the Inverted Pendulum Controller	43
8.1	Design of Inner Loop Controller	46
8.2	Design of Outer Loop Controller	50
8.3	Verifying the total controller	57
9	Design of the Rocket and Gimbal Controller	59
9.1	Rocket Design	59
9.2	Rocket Controller Design	63

III Implementation	73
10 Implementation	75
10.1 Inverted Pendulum Implementation	75
10.2 Rocket Implementation	86
IV Test & conclusion	89
11 Inverted Pendulum Acceptance Tests	91
11.1 Acceptance Test 2.	91
11.2 Acceptance Test 3.	93
12 Discussion	95
12.1 Inverted Pendulum possible improvements	95
12.2 Rocket	95
12.3 Differences between the Rocket and the Inverted Pendulum	95
Bibliography	97
A Test Journal: Template	99
B Test Journal: Gear Train System	101
B.1 Electronics characteristics	101
B.2 Mechanical Characteristics	110
C Linearization of the Arm and Stick Model	117
D Test Journal: Tachometer	119
E Test Journal: Potentiometer	123
F Test Journal: rocket motor test	129
G Test Journal: Servomotors	133
H Test Journal: Attached Flight	139

Part I

Pre-analysis & requirements

Chapter 1

Introduction

The stabilization of an inverted pendulum is one of the well-known example used in education to explain classical mechanics and physics. It started to appear in the 1960's with Roberge's bachelor thesis "The Mechanical Seal" [1]. It is now one of the main benchmark for testing nonlinear control techniques. The principle of it is to balanced a rod in a upright position.

Should be revised -
Mathias

The goal of this project is to model and control an unstable dynamic system. The inverted pendulum being one of the available system, it is chosen for its textbook case as explained before. However, a concrete application of the inverted pendulum is wanted as it is an abstract system. The flight control of a rocket during the initial stage of its launch presents similarities [1]. These similarities can already be intuitively seen as both has aim to stabilize a stick by applying a force at its bottom. Therefore a comparison between the solutions of the inverted pendulum and the rocket will be drawn in the report.

Chapter 2

Initial Problem Statement

In order to design and implement a controller that can ensure a stable launch and flight of a rocket the following questions needs answering:

How much is the stabilization of the inverted pendulum similar to the flight control of a rocket in the early stages?

- Is the model of the inverted pendulum is similar rocket's flight control?
- Can the inverted pendulum and the rocket be controlled using similar control methods?

Chapter 3

Preliminary Analysis of a Rocket

The following chapter describes the functionality and structure behind a rocket. The goal is to determine which factors that leads to instability in flight and launch of a rocket.

The full scale rocket model that will be described consist of,

- a payload system.
- a guidance system.
- a propulsion system.
- a structural system.

The model is seen cf. figure 3.1.

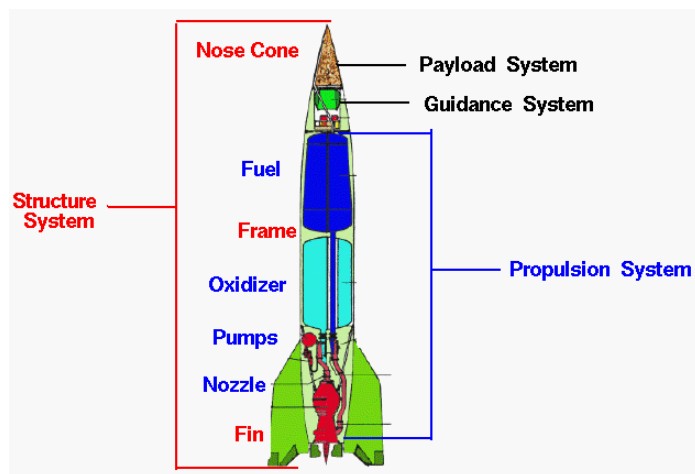


Figure 3.1: Structure of a full scale rocket[2].

Payload System

Most rockets has some form of payload system. The goal of the payload system is to carry different objects to its wanted destination. The payload can be everything from satellites and astronauts to fireworks depending on the purpose of the rocket. The payload should be considered when looking at the stability of the rocket, because incorrect weight distribution in the rocket, could lead to aerodynamic and structural instability.

Guidance System

All rockets that has the goal to be directed or controlled includes a guidance system. The guidance system consist of a processors, sensors, radars, and a form of wireless communication. Its purpose is to control the stability, direction and rotation of the rocket during launch and in flight. The guidance system is developed based on the understanding of forces acting rocket and its motion. The guidance system in modern rockets often actuate on the propulsion and nozzle system to correct rotation and direction of the rocket.

Propulsion System

The propulsion system of a rocket is the part which thrust the rocket. Thrust is the main force that makes the rocket launch and fly. All propulsion systems is based on Newton's third law. This means that a propulsion system should be able make a combustion which produces a downwards force high enough to launch the structural system of the rocket.

The propulsion system can either be a liquid rocket engine or a solid rocket engine. A liquid rocket engine is based on a combustion of fuel and a oxidizer which is mixed **an** burned. The resulting gas of the burn, is directed **trough** a nozzle which accelerates it. A solid rocket engine has premixed oxidizer and fuel which becomes the propellant. This propellant is compressed into a cylinder with **an** hole in it that functions as a combustion chamber. Which means that after ignition the propellants surface functions as the combustion chamber. The gas is therefore also forced **trough** a nozzle that accelerates it. Which applies **i** force to the engine that gives a launch of the rocket.

Structural System

Close to all full scale rockets consist of a structural system. The system consist of the cylindrical body/frame, a nose cone with the payload system and the fins that ensures a stable aerodynamic profile. Though most newer full scales rocket does not rely only on aerodynamics to ensure stability[2].

The correct combination of the system modules and design should ensure a stable flight, but as described cf. section 1 it is shown that most rockets would benefit from a control system to ensure directional stability. Further investigation of the stability of rocket is proceeded.

3.0.1 Stability of a Rocket

A rocket often has a target, either if it is space travelling or just collecting orbit data on earth, but in order to succeed it has to be stable [3]. The flight direction of a rocket can change due to disturbances as wind and thrust instabilities.

Stability can be defined within many categories. In the case of a rocket the stability is considered as the directional and flight stability.

Figure 3.2 describes a example of a chaotic path for a badly designed rocket. Where the center and gravity and pressure is incorrect placed on the unstable rocket, which make it deviate from its goal trajectory.

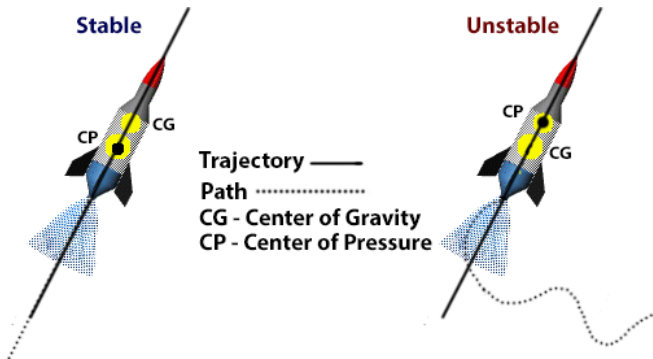


Figure 3.2: Example of the path for an unstable rocket [3].

Center of gravity and pressure is related to the forces acting on the rocket. An analysis of these forces is proceeded. Figure 3.3 describes the different situations a rocket encounters during its flight and describes the forces applied in these cases.

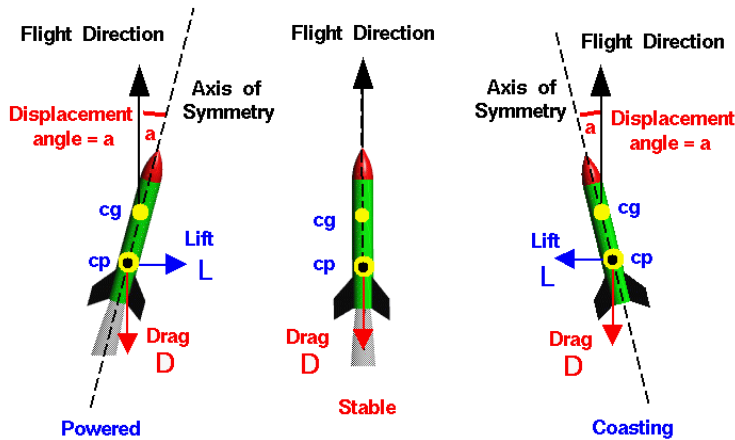


Figure 3.3: Summary of forces applied to a rocket during its flight [3].

In Figure 3.3 two points can be seen on the rockets. One is CP the Center of Pressure where the lift and the drag force apply [3] a rocket. The other one is CG the Center of Gravity, which is the point which the rocket rotate around [3]. Due to this characteristics the torque applied by the lift and the drag is dependent of the relative positioning between the CG and the CP. Since a rocket tilts due to a torque applied by external forces such as the wind, then lift and the drag has to be oriented so it counters these forces. In order to do so the CG has to be above the CP [3]. This means depending of the position of the CP compared to the CG the rocket flight will be either stable or unstable. That is why in simpler rockets without any control system, its design is made that CP is indeed above CG.

This preliminary analysis makes gives the possibility to further examine on how to control the stability of a rocket.

3.1 Controlling a Rocket's Stability

The previous design method does not provide a perfectly stable attitude control. Indeed to have such precision an active control system is necessary. Full scale rockets use the thrusting force to achieve alike control. In order to do so most of them operate with the gimballed thrust method. It consists of steering the engine's nozzle to get the thrusting force in right incidence, an example is seen cf. figure Figure 3.4.

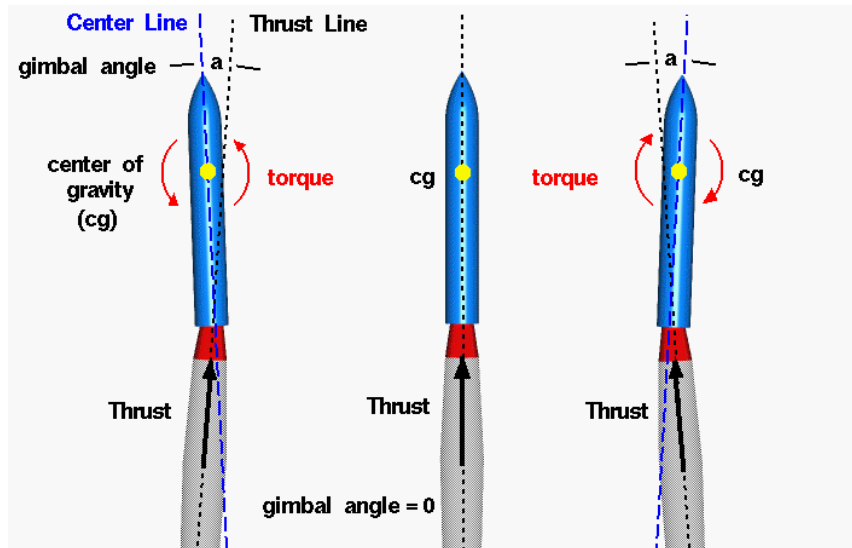


Figure 3.4: Example of gimbaling a rocket nozzle [3].

Where a torque is applied to create a rotation around the rocket's center of gravity. The thrust direction is relative to the position of the center of gravity. This should

compensate for direction deviations from the rocket's center line or trajectory, and keep the rocket stable.

However Space X introduces a new propulsion method by using multiple small engines instead of a big one. With this method the thrusting force direction can be instead controlled by the output of each engine. For smaller rockets orientable fins are used. By changing the orientations of the fins the drag and the lift are modified and so is the attitude of the rocket.

Stabilization of rockets are therefore feasible with different types of control types. Most rockets are one time use which means that implementing and testing of a stabilization system would be of high cost. Therefore will similar control systems be examined to research the possibility for making a ground based control system, which can be related to the motion and stabilization of a rocket in flight.

3.2 Systems with Similar Instability Problems

In order to stabilize the rocket in flight, a controller must be implemented to correct the rockets trajectory deviation during flight.

The possibility of damaging the rocket or the controller needs to be countered by the efficiency of the control system.

Experimenting such a system during flight is expensive and presents nonnegligible hazards. Is there a system that has similar instability properties of rockets, and presents fewer restrictions to experiment? 

The Cubli is a system known for its instability. It is commonly used in Control Theory to analyze the behavior of a reaction of a wheel inverted system. The advantages of the usage a Cubli is its ability to reach its equilibrium position in microgravity environments, such as asteroids. This is not relevant for a rocket instability project. And can therefore not be directly related to the instability of a rocket.

A recent technology facing instability is Segway. A Segway is an application of an inverted pendulum to a two wheeled self-balance vehicle. The objective is to detect and stabilize the instability of the vertical stick to move the vehicle and prevent the user to fall. This vehicle requires three body directions instead of the linear motion of an inverted pendulum. The study of instability properties of a Segway system would mean the study of elements nonexistent or negligible in a rocket system.

An inverted pendulum objective is to stabilize a stick whose center of mass is above pivot point. The process is done using a horizontal force, resulting in a first degree of freedom rotation, as found in a rocket system. A double inverted pendulum is a combination of an inverted pendulum and a double pendulum. The stability of the stick is reached by applying a torque between the two pendulums.

In consideration of the different applications and similarities of the three systems, the double inverted pendulum will be further analyzed. The objective is to model the dynamics of both the double inverted pendulum and the rocket, and then compare and relate the models to determine similarities. This should lead to designing a control system for stabilizing the inverted pendulum, which could be implemented on the rocket as a stabilization control system.

Chapter 4

Delimitation

In the project some limits has to be set for the use of models and materials. The objective of the control system is to find the similarities of using a electronic stabilization system for rockets and for inverted pendulums. The system is developed as a proof-of-concept solution. The models in the project can only be approximations of reality, and it is therefore observable that the transfer to a larger scale project will not be linear.

Physical delimitation: The inverted pendulum setup used in the project is pre-fabricated and made available by the university. The choice of motor, gears, and other components will therefore not be further considered. The setup is a double inverted pendulum, and contains therefore of both a arm and a stick. The double inverted pendulum setup will be from here on be called "inverted pendulum". The setup is shown cf. figure 4.1.

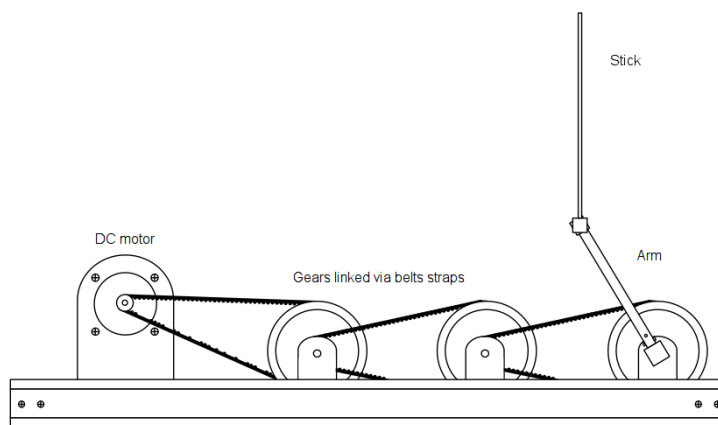


Figure should be updated with lengths and gear teeth, block separating the individual systems.

Figure 4.1: Diagram of the inverted pendulum setup[4].

Construction and modeling of the rocket will be limited to a minor-scale rocket with a similarities to the design behind a full-scale rocket. The rocket will be designed around a solid propellant thruster, and will therefore not contain any liquid fuel. This is to limit the constraints from laws and keep the cost low. Further more weight and dimension limits is set before designing the rocket.

Control delimitation: A choice is made that the starting point for controlling the stick is as illustrated cf. figure 4.1 in upwards vertical position. Therefore the controller will not be able to balance the stick, if its vertical balance limits is surpassed. The delimitation is made to simplify the controlling, and make it as similar as possible to controlling a rocket.

Test delimitation: Launching and flight of a rocket for testing a controller is a high cost procedure because of the chance of damaging the rocket and the cost of thrusters per launch. The testing of the rockets stabilization will be ground based test setup, where the controller can be tested without the risk of damaging the rocket. If, and only if the control system proves stable and safe, a launch and flight of the rocket will be conducted under circumstances fulfilling given laws.

The delimitation sets the boundaries for the project and describes which models is available. This gives possibility for describing and modeling of both the inverted pendulum and rocket, to examine if there is similarities behind controlling them.

Chapter 5

Inverted Pendulum Analysis

5.1 Inverted Pendulum Description

For this project an inverted pendulum set up is given. It consists of:

- A DC motor
- A gear system
- An arm
- A stick connected to the end of the arm.

A diagram of the setup when fully assembled is seen on Figure 5.1.

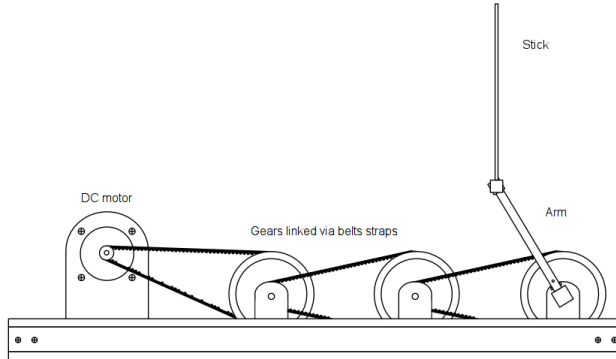


Figure 5.1: Diagram of the set up fully assembled.

Each part will be described with its specifications and use in the setup. The input and output relation of each block is illustrated on Figure 5.2, where the goal throughout the chapter will be determining the transfer functions that describe these relations.

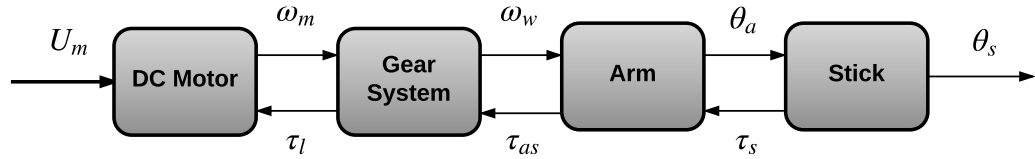


Figure 5.2: Block diagram of the input/output relations of the system.

Where:

U_m	is the motor input voltage	[V]
ω_m	is the angular velocity of the motor	[rad s ⁻¹]
ω_w	is the angular velocity of the gear connected to the arm	[rad s ⁻¹]
τ_l	is the total friction of the gears, arm and stick	[N m]
τ_{as}	is the load of the arm and the stick	[N m]
τ_s	is the load of the stick	[N m]
θ_a	is the angle from the arm to the y-axis	[rad]
θ_s	is the angle from the stick to the y-axis	[rad]

DC Motor

An Axem DC servo motor model F9M2 is attached to the gears to create an angular velocity in the system. The integrated tachometer of the motor is used as feedback to ensure control precision. This is done so it is possible to see the velocity and direction of the motor and relate it to the position of the arm. Using the DC motor also means implementing a motor controller. Already implemented in the setup is a Maxon Escon 50/5 Servocontroller, which can be controlled through PWM [5]. The servocontroller is supplied through a 230 V regulator that can supply the servocontroller with up to 56 V and 15 A depending the power supply. The regulator in itself will be considered a blackbox, because of user limitations when working with 230 V at the university. The DC motor and servocontroller will in system diagrams be evaluated as one unit, but further considered when implementing a system controller.

Gear System

Between the DC motor and arm is the gear system. The goal of the gear system is to reduce the ratio between the rotation of the motor versus the arm. The gear system is series of the same size small and big gear connected with belts. The setup is seen on Figure 5.1, where the number of gear is illustrated. The parameters of the gear system is listed cf. Table 5.1.

Table 5.1: Parameters of gear system.

Piece	Parameter	Value	Unit
Gear _{big}	Teeth	40	[1]
Gear _{big}	Diameter	0.12	[m]
Gear _{small}	Teeth	12	[1]
Gear _{small}	Diameter	0.04	[m]
Belt	Length	0.6	[m]

Stick and Arm

The arm and stick are elements that always appears in the double inverted pendulum setup. The goal is for the arm to apply force on their common joint, which would affect the position of the stick. The physical parameters for the stick and arm is listed cf. Table 5.2.

Table 5.2: Physical parameters of the arm and sticks.

Piece	Parameter	Value	Unit
Stick _{long}	Length	0.8	[m]
Stick _{long}	Weight	0.344	[kg]
Stick _{short}	Length	0.4	[m]
Stick _{short}	Weight	0.170	[kg]
Arm	Length	0.33	[m]
Arm	Weight	0.288	[kg]

Some feedback is needed to be able to control the stick through the arm and gears. The sensors used are implemented as an integrated part of the setup, and will therefore be the choice and will not be further discussed.

A necessary feedback to know is the angle between the stick and arm. This is needed to balance the stick via the controller. The angle between the stick and arm is detected and sampled from a potentiometers rotational position. Equally the position of the arm is needed, this is to determine the amount of change needed to counteract the change in the stick. The position of each potentiometer can be seen Figure 5.3.

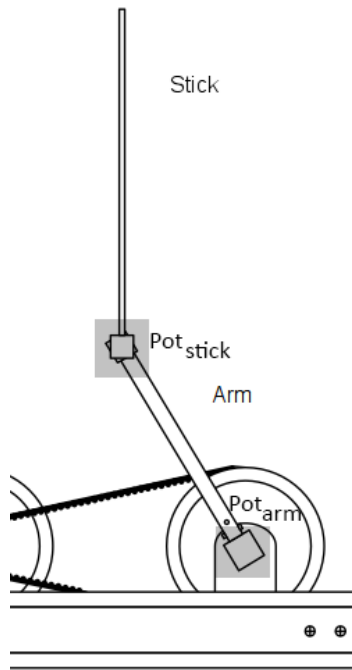


Figure 5.3: Diagram of the arm and stick with sensors illustrated.

The block diagram for the standard feedback control system with the known system plant is seen on Figure 5.4.

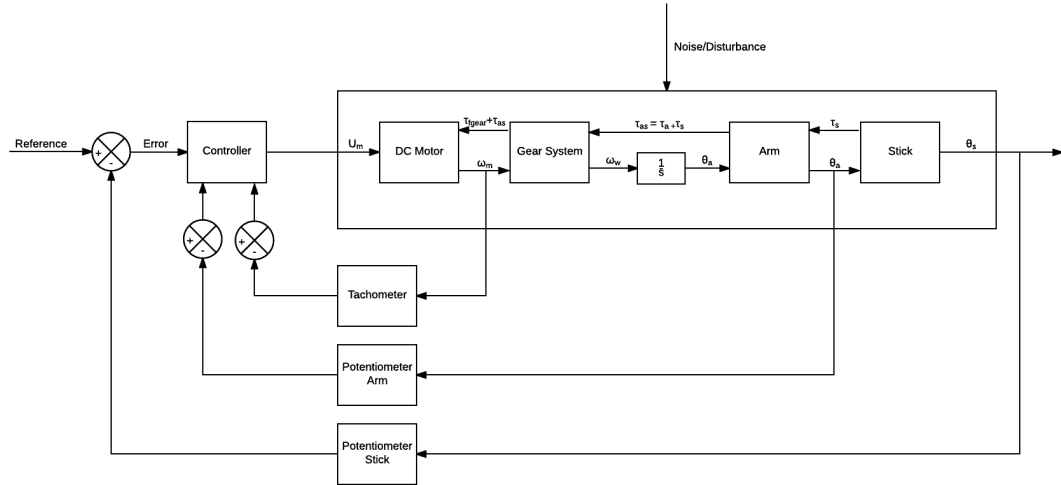


Figure 5.4: Block diagram of the setups feedback loop.

Might be changed, was not sure how we would handle the feedback of the sensors.

The basics of each system in the Inverted Pendulum is now described with its specifications, and the dynamics of the system can be modelled. Each section will be modeled from the output to the input as the sections generate a torque that effects the previous sections of the system.

5.2 Modelling of the Arm and Stick

The goal of this section is to have a mathematical model for the behaviour of the angle of the stick in relation to the angle of the arm on the motor. The inputs and outputs of this system can be seen by the block diagram in Figure 5.5.

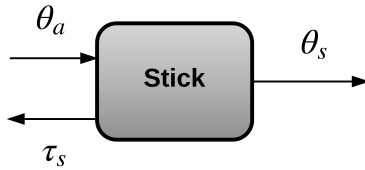


Figure 5.5: Block diagram of the inputs and outputs of the stick section of the inverted pendulum setup.

The angles, constants and forces used to describe the system are seen on Figure 5.6. Where:

F_x is the force in the x direction	[N]
F_y is the force in the y direction	[N]
x_s is the position of the center of mass of the stick in the x direction	[m]
y_s is the position of the center of mass of the stick in the y direction	[m]
l_a is the length of the arm	[m]
l_s is the length of the stick	[m]
θ_a is the angle from the arm to the y-axis	[rad]
θ_s is the angle from the stick to the y-axis	[rad]

Jacob: Add the reactionary forces where arm and stick connects. Fpx and Fpy.

All forces, constants and variables that relates to the arm and stick are denoted by a subscripted a and s respectively.

The behaviour of the stick can be fully described by three movements; two translatory and one rotary. It can move in the x and y direction and rotate around it's own axis. To fully describe the system two geometric equations are also needed.

The two translatory forces acting on the stick in the x and y directions are found by Equation (5.1) using Newton's 2nd law of motion.

$$\ddot{x}_s M_s = F_x \quad (5.1a)$$

$$\ddot{y}_s M_s = F_y - g M_s \quad (5.1b)$$

$$F_y = (\ddot{y}_s + g) M_s \quad (5.1c)$$

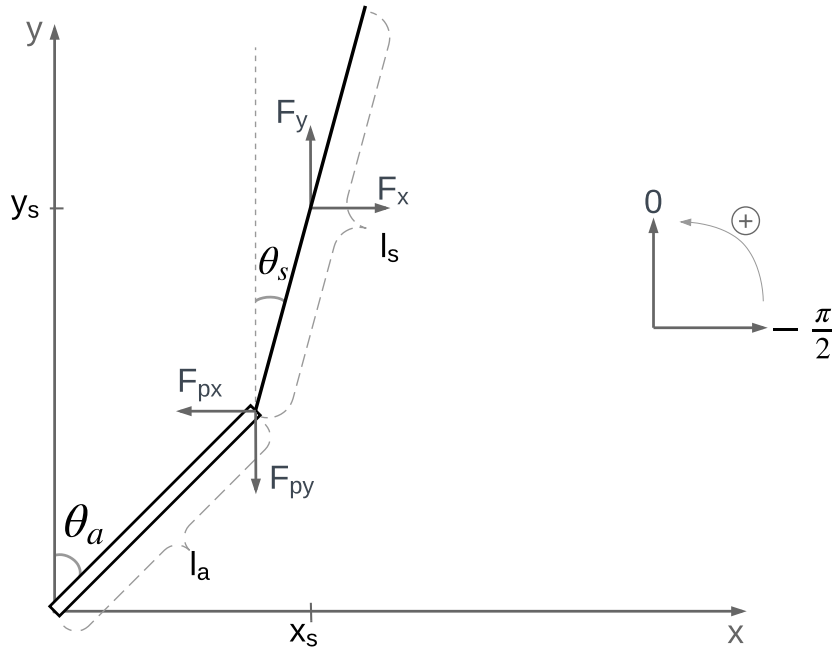


Figure 5.6: Diagram of the angles and forces acting on the arm and the stick.

Where:

g is the standard gravitational acceleration near the surface of the earth [m s⁻²]

M_s is the mass of the stick [kg]

The rotational movement of the stick is described by Equation (5.2).

$$J_s \ddot{\theta}_s = \frac{l_s}{2} (F_x \cos(\theta_s) + F_y \sin(\theta_s)) - b_{as} \dot{\theta}_{as} \quad (5.2)$$

Finally the position of the center of mass of the stick in the x and y direction is found by Equation (5.3) using geometry.

$$x_s = l_a \sin(-\theta_a) + \frac{l_s}{2} \sin(-\theta_s) \quad (5.3a)$$

$$x_s = -l_a \sin(\theta_a) - \frac{l_s}{2} \sin(\theta_s) \quad (5.3b)$$

$$y_s = l_a \cos(-\theta_a) + \frac{l_s}{2} \cos(-\theta_s) \quad (5.3c)$$

$$y_s = l_a \cos(\theta_a) + \frac{l_s}{2} \cos(\theta_s) \quad (5.3d)$$

Equation (5.1a), Equation (5.1c), Equation (5.2), Equation (5.3b) and Equation (5.3d) are all the equations necessary to fully describe the behaviour of the system. The

goal of the modeling is to end with a transfer function that relates the angle of the stick to the angle of the arm. There are 6 unknown variables in the 5 equations: F_x , F_y , x_s , y_s , θ_a and θ_s . It should therefore be possible to end with one equation with the two unknowns θ_a and θ_s i.e. the transfer function.

The derivatives of x_s and y_s is found in Equation (5.4).

$$\dot{x}_s = -l_a \dot{\theta}_a \cos(\theta_a) - \frac{l_s}{2} \dot{\theta}_s \cos(\theta_s) \quad [\text{m s}^{-1}] \quad (5.4\text{a})$$

$$\ddot{x}_s = -l_a \ddot{\theta}_a \cos(\theta_a) + l_a \dot{\theta}_a^2 \sin(\theta_a) - \frac{l_s}{2} \ddot{\theta}_s \cos(\theta_s) + \frac{l_s}{2} \dot{\theta}_s^2 \sin(\theta_s) \quad [\text{m s}^{-2}] \quad (5.4\text{b})$$

$$\dot{y}_s = -l_a \dot{\theta}_a \sin(\theta_a) - \frac{l_s}{2} \dot{\theta}_s \sin(\theta_s) \quad [\text{m s}^{-1}] \quad (5.4\text{c})$$

$$\ddot{y}_s = -l_a \ddot{\theta}_a \sin(\theta_a) - l_a \dot{\theta}_a^2 \cos(\theta_a) - \frac{l_s}{2} \ddot{\theta}_s \sin(\theta_s) - \frac{l_s}{2} \dot{\theta}_s^2 \cos(\theta_s) \quad [\text{m s}^{-2}] \quad (5.4\text{d})$$

The forces F_x and F_y have an equal and opposite force at the point where the arm and stick connect. These can be decomposed into perpendicular and parallel forces. The parallel forces are negligible when assuming the stick is perfectly solid and unable to stretch or compress. The perpendicular forces are found by using geometry and shows up in Equation (5.2) for the rotary force and are seen on Figure 5.6.

The derivatives of the two geometric equations are inserted into Equation (5.1a) and Equation (5.1c) which are then inserted into Equation (5.2) in Equation (5.5b).

$$J_s \ddot{\theta}_s = \frac{l_s}{2} (\ddot{x}_s M_s \cos(\theta_s) + (\ddot{y}_s + g) M_s \sin(\theta_s)) - b_{as} \dot{\theta}_{as} \quad (5.5\text{a})$$

$$\begin{aligned} J_s \ddot{\theta}_s = & \frac{l_s}{2} M_s \left(-l_a \ddot{\theta}_a (\cos(\theta_a) \cos(\theta_s) + \sin(\theta_a) \sin(\theta_s)) \right. \\ & + l_a \dot{\theta}_a^2 (\sin(\theta_a) \cos(\theta_s) - \cos(\theta_a) \sin(\theta_s)) \\ & - \frac{l_s}{2} \ddot{\theta}_s (\cos(\theta_s) \cos(\theta_s) + \sin(\theta_s) \sin(\theta_s)) \\ & + \frac{l_s}{2} \dot{\theta}_s^2 (\sin(\theta_s) \cos(\theta_s) - \cos(\theta_s) \sin(\theta_s)) \\ & \left. + g \sin(\theta_s) \right) - b_{as} \dot{\theta}_{as} \end{aligned} \quad (5.5\text{b})$$

Using the trigonometric properties in Equation (5.6), Equation (5.5b) is reduced to Equation (5.7).

$$\cos(\theta_a) \cos(\theta_s) \pm \sin(\theta_a) \sin(\theta_s) = \cos(\theta_a \mp \theta_s) \quad (5.6\text{a})$$

$$\sin(\theta_a) \cos(\theta_s) \pm \cos(\theta_a) \sin(\theta_s) = \sin(\theta_a \pm \theta_s) \quad (5.6\text{b})$$

$$\cos(\theta_s)^2 + \sin(\theta_s)^2 = 1 \quad (5.6\text{c})$$

$$J_s \ddot{\theta}_s = \frac{l_s}{2} M_s \left(-l_a \ddot{\theta}_a \cos(\theta_a - \theta_s) + l_a \dot{\theta}_a^2 \sin(\theta_a - \theta_s) - \frac{l_s}{2} \ddot{\theta}_s + g \sin(\theta_s) \right) - b_{as} \dot{\theta}_{as} \quad (5.7)$$

This is the nonlinear mathematical model for the system. This will be linearized in order to perform a Laplace transformation. The linearization is found in Appendix C.

The linearized model is Equation (5.8).

$$J_s \ddot{\theta}_s = \frac{l_s}{2} M_s \left(-l_a \ddot{\theta}_a - \frac{l_s}{2} \ddot{\theta}_s + g \theta_s \right) - b_{as} \dot{\theta}_{as} \quad (5.8)$$

Inserting the moment of inertia for a rotating stick, $J_s = \frac{1}{12} M_s l_s^2$, the linearized model becomes (5.9d) [6].

$$\frac{1}{12} M_s l_s^2 \ddot{\theta}_s = \frac{l_s}{2} M_s \left(-l_a \ddot{\theta}_a - \frac{l_s}{2} \ddot{\theta}_s + g \theta_s \right) - b_{as} \dot{\theta}_{as} \quad (5.9a)$$

$$\frac{1}{12} M_s l_s^2 \ddot{\theta}_s + \frac{1}{4} M_s l_s^2 \ddot{\theta}_s = \frac{l_s}{2} M_s \left(-l_a \ddot{\theta}_a + g \theta_s \right) - b_{as} \dot{\theta}_{as} \quad (5.9b)$$

$$\frac{1}{3} M_s l_s^2 \ddot{\theta}_s = \frac{l_s}{2} M_s \left(-l_a \ddot{\theta}_a + g \theta_s \right) - b_{as} \dot{\theta}_{as} \quad (5.9c)$$

$$\ddot{\theta}_s = \frac{3}{2l_s} \left(-l_a \ddot{\theta}_a + g \theta_s \right) - \frac{3b_{as} (\dot{\theta}_s - \dot{\theta}_a)}{M_s l_s^2} \quad (5.9d)$$

The linearized model is now Laplace transformed in Equation (5.10c) in order to find the transfer function.

$$s^2 \Theta_s = \frac{3}{2l_s} \left(-s^2 l_a \Theta_a + g \Theta_s \right) - s \frac{3b_{as}}{M_s l_s^2} \Theta_s + s \frac{3b_{as}}{M_s l_s^2} \Theta_a \quad (5.10a)$$

$$\Theta_s \left(s^2 + \frac{3b_{as}}{M_s l_s^2} s - \frac{3g}{2l_s} \right) = \Theta_a \left(-\frac{3l_a}{2l_s} s^2 + \frac{3b_{as}}{M_s l_s^2} s \right) \quad (5.10b)$$

$$\frac{\Theta_s}{\Theta_a} = \frac{-\frac{3l_a}{2l_s} s^2 + \frac{3b_{as}}{M_s l_s^2} s}{s^2 + \frac{3b_{as}}{M_s l_s^2} s - \frac{3g}{2l_s}} \quad (5.10c)$$

The system has a zero in 0 (two if the friction is considered negligible) which gives a 0 dB DC gain. This makes sense as the stick shouldn't move if the angle of the arm is constant. The poles show that the natural frequency of the system depends only on the gravity and length of the stick. This is similar to Equation (5.11) for the frequency of a simple pendulum [7].

$$\omega_n = \sqrt{\frac{g}{L}} \quad (5.11)$$

A linearized model in the Laplace domain for the arm and the stick has been derived and the model for the motor and gears is now derived. The load torque generated by the arm and stick is significantly smaller than that of the gear system at the DC motor and is therefore assumed negligible.

5.3 Modeling of the Gear System

This section aims to describe the behaviour of the gear system and the transfer functions that need to be found are shown on Figure 5.7. Two transfer functions are going to be determined in this section: The relation between the motor velocity, ω_m , and the angle of the arm, θ_a , and the load torque, τ_l , generated by the gears. Where:

τ_l is the torque of the motor's load	[N m]
ω_m is the motor's angular velocity	[m s ⁻¹]
τ_{as} is the torque of the arm and the stick	[N m]
ω_{w3} is the third wheel's angular velocity	[m s ⁻¹]

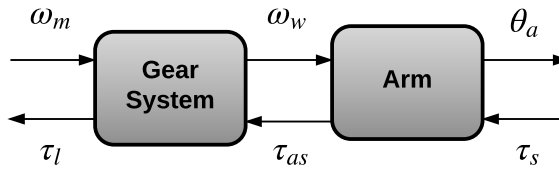


Figure 5.7: Block diagram of the inputs and outputs of the gear system.

5.3.1 Relation between Motor Velocity and Angle of the Arm

The motor is connected to the first wheel of the gear system by a belt as shown on Figure 5.8. The first wheel has a smaller wheel rigidly attached and turning in the same direction. The smaller first wheel is attached to the second wheel in the same fashion as the motor to the first wheel. Wheel two and three are exactly the same as wheel one and two. The entire system can thus be described Figure 5.8 by replacing the motor wheel with the smaller wheels 1 and 2 and the larger wheel 1 with the larger wheels 2 and 3.

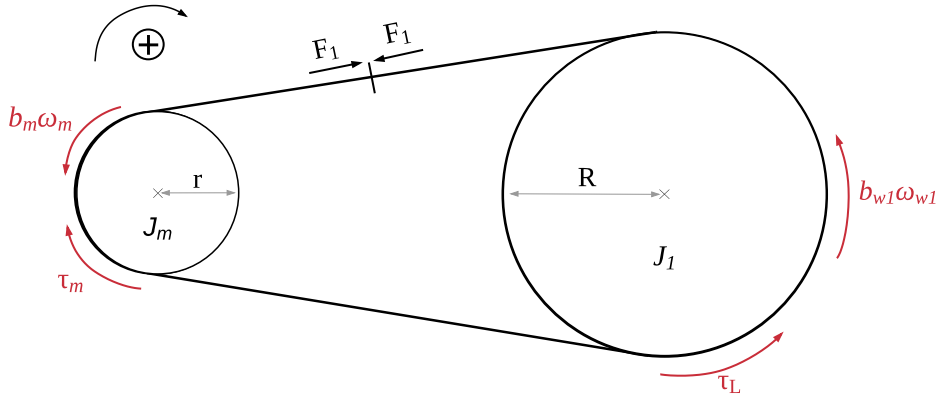


Figure 5.8: Free body diagram of the motor wheel system.

Where:

J_m is the moment of inertia of the motor	[kg m ²]
J_w is the moment of inertia of the wheel	[kg m ²]
ω_m is the motor's angular velocity	[m s ⁻¹]
τ_m is the torque of the motor	[N m]
F_1 is the force transferred from the motor to the wheel	[N]
r is the radius of the motor's wheel	[m]
R is the radius of the wheel	[m]
τ_f is the torque of the gear train friction	[N m]
τ_L is the torque of the wheel's load	[N m]
b_w is the viscous friction coefficient of the wheel	[N m s]

If the motor shaft turns, the belt joining the small and the big wheel will make them turn the same distance, giving relation in Equation (5.12).

$$\theta_m r = \theta_w R \quad (5.12)$$

This expression is then differentiated to find the relation with the angular velocities in Equation (5.13).

$$\omega_m r = \omega_w R \quad (5.13)$$

The gear ratio can then be defined by Equation (5.14).

$$N = \frac{r}{R} \quad (5.14)$$

As the gear system is composed by three similar connected wheels structures like Figure 5.8, the ratio between one of the small wheels, r_x , and the big wheel connected

by the belt, R_x is the same and is seen in Equation (5.15).

$$\frac{r_x}{R_x} = \frac{r_{\text{motor}}}{R_{w_1}} = \frac{r_{w_1}}{R_{w_2}} = \frac{r_{w_2}}{R_{w_3}} = N \quad (5.15)$$

Knowing this and since ω_m is transferred through three gears reductions, the relation between the angular velocity of the motor ω_m and the angle of the arm θ_a is found following the principle of Equation (5.13).

$$\omega_a(t) = N^3 \omega_m(t) \quad (5.16a)$$

$$\theta_a(t) = N^3 \int_0^t \omega_m(v) dv \quad (5.16b)$$

$$\mathcal{L}\{\theta_a(t)\} = \Theta_a(s) = N^3 \cdot \frac{1}{s} \Omega_m(s) \quad (5.16c)$$

The transfer function from the motor's angle velocity to the angle of the arm becomes Equation (5.17).

$$\frac{\Theta_a(s)}{\Omega_m(s)} = \frac{N^3}{s} \quad (5.17)$$

5.3.2 Determining the Load Torque Produced by the Gears

The torque of the load put on the motor is the sum of the torque produced by the gears and the torque produced by the arm and stick. As the torque from the arm and stick are considered negligible c.f. Section 5.2, only the torque of the gears needs to be described.

The torque on the wheel of the motor can be described by Equation (5.19).

$$J_m \dot{\omega}_m = \tau_m - \tau_l - \tau_{fm} \quad (5.18)$$

$$J_m \dot{\omega}_m = \tau_m + F_1 r - b_m \omega_m \quad (5.19)$$

This means that the torque of the load produced by the gears is equal to $-F_1 r$. To find F_1 the torque on the wheel is examined and seen in Equation (5.20).

$$J_w \dot{\omega}_w = -F_1 R - \tau_L - b_w \omega_w \quad (5.20)$$

Here τ_L is the load on wheel 1 that comes from the rest of the wheels connected to it. Wheel 2 is connected to wheel 1 similar to how wheel 1 is connected to the motor. This means that the load torque on wheel 1 is related to F_2 and the load torque on wheel 2 is related to F_3 . Substituting the load torque for the forces, the torques for each wheel is Equation (5.21).

$$J_{w_1} \dot{\omega}_{w_1} = -F_1 R + F_2 r - b_{w_1} \omega_{w_1} \quad (5.21a)$$

$$J_{w_2} \dot{\omega}_{w_2} = -F_2 R + F_3 r - b_{w_2} \omega_{w_2} \quad (5.21b)$$

$$J_{w_3} \dot{\omega}_{w_3} = -F_3 R - b_{w_3} \omega_{w_3} \quad (5.21c)$$

Using the relation in Equation (5.13), the angular velocity of each wheels can be found to be Equation (5.22).

$$\omega_{w_1} = N\omega_m \quad (5.22a)$$

$$\omega_{w_2} = N\omega_{w_1} = N^2\omega_m \quad (5.22b)$$

$$\omega_{w_3} = N\omega_{w_2} = N^3\omega_m \quad (5.22c)$$

The same equations are valid with angular accelerations and are inserted in Equation (5.21) giving Equation (5.23).

$$J_{w_1}N\dot{\omega}_m = -F_1R + F_2r - b_{w_1}N\omega_m \quad (5.23a)$$

$$J_{w_2}N^2\dot{\omega}_m = -F_2R + F_3r - b_{w_2}N^2\omega_m \quad (5.23b)$$

$$J_{w_3}N^3\dot{\omega}_m = -F_3R - b_{w_3}N^3\omega_m \quad (5.23c)$$

The forces F_1 , F_2 and F_3 are isolated giving Equation (5.24).

$$F_1 = -\frac{1}{R}N \left(b_{w_1}\omega_m + J_{w_1}\dot{\omega}_m - \frac{F_2r}{N} \right) \quad (5.24a)$$

$$F_2 = -\frac{1}{R}N^2 \left(b_{w_2}\omega_m + J_{w_2}\dot{\omega}_m - \frac{F_3r}{N^2} \right) \quad (5.24b)$$

$$F_3 = -\frac{1}{R}N^3 (b_{w_3}\omega_m + J_{w_3}\dot{\omega}_m) \quad (5.24c)$$

Inserting Equation (5.24c) in Equation (5.24b) gives Equation (5.25).

$$F_2 = -\frac{1}{R}N^2 \left(b_{w_2}\omega_m + J_{w_2}\dot{\omega}_m + \frac{r}{R} \frac{N^3}{N^2} (b_{w_3}\omega_m + J_{w_3}\dot{\omega}_m) \right) \quad (5.25)$$

Equation (5.25) is then inserted in Equation (5.24a) giving Equation (5.26) while remembering that the gear ratio is defined by Equation (5.14).

$$\begin{aligned} F_1 = & -\frac{1}{R}N \left(b_{w_1}\omega_m + J_{w_1}\dot{\omega}_m \right. \\ & \left. + N^2 \left(b_{w_2}\omega_m + J_{w_2}\dot{\omega}_m \right. \right. \\ & \left. \left. + N^2 (b_{w_3}\omega_m + J_{w_3}\dot{\omega}_m) \right) \right) \end{aligned} \quad (5.26)$$

Since $\tau_l = -F_1r$ and the torque of the load on the motor is the torque of the gears, τ_{gear} can be expressed by Equation (5.27).

$$\begin{aligned}\tau_{\text{gear}} = & N^2 \left(b_{w1}\omega_m + J_{w1}\dot{\omega}_m \right. \\ & + N^2 \left(b_{w2}\omega_m + J_{w2}\dot{\omega}_m \right. \\ & \left. \left. + N^2(b_{w3}\omega_m + J_{w3}\dot{\omega}_m) \right) \right)\end{aligned}\quad (5.27)$$

Equation (5.27) is Laplace-transformed and reorganized giving Equation (5.28b).

$$\begin{aligned}\mathcal{L}\{\tau_{\text{gear}}(t)\} = \tau_{\text{gear}}(s) = & N^2 \left(B_{w1}\Omega_m + sJ_{w1}\Omega_m \right. \\ & + N^2 \left(B_{w2}\Omega_m + sJ_{w2}\Omega_m \right. \\ & \left. \left. + N^2(B_{w3}\Omega_m + sJ_{w3}\Omega_m) \right) \right)\end{aligned}\quad (5.28a)$$

$$\tau_{\text{gear}} = \left((N^2J_{w1} + N^4J_{w2} + N^6J_{w3})s + (N^2B_{w1} + N^4B_{w2} + N^6B_{w3}) \right) \Omega_m \quad (5.28b)$$

The moments of inertia and the frictions for each wheel is grouped into two variables J_{gear} and B_{gear} respectively giving the torque for the gears in Equation (5.29).

$$\tau_{\text{gear}} = (J_{\text{gear}}s + B_{\text{gear}}) \Omega_m \quad (5.29)$$

5.4 Modeling of the DC-Motor

The purpose of this section is to establish a dynamic model of the DC-motor. The inputs and outputs of the model can be seen on the block diagram on Figure 5.9.

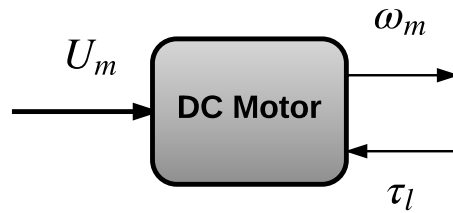


Figure 5.9: Block diagram showing the inputs and outputs of the DC motor part of the inverted pendulum setup.

Only the transfer function from the voltage input, U_m , to the angular velocity output, ω_m , needs to be found. It will be done by modeling the electrical and the mechanical part of the motor in that order before combining them.

5.4.1 Electrical Model of the Motor

The electrical circuit of the motor is presented in Figure 5.10.

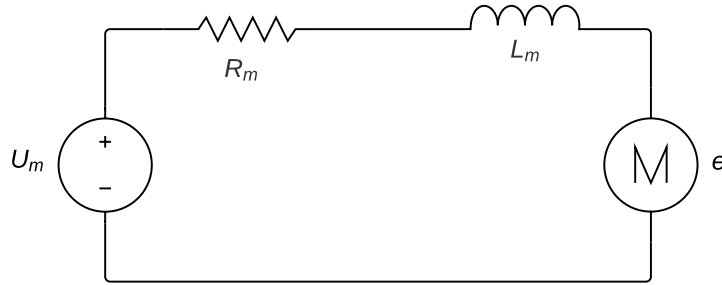


Figure 5.10: Circuit diagram of a DC-motor.

Using Kirchhoff's voltage law, the electric model of the DC-motor is Equation (5.30).

$$U_m = R_m i + L_m \frac{di}{dt} + e \quad (5.30a)$$

$$e = K_e \omega_m \quad (5.30b)$$

Where:

U_m is the voltage output of the generator	[V]
R_m is the resistance of the DC-motor	[Ω]
L_m is the inductance of the DC-motor	[H]
i is the current in the DC-motor	[A]
e is the electromotive force	[V]
K_e is the motor velocity constant	[V s rad ⁻¹]
ω_m is the angular velocity of the motor	[rad s ⁻¹]

This is all that's needed for the electrical part to find the model of the motor.

5.4.2 Mechanical Model of the Motor

The mechanical free body diagram of the motor is presented in Figure 5.11.

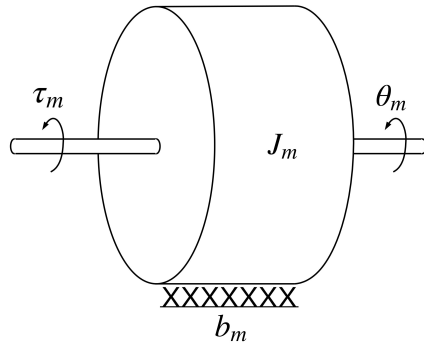


Figure 5.11: Free body diagram of a DC-motor.

From Figure 5.11, the sum of the torques for the mechanical part of the motor is Equation (5.31).

$$J_m \dot{\omega}_m = \tau_m - \tau_l - \tau_{fm} \quad (5.31)$$

Where:

J_m is the moment of inertia of the motor $[\text{kg m}^2]$

τ_m is the torque of the DC-motor $[\text{N m}]$

τ_l is the torque of the load $[\text{N m}]$

τ_{fm} is the torque of the friction $[\text{N m}]$

The motor's torque and the friction's torque, respectively τ_m and τ_f , are defined by Equation (5.32) while τ_l is the torque of the gears, τ_{gear} , found in Section 5.3.2.

$$\tau_m = K_t \cdot i \quad (5.32a)$$

$$\tau_{fm} = b_m \cdot \omega_m \quad (5.32b)$$

Where:

K_t is the motor torque constant $[\text{N m A}^{-1}]$

b_m is the viscous friction coefficient $[\text{N m s rad}^{-1}]$

Inserting Equation (5.32) into Equation (5.31) gives Equation (5.33).

$$J_m \dot{\omega}_m = K_t i - \tau_{\text{gear}} - b_m \omega_m \quad (5.33)$$

The mechanical and electrical model of the motor can now be combined.

5.4.3 Combined Model of the Motor

First the electrical and mechanical equations of the motor are Laplace-transformed in Equation (5.34)

$$U_m(s) = R_m I(s) + sL_m I(s) + K_e \Omega_m(s) \quad (5.34a)$$

$$sJ_m \Omega_m(s) = K_t I(s) - \tau_{\text{gear}} - B_m \Omega_m(s) \quad (5.34b)$$

The current, $I(s)$, is isolated and inserted in Equation (5.34b) giving Equation (5.35).

$$sJ_m \Omega_m(s) = K_t \frac{U_m(s) - K_e \Omega_m(s)}{R_m + sL_m} - \tau_{\text{gear}} - B_m \Omega_m(s) \quad (5.35)$$

Equation (5.29) is inserted in Equation (5.35) and rearranged giving Equation (5.36c). The equation is simplified by setting $J_t = J_m + J_{\text{gear}}$ and $B_t = B_m + B_{\text{gear}}$.

$$\Omega_m(s) \left((J_m + J_{\text{gear}}) s + (B_m + B_{\text{gear}}) \right) = K_t \frac{U_m(s) - K_e \Omega_m(s)}{R_m + sL_m} \quad (5.36a)$$

$$\Omega_m(s) \left(J_t L_m s^2 + (J_t + B_t L_m) s + B_t R_m + K_t K_e \right) = K_t U_m(s) \quad (5.36b)$$

$$\frac{\Omega_m(s)}{U_m(s)} = \frac{K_t}{J_t L_m s^2 + (J_t R_m + B_t L_m) s + B_t R_m + K_t K_e} \quad (5.36c)$$

As L_m is significantly smaller than R_m it is assumed to be 0. This assumption is made to simplify the motor model and is fair as a small L_m would have almost no influence on the system as seen in Equation (5.35). This gives Equation (5.37) which is the final transfer function for the DC motor model.

$$\frac{\Omega_m(s)}{U_m(s)} = \frac{K_t}{J_t R_m s + B_t R_m + K_t K_e} \quad (5.37)$$

5.5 Combining the Models for the Inverted Pendulum

With a model for each individual part of the inverted pendulum derived, a combined model for the entire system can be made. This model will have voltage, $U_m(s)$, as input and the angle of the stick, $\Theta_s(s)$, as the output. This is done by multiplying all transfer functions together as seen in Equation (5.38).

$$\frac{\Omega_m(s)}{U_m(s)} \cdot \frac{\Theta_a(s)}{\Omega_m(s)} \cdot \frac{\Theta_s(s)}{\Theta_a(s)} = \frac{\Theta_s(s)}{U_m(s)} \quad (5.38)$$

By combining Equation (5.37), Equation (5.17) and Equation (5.10c) the model for the inverted pendulum becomes Equation (5.39).

$$\frac{\Theta_s(s)}{U_m(s)} = \frac{K_t}{J_t R_m s + B_t R_m + K_t K_e} \cdot \frac{N^3}{s} \cdot \frac{-\frac{3l_a}{2l_s}s^2 + \frac{3b_{as}}{M_s l_s^2}s}{s^2 + \frac{3b_{as}}{M_s l_s^2}s - \frac{3g}{2l_s}} \quad (5.39)$$

The values for all variables for the inverted pendulum along with their origin is shown in Table 5.3. The friction between the arm and the stick is assumed to be zero as the joint consists of a ball bearing.

Table 5.3: Parameters for the inverted pendulum and their origin.

Variable	Value	Parameter	Unit	Origin
K_t	$29.3 \cdot 10^{-3}$	Mechanical motor constant	N m A^{-1}	Section B.1.4
K_e	$35.5 \cdot 10^{-3}$	Electrical motor constant	$\text{V}/(\text{rad/s})$	Section B.1.3
J_m	$29.0 \cdot 10^{-6}$	Moment of inertia of motor	kg m^2	[8]
J_{gear}	$0.153 \cdot 10^{-3}$	Moment of inertia of gear	kg m^2	Section B.2.2
R_m	0.8	Resistance	Ω	Section B.1.1
B_m	$0.159 \cdot 10^{-3}$	Friction in motor	$\text{N}/(\text{rad/s})$	Section B.2.1
B_{gear}	$1.11 \cdot 10^{-3}$	Friction in the gears	$\text{N}/(\text{rad/s})$	[4]
N	0.3	Gear ratio	1	Table 5.1
l_a	0.33	Length of arm	m	Table 5.2
l_s	0.8	Length of stick	m	Table 5.2
M_a	0.288	Mass of arm	kg	Table 5.2
M_s	0.344	Mass of stick	kg	Table 5.2
b_{as}	0	Friction in arm and stick	$\text{N}/(\text{rad/s})$	Assumption
g	9.8	Standard gravity	m s^{-2}	[9]

With the mathematical model of the inverted pendulum found a controller for the system can be designed.

Chapter 6

Rocket Analysis

A rocket presents a large number of similarities with an inverted pendulum in terms of modeling and control as it will be demonstrated in this chapter. It also adds one degree of freedom compared to the inverted pendulum, since it can be controlled in two horizontal directions. A model of the rocket is made to be able to compare the two systems' dynamics.

Appendix reference not working, find a way to include path i guess.

Two different parameters can be controlled in the rocket: the angle of its body compared to vertical and its position. The purpose is to minimize the angle and to keep the initial position, but not the initial altitude.

6.1 Modeling of the angle

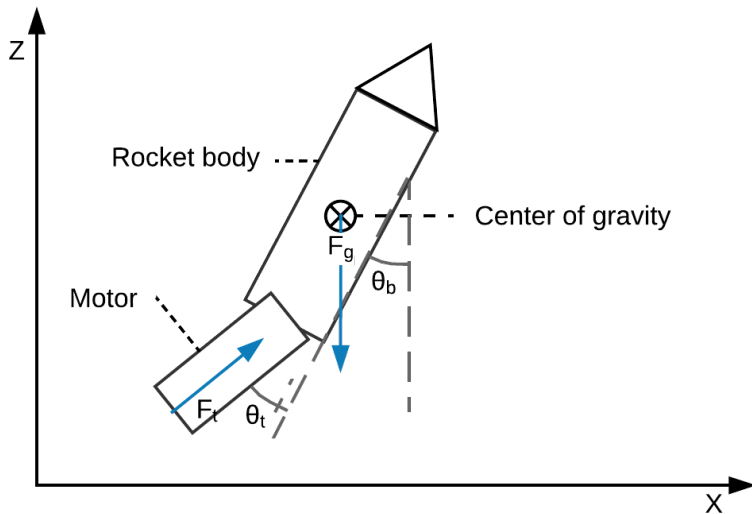


Figure 6.1: Simplified sum of forces on the rocket.

This section will focus on the forces acting perpendicularly to the rocket body, thus creating torques. The resulting transfer function will take θ_t , the thruster angle compared to the body, as an input and θ_b , the body angle compared to vertical as an output.

The thruster force F_t will be considered as constant. See the rocket motor test experiment for details: [??](#). F_g is the gravity force on the rocket's center of gravity. The force of drag is neglected due to the low-speed conditions of the tests, and the absence of air in most real-life scenarios.

Using Newton's second law the following equation can be derived.

$$I_r \cdot \ddot{\theta}_b = \tau_t \quad [N \cdot m] \quad (6.1)$$

Where:

I_r is the inertia of the rocket	$[kg \cdot m^2]$
$\ddot{\theta}_b$ is the angular acceleration of the rocket body	$[s^{-2}]$
τ_t is the torque created by the thruster on the rocket	$[kg \cdot m^2 \cdot sec^{-2}]$

By going to the Laplace domain and grouping elements the following transfer function  is obtained:

Calculating I_r assuming that all the mass is concentrated at the electronics/battery stage of the rocket. 70% of the weight is in fact concentrated on this part (rocket is about 300 grams and the electronics stage is around ~~0~~210 grams). The rocket is rotating around its center of gravity.

$$I_r = m_{Es} \cdot l_{Es}^2 \quad (6.2)$$

Where:

m_{Es} is the mass of the electronics stage	$[kg]$
l_{Es} is the distance from the electronics stage to the center of gravity	$[m]$

The torque τ_t can be expressed as:

$$\tau_t = F_t \cdot \sin(\theta_t) \cdot l_{Cg} \quad [N \cdot m] \quad (6.3)$$

Where:

F_t is the thruster force	$[N]$
θ_t is the angle of the thruster compared to the body's longitudinal axis	$[1]$
l_{Cg} is the distance from the thruster end to the center of gravity	$[m]$
τ_t is the torque created by the thruster on the rocket	$[N \cdot m]$

The small angle approximation is used on τ_t :

$$\tau_t = F_t \cdot \theta_t \cdot l_{Cg} \quad [\text{N}\cdot\text{m}] \quad (6.4)$$

The transfer function becomes:

$$H = \frac{\theta_b}{\theta_t} = \frac{F_t \cdot l_{Cg} \cdot \frac{1}{m_{Es} \cdot l_{Es}^2}}{s^2} \quad (6.5)$$

The servomotors also present a transfer function to be taken into consideration. The transfer function is obtained in ???. It is a first order system. The time constant of the servomotors is determined in Appendix G.

$$\frac{\theta_{out}}{\theta_{in}} = \frac{1}{\tau s + 1} \quad (6.6)$$

Where:

- | | |
|--|-----|
| θ_{in} is the angle sent to the servo by the controller | [1] |
| θ_{out} is the angle outputed by the servo | [1] |

6.2 Comparison of the Inverted Pendulum and Rocket Models

From Chapter 5 and Chapter 6 it is found, that the models are slightly different. First of all, opposite angles were chosen in the beginning of the modeling process. Moreover, the the pendulum is fixed to the gears and motor, while the rocket is floating in the air, and thus canceling the gravity. Regarding to root locus, the inverted pendulum has two more zeros in 0 and two real poles equidistant from zero, whereas the rocket has two poles in 0. The difference in poles is due to the absence of gravity into the rocket modeling, while the difference in zeros might be due to the fact that the arm is rigidly attached compared to the thruster.

Due to this difference a different controller needs to be designed for each model.

Chapter 7

Requirements and Specifications

The following chapter describes requirements and specifications determined for controlling both the rocket and the inverted pendulum. The requirements are set to obtain a system which fulfils the problem statement .

As described previously the goal of both systems is to react to deviations from its stable position. The goal of the rocket is the launch and a stable flight, versus the inverted pendulum where the goal is to balance the stick in vertical upwards position.

Ref to section - Mathias and might be changed in formulation

Both systems will be described with physical and control requirements in separate sections. The physical requirements will be set based on the limits of the models. The controller requirements will be based on speed, precision and stability, which means that control parameters would be set for:

- Settling Time
- Overshoot
- Rise Time
- Steady State Error

Each parameter would affect each other, and therefore a discussion of the best combination will be considered.

7.0.1 Requirements for the Inverted Pendulum

The requirements are based on figure 5.1, and the modeling behind where the angle relations and positions is described between the gears, arm and stick. It is yet decided that the main requirement set is to balance the stick. But requirements have to be set considering when the stick is balanced and when not.

- The figure can be added, to simplify the explanation.
- 1. The control position of the arm must not exceed $\pm \frac{\pi}{4}$ radians from the 0 radians vertical position.**

A choice made to limit the arms movements around vertical upwards position which will act as the initial position. The arm should not exceeded the limit because the control of the stick will become more vertical than horizontal. It is therefore considered that the arm is not able to control the stick in a stable manor.

- 2. The angle of the stick must not exceed $\pm \frac{\pi}{18}$ radians from vertical position.**

An assumption made to simplify and limit the sticks movement, which would relate it to the control of a rocket. Assuming that the arm can not move to more than $\frac{\pi}{4}$, gives that the overshoot of the arm can be at maximum:

$$\frac{\pi}{4} - \frac{\pi}{18} = \frac{7\pi}{36} \quad (7.1)$$

$$\frac{\frac{7\pi}{36}}{\frac{\pi}{18}} = 350 \% \quad (7.2)$$

This only apply when considering the worst case position of the stick when the arm is still in vertical position. It means that arm should be able to catch the stick without overshooting more than 350%. The overshoot is limit, because 350% is considered unstable when the goal is to balance the stick. The maximum overshoot is limited to a tenth of the sticks angular position $\frac{\pi}{180}$. And may therefore not exceed:

$$\frac{\frac{\pi}{180}}{\frac{\pi}{18}} = 10 \% \quad (7.3)$$

3. Deviation from the upright position of the stick must not exceed $\pm \frac{\pi}{36}$ radians when considered balanced.

A choice made to ensure stability and avoid oscillation around the equilibrium position. This means that if the angle is exceeded the controller needs to react. The requirement is mainly set to ensure that the stick balancing precision is within the sampling precision of the sensors. The controller will be designed based on a steady state error of zero, which means that errors from balanced position are from disturbance and not from the controller's steady state error.

4. The system should be able to regain balance if an impulse of $\frac{\pi}{18}$ radians is applied, in form of a push on the stick.

If an impulse from the external disturbance is acting on the stick then the control should be able to counteract the stick back into equilibrium position.

7.0.2 Requirements for the Rocket

Some limits has to be set based on the capability of building and using a rocket. The controller requirements will be the same as with the inverted pendulum. The physical dimensions of the rocket can not exceed:

Parameter	Value	Unit
Length	0.25	[m]
Width	0.25	[m]
Height	0.5	[m]
Total volume	0.03	[m ³]
Weight	0.3	[kg]

Table 7.1: Maximum size and weight of the rocket.

5. Deviation from the rockets initial trajectory must not exceed $\pm \frac{\pi}{18}$ radians.

A choice made to limit the movement of the rocket during flight. If the limit is exceeded the rocket controller will not guarantee stability, but might stabilize the rocket none the less.

Might be changed based on resolution and precision of gyroscope

- 6. The system should be able to regain its stability and direction if an external disturbance impulse of $\frac{\pi}{36}$ radians is applied on the rocket.**

A choice made to ensure flight stability even if the rocket is influenced by a external disturbance.

7.1 Acceptance Test Specification

The following section describes how the requirements can be tested. This verification is made to ensure that the system fulfils the set requirements.

Acceptance Test 1.

Verification of requirement 1 will not be proceeded, but simply implemented in the software based on feedback from the arm potentiometer. The software will, if the angle exceeds $\pm \frac{\pi}{4}$ radians, set the arm to initial vertical position and no longer react on feedback from the stick, until the stick has been balanced around $\pm \frac{\pi}{18}$ radians in at least 5 seconds. The controller will then again react to changes on the stick.

Acceptance Test 2.

Requirement 2 and 3 is tested based on placing the stick and arm in vertical balanced position. The controller is engaged and the system is ran for ten minutes. The feedback data of the sensors will be collected to determine if the sticks angle have exceeded the requirement. As well is the sampled data from the motor used to compare with the position changes of the stick and see if the controller consider the stick balanced when the angle of the stick is within $\pm \frac{\pi}{36}$ of 0 radians.

Acceptance Test 3.

Requirement 4 is tested from holding the stick in $\pm \frac{\pi}{18}$ radians when the arm is at 0 radians vertical position. The control system is activated and the stick is released. The test is repeated 5 times and the sensor data is sampled and saved each time.

Maxime: Should we try again for the last test?

Mathias - Add rocket test if it will be testable

Part II

Design

Chapter 8

Design of the Inverted Pendulum Controller

The goal of the controller is to balance the stick in an upright position. The system is seen as a block diagram on Figure 8.1. Inserting all the constants from Table 5.3 gives the transfer function seen in Equation (8.1).

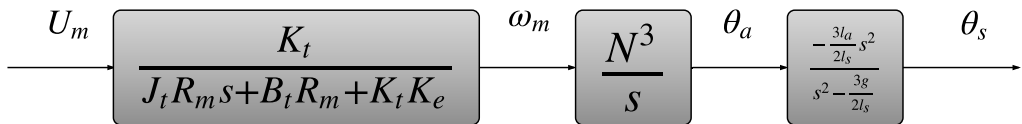


Figure 8.1: Block diagram of the inverted pendulum system.

$$\frac{\Theta_s}{U_m} = \frac{-3.36s^2}{s^4 + 14.11s^3 - 18.37s^2 - 259.41s} \quad (8.1)$$

The system is inherently unstable as it is evident by the pole in the right half plane of the pole-zero plot in Figure 8.2.

In order to achieve a stable system the right half plane pole needs to be moved to the left half plane.

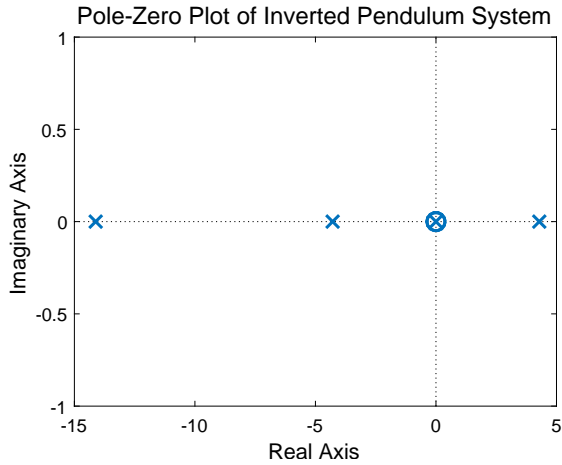


Figure 8.2: Pole-zero plot for the inverted pendulums transfer function.

There's a plethora of different options for the controller to use; the simplest being a proportional controller. A simple way to check whether the proportional controller is feasible is by examining the root locus of the transfer function in Figure 8.3a. The pole in the right half plane moving towards infinity is caused by the transfer function being negative and can be fixed with a negative gain as shown on figure Figure 8.3b.

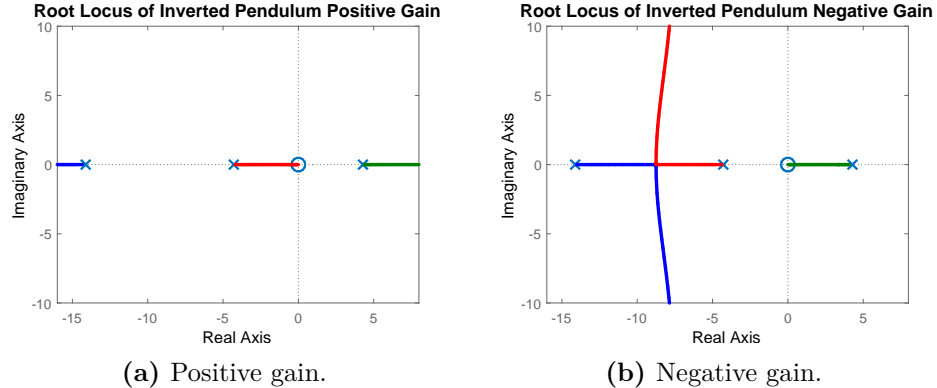


Figure 8.3: Root locus of the inverted pendulums transfer function.

The proportional controller isn't feasible as the pole in the right half plane never enters the stable region even with a negative gain. This is because the pole will always end at a zero if available. The zero in 0 blocks the unstable pole from moving into the stable region.

The controller can be simplified by using cascade control. This means two controllers should be designed; one that controls the angle of the arm and one that controls the angle of the stick. The cascade control system can be seen on Figure 8.4.

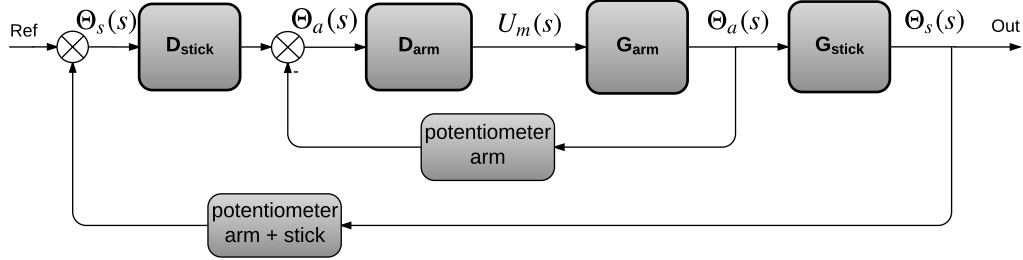


Figure 8.4: Block diagram of the inverted pendulum system with cascade control.

If the inner loop is fast enough compared to the outer loop, it is negligible to the outer loop controller. This means the root locus of the can be split into two separate systems with a respective controller that needs to be designed. The two new loops will be referred to as the inner loop and outer loop and their transfer function is seen in Equation (8.2).

$$\frac{\Theta_a}{U_m} = \frac{5.43}{s^2 + 14.11s} \quad (8.2a)$$

$$\frac{\Theta_s}{\Theta_a} = \frac{-0.62s^2}{s^2 - 18.38} \quad (8.2b)$$

The root locus of the two subsystems is seen on Figure 8.5.

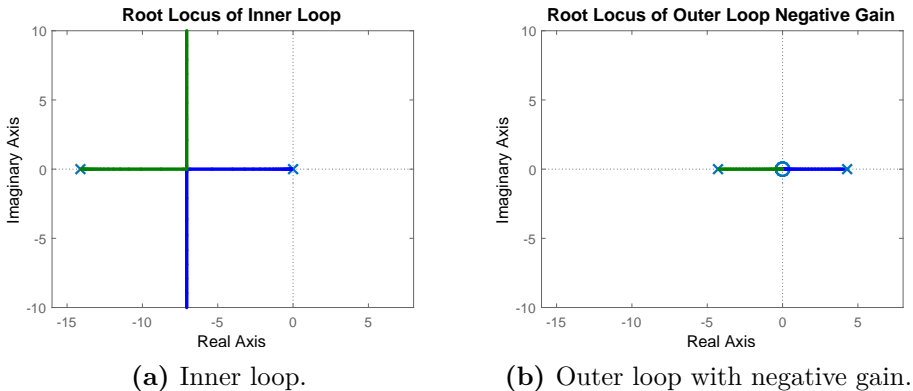


Figure 8.5: Root locus of the inverted pendulum with cascade control.

With this split it's simpler to design a controller that can move the unstable pole to the stable region. The inner loop controller will be designed first as it's essential

to this split that the inner loop is faster than the outer loop. The inner loop controller will be designed to be as fast as possible before the outer loop controller is designed.

8.1 Design of Inner Loop Controller

For the design of the inner loop controller, it is important that it settles faster than the outer loop controller without any overshoot. This means the natural frequency of the system with the controller needs to be larger and the poles close to the real axis. With the help of Figure 8.6 a gain of 9.17 is chosen as it is the maximum gain obtainable without having any overshoot.

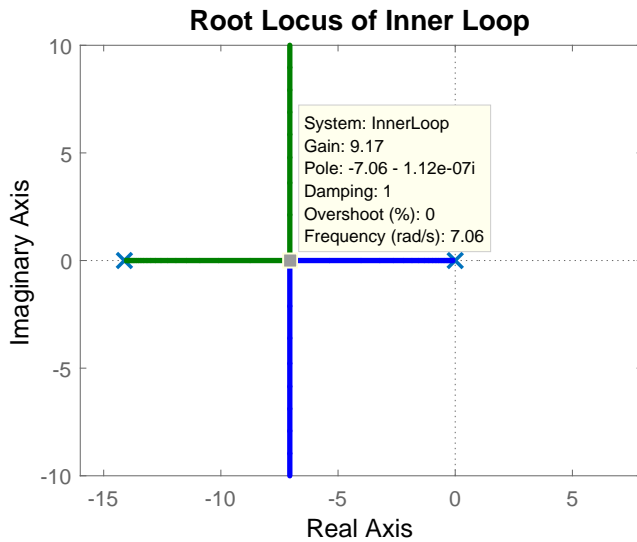


Figure 8.6: Root locus of the inner loop showing the gain required for the poles to meet.

However this system the two poles are still very close to the outer loop system.

In order to speed up the inner loop two options are available. The first one is to use a more elaborate controller than the P controller such as a PD controller or a lead. The second one is to once again divide the inner loop into two loops. The second method is the motor has already a tachometer integrated, and it is simpler to implement this method. Furthermore when testing for the motor parameters, the driver did not deliver a constant speed for a constant voltage. A feedback loop of the velocity would be able to reduce the inconsistencies generated by the driver.

The two new loops will thus control the motor velocity and angle of the arm and will be called motor loop and arm loop respectively.

The first loop which will be designed will be the motor loop as it is the most inner loop. The new control loop is added to Figure 8.4 to form the final block diagram presented in Figure 8.7.

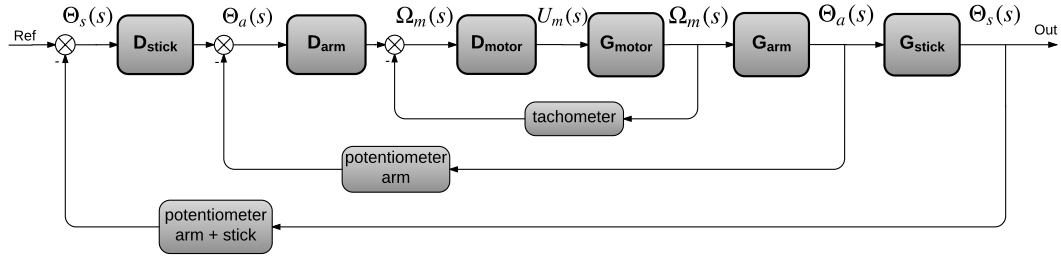


Figure 8.7: New block diagram of the inverted pendulum system with cascade control.

8.1.1 Design of the Motor Loop Controller

The very first loop control is the one adjusting the motor velocity, ω_m , according to the voltage. The transfer function from U_m to ω_m is taken from Section 5.4. The values for the variables in Equation (5.37) is inserted giving Equation (8.3).

$$\frac{\Omega_m(s)}{U_m(s)} = \frac{201.24}{s + 14.11} \quad (8.3)$$

As it is the most inner loop of the system, the step response has to be faster than the outer loops controlling the arm and the stick. The transfer function has a negative pole making the system stable. It also has a pretty large gain already so simply closing the loop is enough to get a faster response. The step response of the closed motor loop is seen on Figure 8.8.

There is a small steady state error that will be corrected slightly by increasing the gain. The gain is increased until the steady state error is less than 5%. The gain required is 1.35. The step response of the closed motor loop with a gain of 1.35 can be seen on Figure 8.9. This has a settling time of 0.0137 seconds.

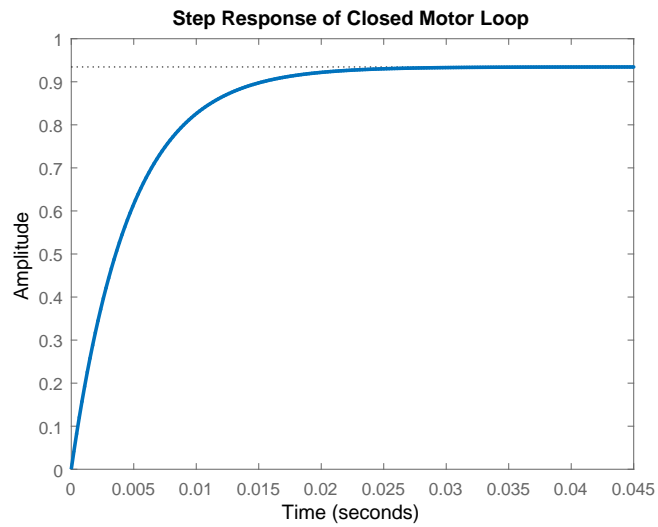


Figure 8.8: Step response of the closed motor loop with a gain of 1.

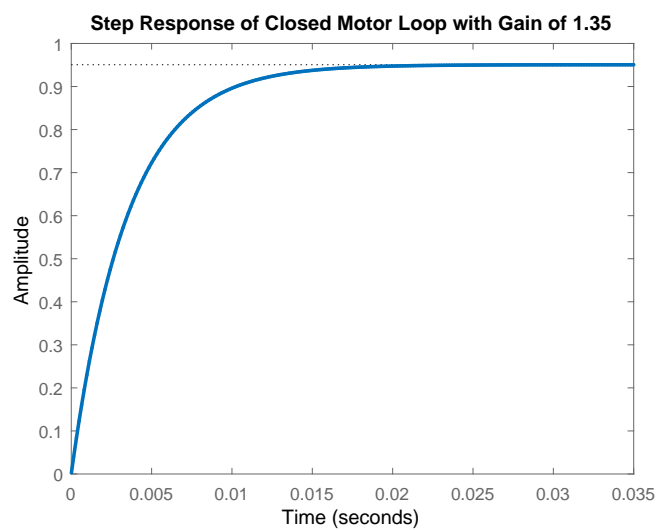


Figure 8.9: Step response of the closed motor loop with a gain of 1.35.

The controller for the motor loop thus becomes Equation (8.4).

$$D_{\text{motor}} = 1.35 \quad (8.4)$$

8.1.2 Design of the Arm Loop Controller

The motor loop part has a settling time of 0.0137 s, so the settling time of the arm's loop has to be at least 0.137 s in order to make the assumption that the motor's loop transfer function is equal to 1 for the arm's loop. The transfer function for the arm loop is found by inserting the values in Equation (5.17) giving Equation (8.5).

$$\frac{\Theta_a}{\Omega_m} = \frac{0.027}{s} \quad (8.5)$$

The root locus of Equation (8.5), in Figure 8.10, shows that there is theoretically no gain limitation for the arm as the pole moves to the left side plan making the system stable, as long as the gain is high enough. The pole is also always on the real axis which means there will be no overshoot no matter the gain.

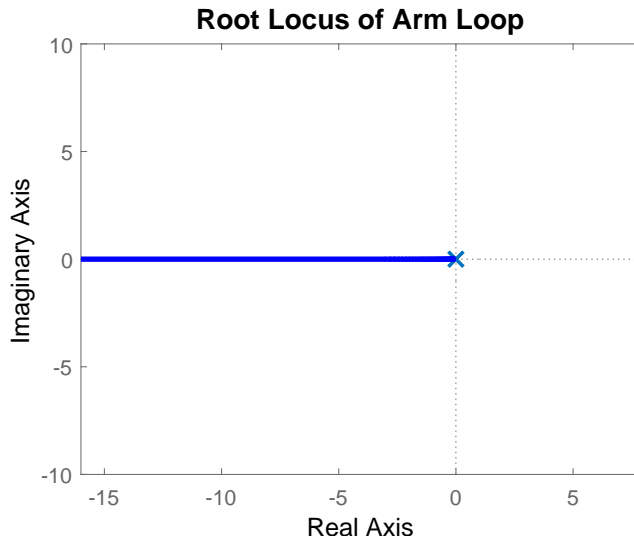


Figure 8.10: Velocity as input and Arm's angle as the output

The gain for the closed loop will be chosen to give a settling time slower than 0.137. A gain of 900 is satisfactory as it gives a settling time of 0.16 seconds as seen on the step response on Figure 8.11.

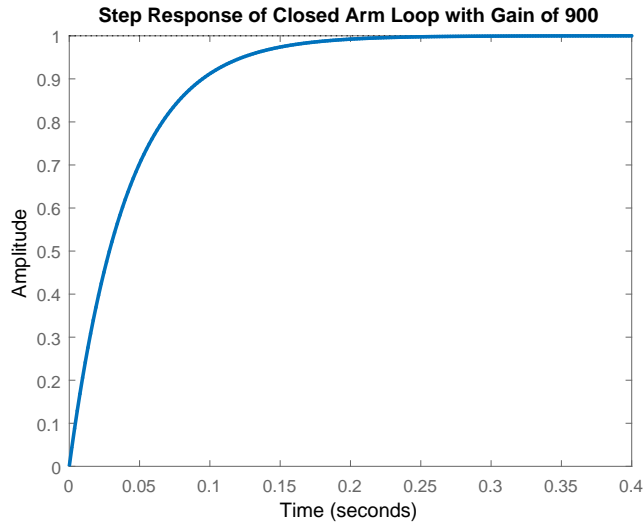


Figure 8.11: Step response of the closed arm loop with a gain of 900.

The arm loop controller then becomes Equation (8.6).

$$D_{\text{arm}} = 900 \quad (8.6)$$

8.2 Design of Outer Loop Controller

As the poles in feedback will eventually end up at the zeros with a large enough gain, there are two options to bring the unstable pole into the stable region: Remove all zeros in 0 so the pole can cross the into the stable region along the real axis or add another unstable open loop pole to force the poles off the real axis and then try to circumvent the zeros in 0.

Removing the zeros in 0 can't be done by adding poles as $\infty \cdot 0$ isn't defined. Instead it's better to try and redefine the model output to something with a DC gain but at the same time requires the stick to be balanced to achieve the new output. This could be by attempting to control the position of a point on the stick. The stick would need to be balanced in order to have the point always be in the correct position.

8.2.1 Redefining the Inverted Pendulums Output

The inverted pendulum model will be redefined so the output is the distance from a point on the stick to the vertical axis instead of the angle of the stick. The point, α , and the distance to the vertical axis, x_α , are seen on Figure 8.12.

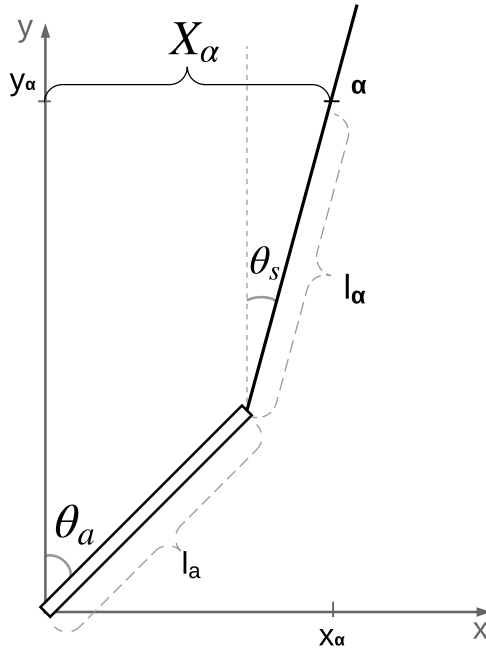


Figure 8.12: Diagram of the distance that will be controlled instead of the angle of the stick.

The distance to the point can be described by Equation (8.7).

$$x_\alpha(t) = l_a \sin(\theta_a(t)) + l_\alpha \sin(\theta_s(t)) \quad (8.7)$$

This is not a linear equation and needs to be linearized in order to Laplace transform it. This is done with a 1st order Taylor approximation around the equilibrium where $\theta_a = \theta_s = 0$ in Equation (8.8)

$$x_\alpha(t) \approx l_a \sin(0) + l_a \cos(0)\theta_a(t) + l_\alpha \sin(0) + l_\alpha \cos(0)\theta_s(t) \quad (8.8a)$$

$$x_\alpha(t) \approx l_a \theta_a(t) + l_\alpha \theta_s(t) \quad (8.8b)$$

This will then be Laplace transformed in Equation (8.9).

$$X_\alpha(s) = l_a \Theta_a(s) + l_\alpha \Theta_s(s) \quad (8.9)$$

By isolating $\Theta_s(s)$ in Equation (5.10c) and inserting it into Equation (8.9), the transfer function in (8.10c) is found. The friction part is removed per Table 5.3.

$$X_\alpha(s) = l_a \Theta_a(s) + l_\alpha \frac{-\frac{3l_a}{2l_s} s^2}{s^2 - \frac{3g}{2l_s}} \Theta_a(s) \quad (8.10a)$$

$$X_\alpha(s) = \frac{l_a \left(s^2 - \frac{3g}{2l_s} \right) + l_\alpha \left(-\frac{3l_a}{2l_s} s^2 \right)}{s^2 - \frac{3g}{2l_s}} \Theta_a(s) \quad (8.10b)$$

$$\frac{X_\alpha(s)}{\Theta_a(s)} = \frac{s^2 \left(l_a - l_\alpha \frac{3l_a}{2l_s} \right) - l_a \frac{3g}{2l_s}}{s^2 - \frac{3g}{2l_s}} \quad (8.10c)$$

The transfer function still ends up with 2 zeros but it's possible to remove them by selecting the point α so $l_\alpha = \frac{2l_s}{3}$. Inserting this into Equation (8.10c) the transfer function becomes Equation (8.11).

$$\frac{X_\alpha(s)}{\Theta_a(s)} = \frac{-l_a \frac{3g}{2l_s}}{s^2 - \frac{3g}{2l_s}} \quad (8.11)$$

The zeros in 0 has been removed but the distance, x_α , now needs to be measured for the feedback. This can be done by measuring the angles, which was also necessary before, but now use Equation (8.7) to calculate the distance instead of using the angle directly. The controller for the transfer function in Equation (8.11) can now be designed.

8.2.2 Controlling the Distance from the Stick to Vertical

The new block diagram for the controllers can be seen on Figure 8.13.

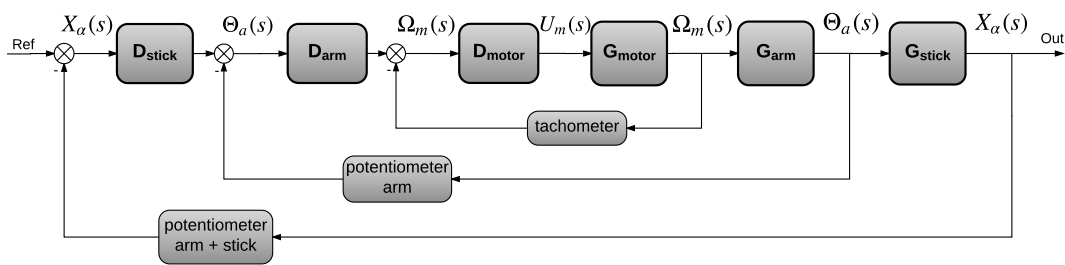


Figure 8.13: Block diagram of the inverted pendulum system with inner and outer loop controllers.

With the redefined transfer function the outer loop will control the transfer function in Equation (8.11). From the root locus in Figure 8.14 it can be seen that a zero

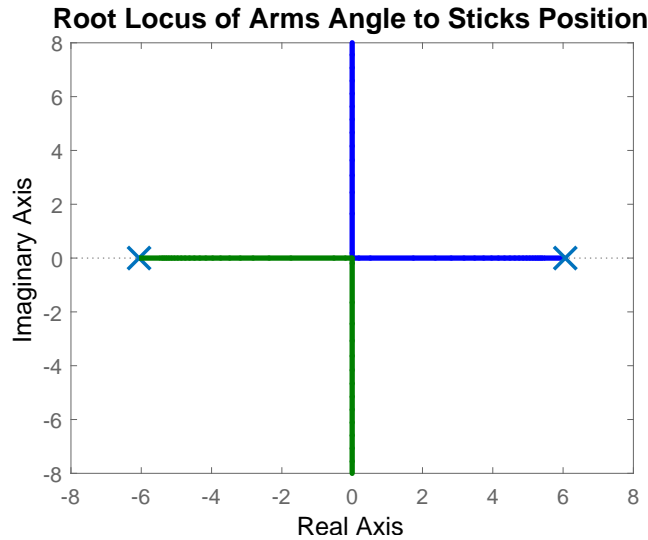


Figure 8.14: Root locus of the transfer function from the angle of the arm to the position of a point on the stick.

needs to be added on the real axis in the left half plane in order to move the pole in the right half plane to the stable region.

If the zero is positioned between the two poles both the right most will move towards the zero while the leftmost moves towards infinity; both along the real axis. Positioning the zero close to the origin doesn't allow for the pole to move far into the left half plane. If it's put far to the left of the stable pole the poles will move off the real axis and to the left of the zero with higher gain. This can move them very far into the left half plane before they come back to the real axis which could cause issues for making the inner loop faster than the outer loop. This is because the further away the poles are from origin the higher the natural frequency and a high natural frequency means small settling time. If the poles are off the real axis it'll introduce overshoot which needs to be under 10% per the specifications.

Placing the zero close to the leftmost pole would allow for the unstable pole to move further into the left half plane without an overly fast response or any overshoot.

The zero could theoretically be placed on the pole to cancel it and allow the pole to move further into the left half plane along the real axis. This would be ideal but the true location of the pole of the real system is difficult to find as small variations in measurements of the system could move the pole slightly.

The zero will initially be placed on the pole as it doesn't change the system drastically whether it's slightly off to either side. The pole is then placed at $-\sqrt{\frac{3g}{2l_s}}$. This can be seen in Figure 8.15.

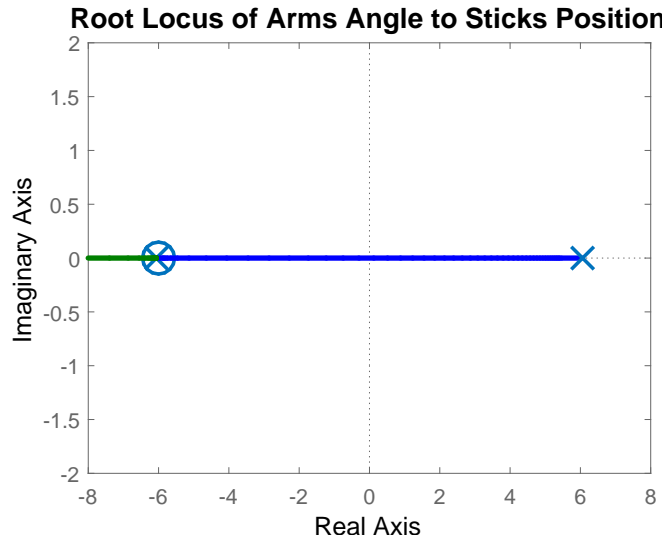


Figure 8.15: Root locus of the outer loop system with a zero cancelling the left pole.

The unstable pole can now enter the stable region by selecting a gain large enough. Simply adding a zero to the system will however amplify high frequencies. This can be avoided by adding a pole further into the left half plane. This effectively makes the controller a lead controller. The position of the pole and the gain will determine the settling time and overshoot of the system. The settling time for the outer loop controller should be more than 10 times slower so the assumption, that the inner loop controller is much faster than the outer loop controller, holds true. As the gain increases the two poles move closer to each other before meeting and moving into the imaginary plane. The gain will be selected to be however much is needed for the poles to meet. The pole can then be selected such that the place where the poles meet will give a settling time 10 times slower than the inner loop.

As the settling time of the inner loop is 0.16 seconds, the natural frequency of the outer loop can be approximated by Equation (8.12).

$$T_{s_{\text{outer}}}(2\%) = -\frac{\ln(0.02)}{\zeta \cdot \omega_n} \quad (8.12a)$$

$$\omega_n = -\frac{\ln(0.02)}{\zeta \cdot T_{s_{\text{inner}}} \cdot 10} \quad (8.12b)$$

$$\omega_n = -\frac{\ln(0.02)}{1 \cdot 0.16 \cdot 10} \quad (8.12c)$$

$$\omega_n = 2.45 \quad (8.12d)$$

This approximation only holds true for 2nd order systems without zeros which this would only be if the zero placed exactly on the pole removes both. This is not the

case however it is still a good place to start. To achieve a natural frequency of 2.45, the lead controller pole needs to be placed so the halfway point between it and the unstable pole is -2.45. The pole location is then found by Equation (8.13).

$$-2.45 = \frac{p_{\text{unstable}} + p_{\text{lead}}}{2} \quad (8.13\text{a})$$

$$p_{\text{lead}} = -2.45 \cdot 2 - \sqrt{\frac{3g}{2l_s}} \quad (8.13\text{b})$$

$$p_{\text{lead}} = -9.19 \quad (8.13\text{c})$$

This can be seen on Figure 8.16.

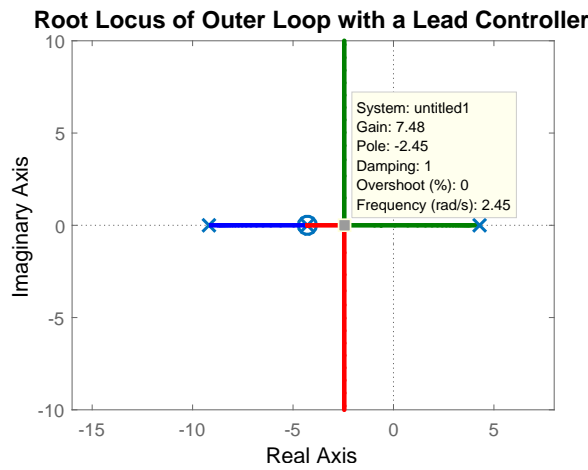


Figure 8.16: Root locus of the outer loop with the lead controller.

To make the two poles meet a gain of 7.48 is needed. This gives a lead controller of Equation (8.14).

$$D_x = 7.48 \frac{s + \sqrt{\frac{3g}{2l_s}}}{s + 9.19} \quad (8.14)$$

The settling time is found by looking at the step response on Figure 8.17.

The settling time is slower than the 1.6 seconds that was expected and this is because the zero placed on the pole still has an influence on the system. A bit of overshoot can also be added in this system to get a faster rise time but a similar settling time. This is okay as the specifications are only for overshoot of the angle of the stick. It's uncertain how an overshoot when controlling the distance to a point on the stick will affect the angle of the stick. A maximum overshoot for the distance is therefore arbitrarily chosen to be the same as the overshoot for the angle. To get a settling

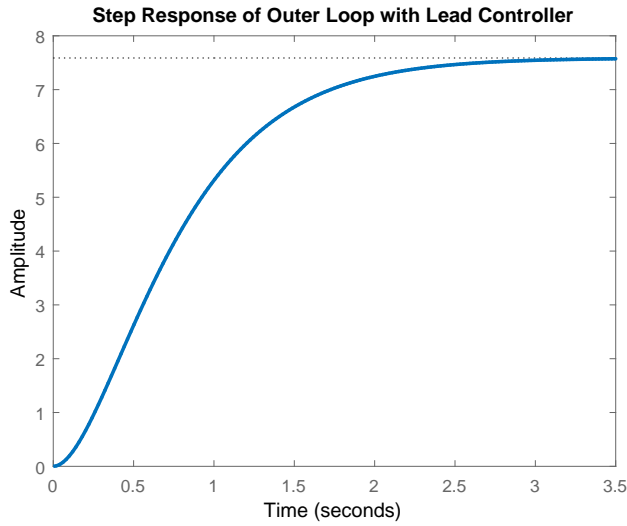


Figure 8.17: Step response showing the settling time of the outer loop with a lead controller.

time of 1.6 seconds a new gain needs to be found to give a faster settling time but no more than 10% overshoot. If it's not possible without more than 10% overshoot the controller pole has to be moved further to the left

The lead controller then becomes Equation (8.15b).

$$D_x = 8.8 \frac{s + \sqrt{\frac{3g}{2l_s}}}{s + 2\frac{\ln(0.02)}{1.6} + \sqrt{\frac{3g}{2l_s}}} \quad (8.15a)$$

$$D_x = 8.8 \frac{s + 4.29}{s + 9.19} \quad (8.15b)$$

This controller gives a fast rise time, a settling time of 1.61 seconds and overshoot of less than 10%. This can be seen on the step response on Figure 8.18.

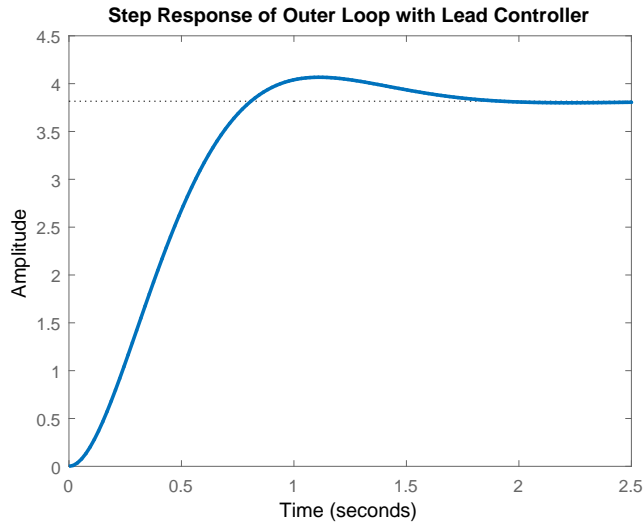


Figure 8.18: Step response of the outer loop with the lead controller that gives less than 10% of overshoot.

8.3 Verifying the total controller

The final controller consists of the motor loop controller, the arm loop controller and the outer loop controller and are seen in Equation (8.16).

$$D_{\text{motor}} = 1.35 \quad (8.16a)$$

$$D_{\text{arm}} = 900 \quad (8.16b)$$

$$D_x = 8.8 \frac{s + 4.29}{s + 9.19} \quad (8.16c)$$

These are implemented as shown on Figure 8.7 and the entire system has the pole-zero plot on Figure 8.19 which shows it should be stable as all poles are in the left half plane.

The step response for the inverted pendulum with the final controller is seen on Figure 8.20.

The controller has a settling time of 3.15 seconds and shows it can balance a point on the stick sufficiently. The controller is deemed satisfactory and will be implemented.

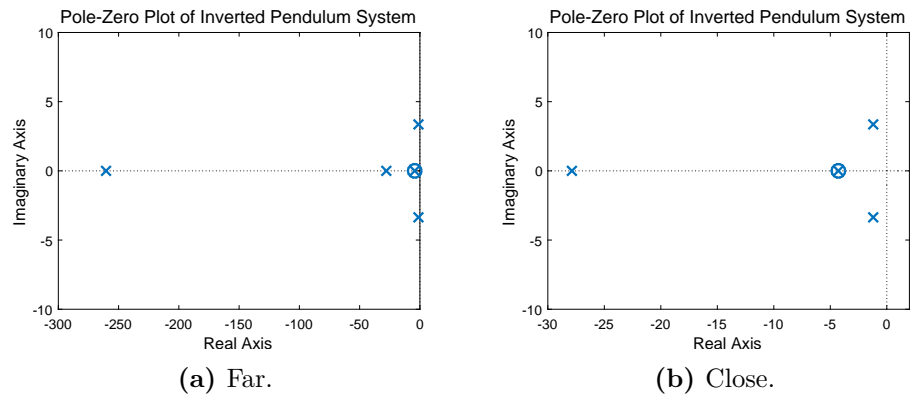


Figure 8.19: Pole-zero plot of the final inverted pendulum system.

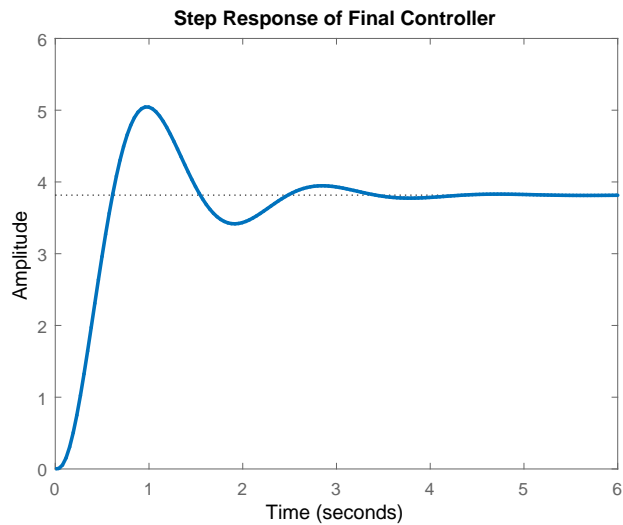


Figure 8.20: Step response of the inverted pendulum with the final controller.

Chapter 9

Design of the Rocket and Gimbal Controller

The following chapter describes the design of the rocket and its control system. The main objective is not to design the rocket, but to implement a control system that can stabilize it during launch and flight.

9.1 Rocket Design

For the purpose of studying the problem of the rocket control, a model rocket was designed and built. Since mechanical design is out of this work's scope, the engineering of this rocket will not be explained, but the design CAD files will be available on the GitHub repository. This design consists of 2 sections, that will be called "stages".

Add the github link later.

First stage: propulsion

- A thruster / Solid Rocket Booster (SRB)
- A thrust vectoring mechanism, also known as gimbal, with two degrees of freedom
- Two servo motors for actuating the gimbal

Interstage:

- An empty fairing separating the propulsion stage from the electronics

Upper stage: control

- A frame to contain the electronics.
- A PCB with a micro-controller.
- A plastic separator with anti-vibration bearings.

Parameter	Value	Unit
Total impulse	17,4	[N]
Average thrust	≈ 3	[N]
Maximum thrust	≈ 9	[N]
Burn duration	$\approx 5,5$	[s]
Weight	0,105	[kg]
Length	0,07	[m]

Table 9.1: DP-3 thruster specifications

- On this separator is placed a gyroscope: the **attitude** sensor.
- A nose fairing.

Choice of thrusters for the rocket

A thruster is a central component in all types of rocket. In the project the thruster will be chosen based on availability and lift force. The maximum weight of the rocket can not exceed 300 grams and the thruster should be able to lift this. The average thrust of the thruster should have at least a average thrust of 3 Newton. The choice is limited to the thrusters which can be acquired within the European regulations. Through superficial research it is found that Klima 18 mm rocket motors is legal in all of Europe, and will be chosen for the thruster. The chosen thruster is the version D3-P with the specifications cf. table 9.1.

Physical Parameters of the Rocket

The important factors for controlling the rocket is the physical parameters. These will effect how the rocket would transfer a input to its output. We will not control the force of the thruster, and this can will therefore not be a part of the important

Piece	Parameter	Value	Unit
Rocket _{overall}	Height	297	[mm]
Rocket _{overall}	Weight	0,28	[kg]
Interstage	Diameter	67	[mm]
Thrust vectoring system	Max. angle	?	[rad]
Thrust vectoring system	Response time	?	[rad/s]

Table 9.2: Parameters of the rocket.

Input the rest of the parameters.

Where:

$Rocket_{overall}$ is the total weight of the system, including thruster, [1]
electronics, and rocket structure.

9.1.1 Choice of Sensors for the Rocket

The following sections describes the sensors chosen for implementation in the rocket. It is chosen that the microcontroller unit, from here on named MCU, used in the system will be a Arduino Nano. The Nano is chosen based on its low weight (7 grams) and small size (18 x 45 mm) which will be an advantage when fitting it in the rocket. Further about the is described cf. section ??.

As described in section 3 the rocket can be a system with instability problems. In the inverted pendulum these instabilities is detected trough sampling sensors and corrected trough a DC motor control system. The same parameters is considered when controlling the rocket. A form of sensor is needed to detect the orientation and position of the rocket, and a control system is needed to counteract changes from the initial trajectory.

Choosing sensors for the rocket will be weighted based on following parameters:

- Compatibility.
- Power consumption.
- Availability.
- Physical dimensions and weight.

Needed is a sensor for measuring:

- Orientation.
- Acceleration.
- Temperature and barometric pressure.

Determining the altitude, orientation and acceleration of the rocket can be done with different types of sensor. Two types of sensors can be considered when involving rockets; reference sensors and inertial sensors. Reference sensors have a external reference to measure from where inertial sensors measures changes in it physical state from its inertial state. Commonly used sensors and applications is listed, these determined from different types of rocket applications:

- Gyroscope
- Accelerometer
- Global Positioning System (GPS)
- Magnetometer
- Barometric pressure sensor

- Infrared camera
- Solar panels

Some sensors can easily be declined from the choice. This is mainly because there application is most commonly with rocket going to higher altitudes or even in-orbit around earth, which is not the interest in this project. For example is the infrared camera implemented in some satellites and rocket to determine the position of the earth relative to the satellite. This will not be implemented in the rocket, because the altitude of the rocket is too low. Equally is solar panels implemented mostly in satellites, because the time span for change is lower than when launching and correcting a rocket. Sensors considered in the project is gyroscopes, accelerometers, magnetometer/compass, GPS, barometric sensor.

GPS is a relatively common used component in flying systems. It is implemented in many quad-copters, where the goal is to hold a position based on GPS. In the rocket it can be used to determined velocity, deviations from trajectory, and altitude. Precise and fast GPS units have a high cost and higher power consumption than alternatives. It is therefore decided that GPS will not be included as a component of choice.

An accelerometer measures acceleration in one to three axis(x,y,z). The reference for measuring is the gravitational force. A single axis accelerometer can measure the acceleration in the direction it is orientated. And can for example be used to determine the velocity upwards flying rocket. This can as well be used to determine a travelled distance based on knowing the acceleration and time. In the case of flying a rocket a three-axis accelerometer would be the implemented, when considering that the rocket can move both lateral and vertical in its position.

A gyroscope is on the other hand measuring the angular velocity changes in three dimensions. The difference between the accelerometer and gyroscope is that the gyroscope is capable of measuring the rate of rotation around an axis. It does not rely on a fixed reference and is commonly used in applications like drones and other flying objects. In the rocket it can be used to determine the orientation and rotation of the rocket based on measuring the rate of changes in any direction.

Combining these gives a Inertial Measurement Unit(IMU), which is commonly used in model planes and quad-copters. The application of this is to obtain the objects position through measuring velocity, orientation, rotation with the gyroscope and accelerometer. Both types of components are dependent of temperature and barometric pressure, so often an IMU includes multiple types of additional sensors for calibration purposes. A choice is made to use an IMU, given that its application in similar types of flying systems verifies that it is suitable for a rocket. Some performance factors must be considered when choosing a IMU. For example is the g-force range of the IMU important. If the maximum ratings is lower than the acceleration of the rocket, then the sensor would not be able to give sufficient data at maximum acceleration. As well is the sensitivity of the accelerometer important. The rocket is a

system with a high amplitude g-force when launching, and therefore a accelerometer with low sensitivity is preferable.

Inertial Measurement Unit - GY-87

GY-87[10] is an IMU made available for use. It includes an MPU6050, which combines a 3-axis accelerometer and a 3-axis gyroscope, a BMP180 thermometer/barometer, and a HMC5883 3-axis magnetometer. It is chosen based on its combination of components, low power consumption of $\approx 6,5$ mA in measurement mode. It is designed so it can be implemented with the Arduino Nano through I2C communication. I2C is a two wire protocol which is working trough serial communication. I2C is based on having two wires between the Arduino and the GY-87. The one wire SCL is the serial clock, and the other wire SDA is the data wire. All components on the GY-87 are convenient to implement with the Arduino. Further analysis is described cf. section [ref]

Ref to to implementation part when it is done.

9.2 Rocket Controller Design

The following sections explains the design procedure behind fitting the transfer function and dynamics of the rocket with a feedback controller. The controllers goal is to change the orientation of the thruster trough regulating the thrust vectoring system.

The goal of the controller is to balance the rocket body in an upright position. The system can be decomposed in a block diagram as shown in Figure 9.1.

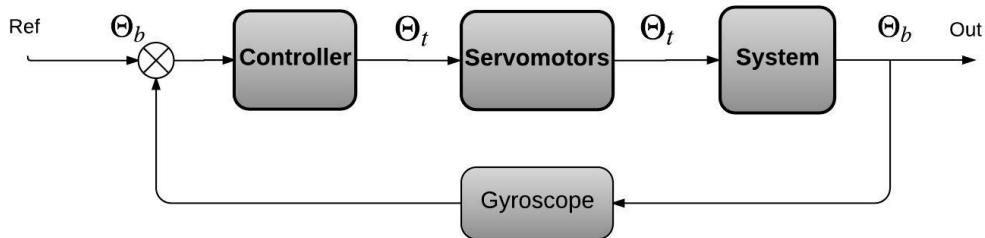


Figure 9.1: Rocket transfer function.

As seen in the modeling of the rocket and on Equation (9.1a), the system presents two poles in the origin of the pole-zero plot.

$$H = \frac{F_t \cdot L_{Cg} \cdot \frac{1}{M_r \cdot L_{Es}^2}}{s^2} \quad (9.1a)$$

$$H = \frac{3 \cdot 0.10 \cdot \frac{1}{0.180 \cdot 0.03^2}}{s^2} \quad (9.1b)$$

Where:

F_t is the thruster force [N]

L_{Cg} is the distance from the thruster end to the center of gravity [m]

M_{Es} is the mass of the electronics stage [kg]

L_{Es} is the distance from the electronics stage to the center of gravity [m]

Looking at the root locus of the system on Figure 9.2 shows the poles goes to infinity on the imaginary axis. This means that any oscillations or noise will never be damped solely by adding a gain.

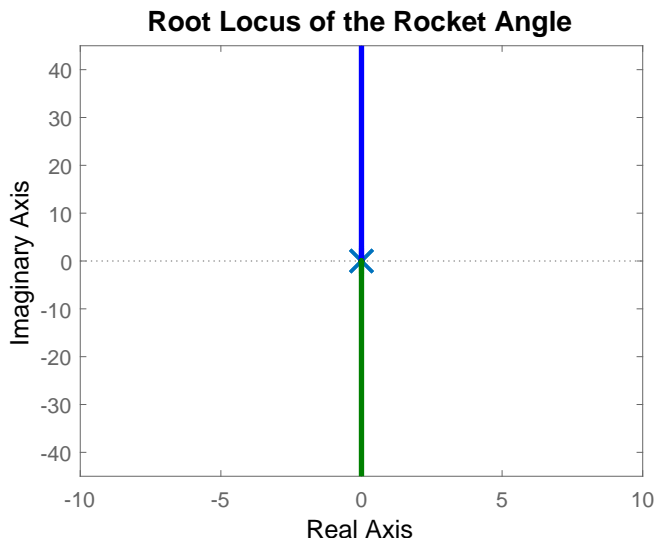


Figure 9.2: Root locus of the rocket angle transfer function.

However the real system is also influenced by the servomotor. The transfer function of the servomotors is shown on Equation (9.2b).

$$H_s = \frac{1}{\tau s + 1} \quad (9.2a)$$

$$H_s = \frac{1}{0.04s + 1} \quad (9.2b)$$

Where:

τ is the time constant of the servomotors

[s]

This function then adds a pole to the initial transfer function, resulting in an unstable system. This is shown on Figure 9.3.

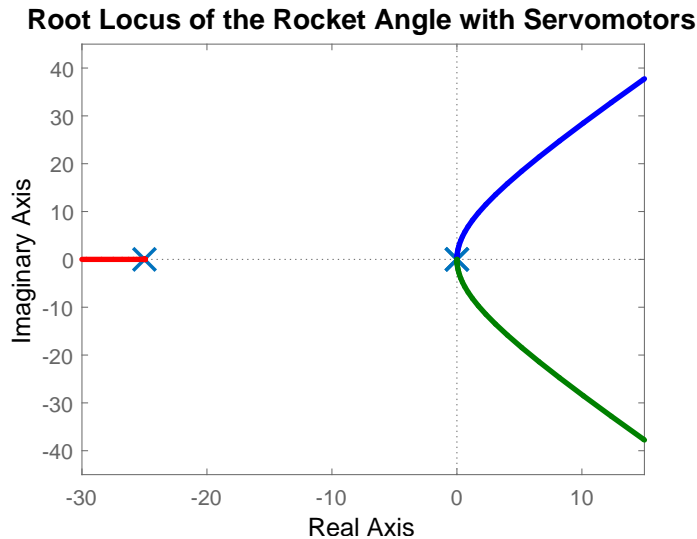


Figure 9.3: Root locus of the system with the pole from the servomotors.

This system could be controlled similarly to the inverted pendulum by doing cascade control. By having an inner loop that controls the servomotors as fast as possible the pole added can be assumed to have no effect. This would make the rocket control design nearly identical to the inverted pendulum by having an inner loop with a simple gain and an outer loop where a compensator in form of a zero needs to be added.

The rocket built however doesn't have any sensors to measure the servomotors so this isn't an option. If the rocket was built differently this would be the preferred way to control it.

Instead an attempt to control the system using an inner loop.

9.2.1 Controlling the Rocket Angle without Cascade Control

To move the poles to the left half plane, a controller C1, adding a zero and a pole on the left side, is implemented to the rocket transfer function. The zero of the controller is chosen to be near the system in order to attract the poles. The pole of the controller is set at high frequency to not temper with the system. Common practice recommends placing the pole at a location 20-40 times larger than the zero. The controller C1 is shown on Equation (9.3).

$$C1 = \frac{s + 2}{s + 40} \quad (9.3)$$

Jacob: Please check these values!

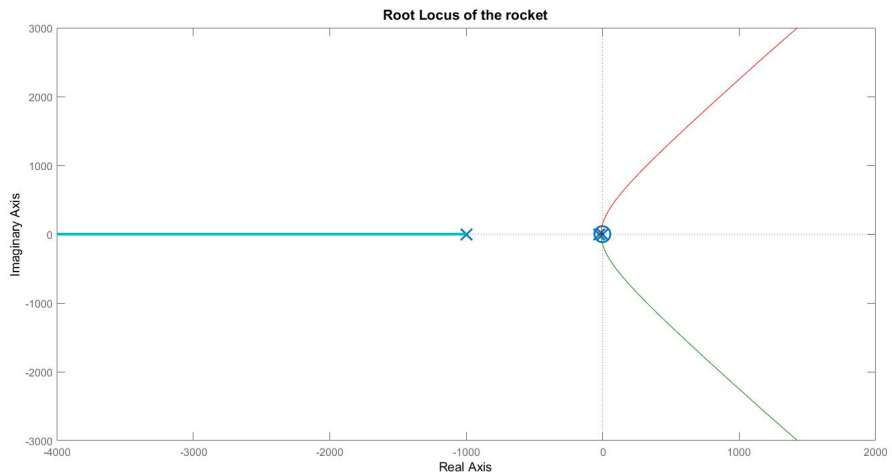


Figure 9.4: Root locus of the system with a lead controller, C1, added.

Jacob: The second controller is useless so you should clean this up. I didn't read any further than here. I can do the root locus graphs once you are sure about your lead controller pole-zero locations.

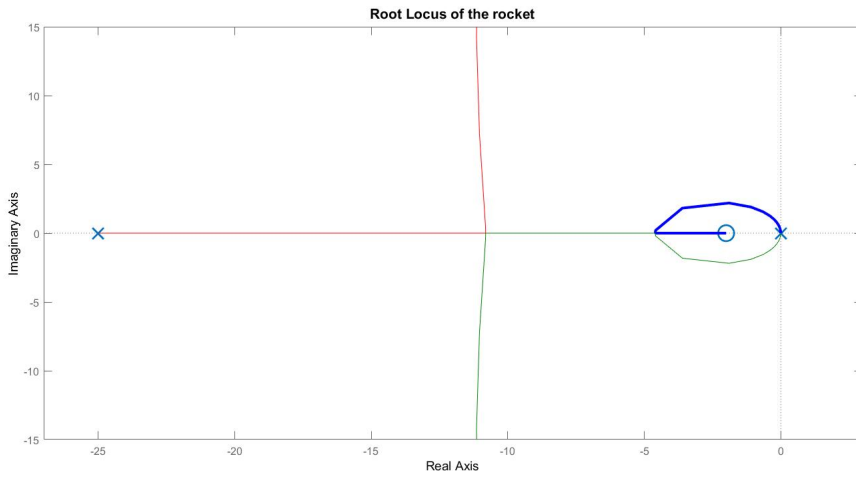


Figure 9.5: Focus on low frequencies.

Another controller C2 is needed to attract the two poles going to infinity along the imaginary axis. The controller and the new rocket transfer function are shown on Equation (G.2b).

$$C2 = \frac{s + 50}{s + 1100} \quad (9.4a)$$

$$H = \frac{s + 2}{s + 1000} \cdot \frac{s + 50}{s + 1100} \cdot \frac{1}{s \cdot \tau + 1} \cdot \frac{F_t \cdot L_{Cg} \cdot \frac{1}{M_r \cdot L_{Es}^2}}{s^2} \quad (9.4b)$$

The pole and zeros of C2 are set at higher frequencies than the first controller C1. The root locus is shown on Figure 9.6.

The rocket requires a fast settling time and rise time in order to act as soon as possible and control the rocket's stability. Lead compensators enable the modulation of the rise time, but impact the overshoot. The overshoot is considered as an inferior error, being in part countered by the play of the gimbal system.

To improve the rise time, the gain is set at 161 dB. This value is chosen by observing the root locus and the gain of a set point, as shown on Figure 9.7.

The system can have a faster rising time according to the step response of the servomotors, as shown on Table 9.3. To further improve the rise time and settling time of the rocket transfer function until the physical limits of the servomotors, a gain of 400 is chosen.

The controlled rocket transfer function is observed on Figure 9.8 and Figure 9.9.

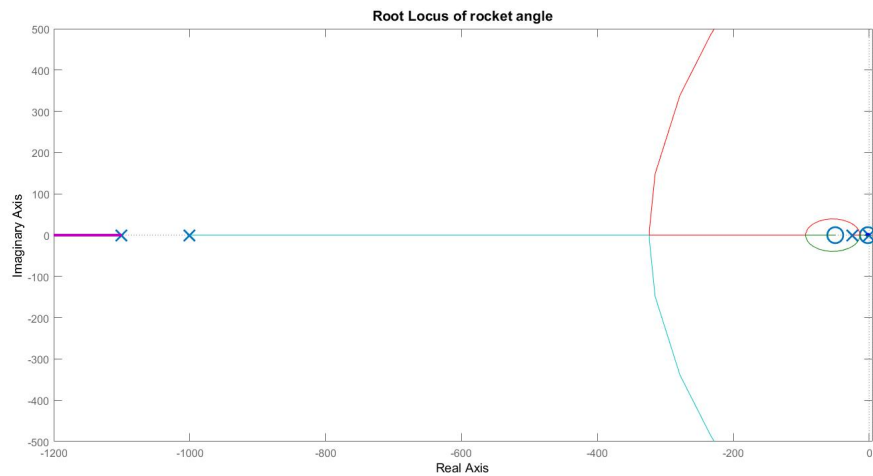


Figure 9.6: Root locus of the rocket transfer function.

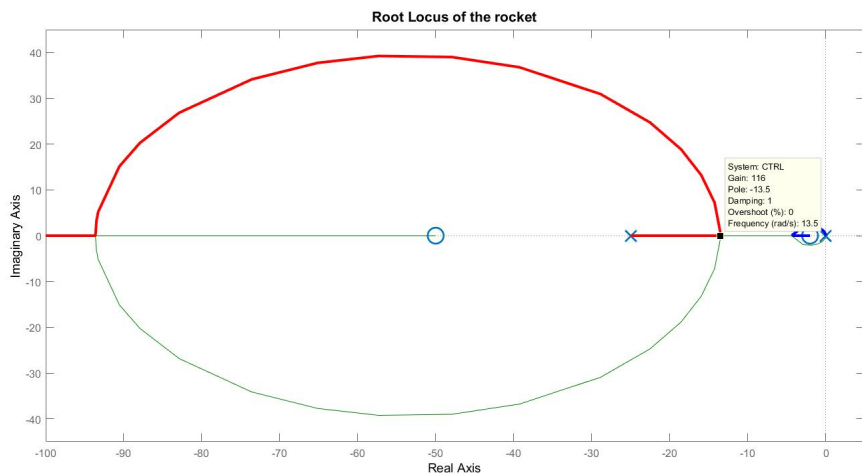


Figure 9.7: Set point at the start of the circle.

Table 9.3: Simulated step responses.

Transfer function	Rise time(s)	Setling time(s)	Overshoot(percentage)
Servomotors	0.0589	0.0782	0
Gain of 1	3.6620	128.1862	77.1429
Gain of 116	0.1666	1.2063	14.5434
Gain of 400	0.0625	0.5757	12.3234

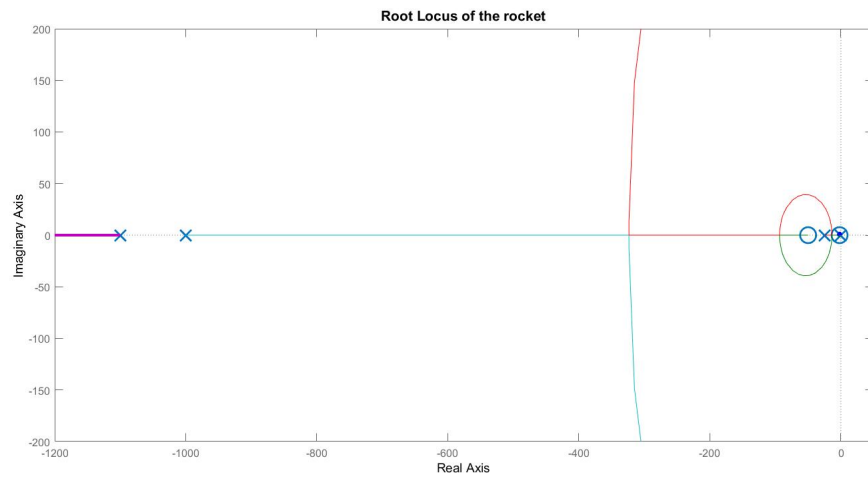


Figure 9.8: Root locus of the rocket transfer function with a gain of 400 dB.

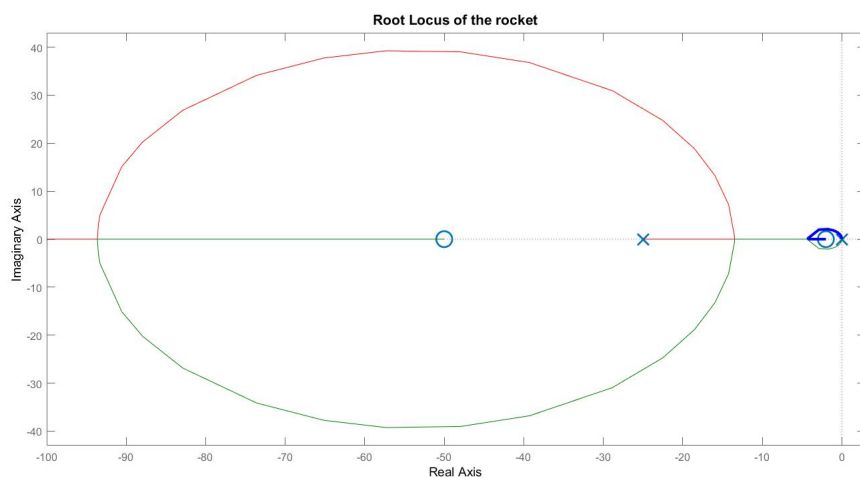


Figure 9.9: Focus on lower frequencies.

The step response of the controlled rocket transfer function is shown on Figure 9.10.

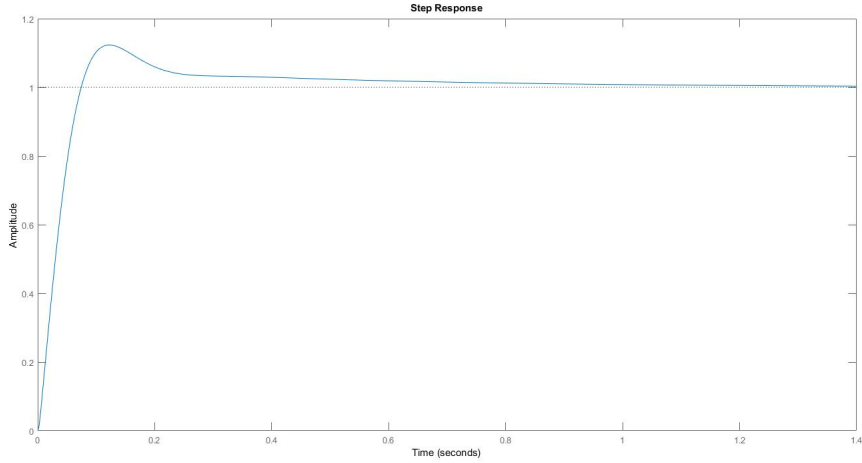


Figure 9.10: Step response of the rocket transfer function.

The bodeplot of the controlled rocket transfer function is shown on ???. The frequency corresponds to a complete rotation of the servomotors. At low frequencies a delay is observed. However the system functions at low speed. This implies that the delay has a tempered effect on the system. Higher frequencies are not physically possible and do not need to be compensated.

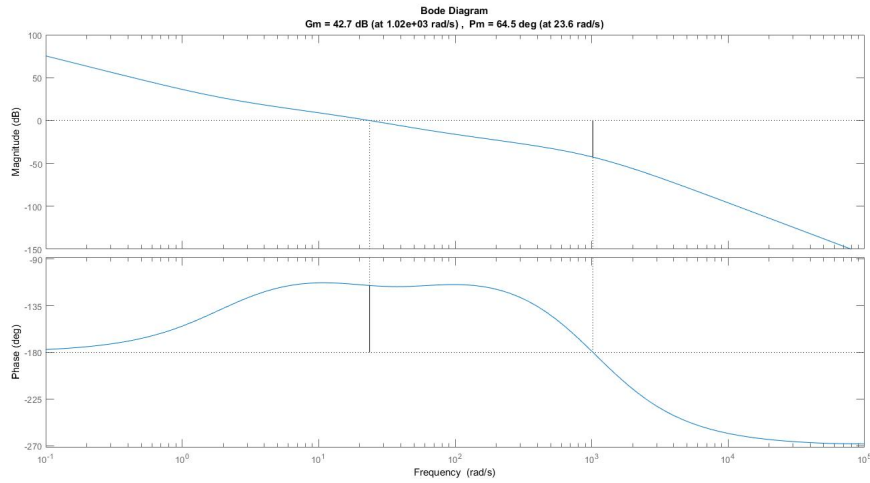


Figure 9.11: Bodeplot of the rocket transfer function.

The controlled rocket transfer function obtained is shown on equation Equation (9.2.1) and Figure 9.12.

$$H = 400 \cdot \frac{s+2}{s+1000} \cdot \frac{s+50}{s+1100} \cdot \frac{1}{s \cdot \tau + 1} \cdot \frac{F_t \cdot L_{Cg} \cdot \frac{1}{M_r \cdot L_{Es}^2}}{s^2} \quad (9.5)$$

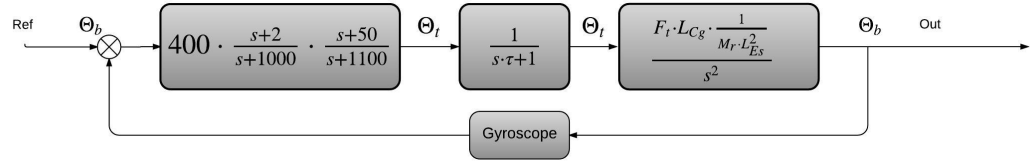


Figure 9.12: Rocket transfer function.

9.2.2 Design of Thrust Vectoring System

Raphael task describe
gimbal. - Mathias

Part III

Implementation

Chapter 10

Implementation

This chapter includes the implementation of controllers and components. The chapter will be separated into two sections, a section for the inverted pendulum and another section for the rocket. An Arduino will be used as the platform to implement the hardware and software on.

10.1 Inverted Pendulum Implementation

This section describes the hardware and software implementation of the controllers designed cf. section 8. The goal is to determine if the designed controllers will balance the stick in the real world application. The section is separated into three different parts about sensors, hardware controller and software controller. The first part is to implement the feedback for the controllers which in the case is sensors.

10.1.1 Implementing Sensors

The following section describes the implementation of the sensors with an Arduino Uno and the double inverted pendulum setup.

Potentiometer

The system consists of multiple sensors, as described cf. section 5.1, where two of these are potentiometers. The potentiometers are tested cf. appendix E. The appendix concluded with a first order approximation of both potentiometers. During implementation it is realized that a slight calibration were needed because of the potentiometer had shifted place in the setup. The approximation for Pot_{arm} is:

$$\theta_a = 63,11 \cdot V_{\text{Pot}_{\text{arm}}} - 117,0 \quad (10.1)$$

Notes:
 $V_{\text{Pot}_{\text{arm}}}$ is the output voltage of the arms potentiometer [V]
 θ_a is the angle of the arm [°]

The approximation for Pot_{stick} is:

$$\theta_s = 66,66 \cdot V_{\text{Pot}_{\text{stick}}} - 163,9 \quad (10.2)$$

Where:

$V_{\text{Pot}_{\text{stick}}}$ is the output voltage of the stick potentiometer. [V]
 θ_s is the angle of the stick, but where zero degrees is when the stick has a zero degree deviation from the arm [°]

An example of implementing this is done **through** a pseudo-code which converts the analogue value to radians. The linear approximations of the potentiometers is used.

```

1 void loop() {
2     // read the input on A0 and A1:
3     int PotArm = analogRead(A0);
4     int PotStick = analogRead(A1);
5
6     double VPotarm = PotArm / 204.8; //Analog2Voltage
7     double ThetaA = 66.66 * VPotarm - 170.46; // Voltage2Degree
8     double ThetaARad = ThetaA * (31.415926 / 1800.0); //Degree2Radians
9     double VPotstick = PotStick / 204.8;
10    double ThetaS = 63.64 * VPotstick - 117.77;
11    double ThetaSRad = ThetaS * (31.415926 / 1800.0);
12 }
```

The sampling time of the sensors is an important aspect when ensuring stability of the control system. The sensor sampling can not be too slow because then the control loops will be slow and not update fast enough. Considering that the sensor is a potentiometer which does not have any active components, then the only limit is the Arduino. Arduino specifies that calling a `analogRead()` takes approximately 100 µs which corresponds to a sampling frequency of 10 kHz. This is considered fast enough for the system and is therefore not a problem.

Tachometer

The tachometer and its precision has been tested in appendix D. The test concluded that the internal tachometers precision is within the limit of what could implemented. The tachometer outputs a voltage which is close to linear with the number of revolutions per minute.

The test concluded with a transfer function for the tachometer, that gives the relation between the tachometer voltage and motor velocity:

$$\frac{\frac{1000 \text{ RPM}}{3.130 \text{ V}} \cdot 2 \cdot \pi}{60 \text{ s}} \cdot T_{\text{Voltage}}[\text{V}] = M_{\text{Velocity}} [\text{rad/s}] \quad (10.3)$$

The function can not directly be implemented with the Arduino. The tachometer will generate a negative and positive voltage corresponding to the direction of the motor. Negative voltage can not be directly input to the Arduino without short circuiting it, and the positive voltage would be to high considering that the motor can go up to 8500 RPM. Interfacing is therefore needed between tachometer and Arduino. This interfacing is done trough the ESCON motor controller included in the inverted pendulum setup. The two outputs of the tachometer is put in to the motor controller via two analogue inputs. The one acts as the positive connection and the other as the negative. How the motor controller is reacting to an input is configured trough the ESCON studio included. In the case it is set with the conversion ratio from voltage to RPM on 3,130 V/1000 RPM, which was determined by external calibration from another tachometer and implemented in the software. The motor controller is set with a output that converts this RPM down between 1 and 4 V to the Arduino. Where 1 V is corresponding to -3000 RPM and 4 V corresponding to +3000 RPM. This gives the possibility to convert these values back to RPM in Arduino. How the motor controller converts the voltages is considered a black box. The wiring for the tachometer can be seen cf. figure 10.1. 

10.1.2 Implementing ESCON Motor Controller

The following sections describes the implementation of the hardware motor controller with the Arduino. The motor controller in the setup is a Maxon Escon 50/5.

The Maxon ESCON 50/5 is a PWM servo controller, that can be used to control DC and EC motors. The application is to amplify signals and control systems **trough**  different control operations. It can also be used with a PWM input signal that can be outputted as an amplified and higher frequency PWM signal to a motor. The servo controller can be used in three different modes which can be configured **trough** the included Maxon ESCON studio. It can be configured in two modes for speed control with open and closed loops with feedback from sensors **trough** the board, and

one mode for motor current control trough inputs from other modules such as an Arduino. In the setup the Escon controller is set to current control.

It is setup **trough** the ESCON studio with current control, and with a external controlled PWM signal. It then gives the possibility to input a PWM signal from the Arduino, which will be amplified so that 90% duty cycle equals 11 A and 10% equals -11 A. This means that 50% will give 0 A.

The Arduino uses a 8-bit timer for PWM as standard so to get a better resolution the TimerOne library is implemented. TimerOne is a 16-bit hardware timer which can be downscaled to give the possibility to have a 10-bit resolution on the PWM signal. A better resolution gives a higher number of duty cycle values which makes the control more precise than with 8-bit.

The configuration file for the ESCON studio is included in the attachment files under **"/Attachment/Implementation/Motor Controller/Motor Controller Configuration File"**. It can be imported into the ESCON studio and loaded onto any 50/5 controller.

The main specifications of the ESCON is listed cf. table 10.1.

Parameter	Value	Unit
Supply voltage V_{cc}	10-50 V	[V]
Output voltage (max.)	$0,98 \cdot V_{cc}$	[kg]
Nominal output current	5	[A]
Maximum output current (<20 s)	15	[A]
Current control PWM frequency	53,6	[kHz]

Table 10.1: Maxon Escon 50/5 specifications[5].

The wiring for the setup can be seen cf. figure 10.1.

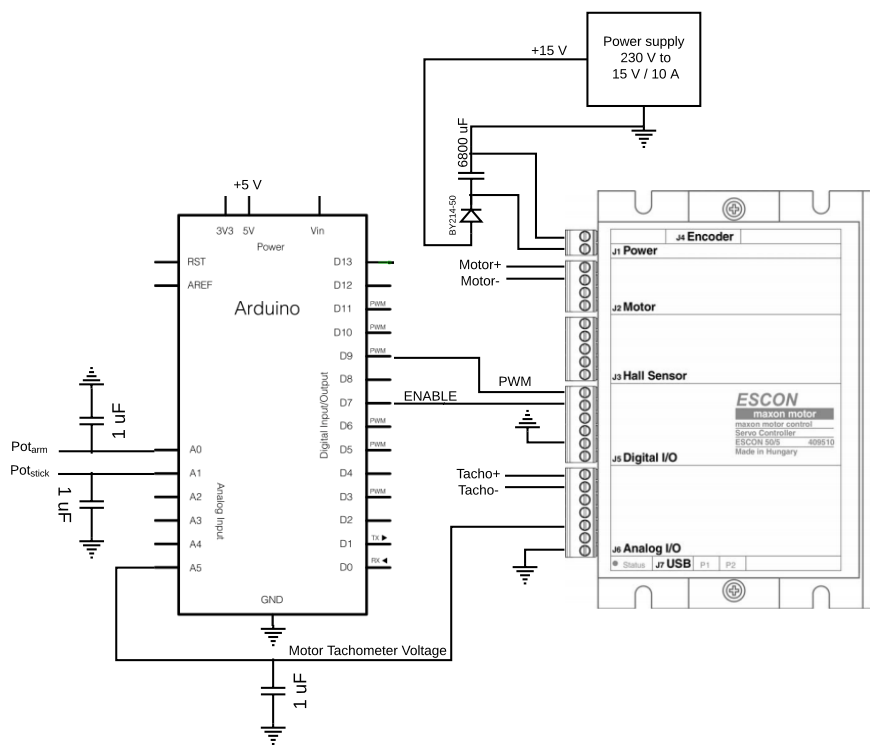


Figure 10.1: Wiring for the control setup.

The control PWM signal from the Arduino is set with a frequency of 5 kHz because that it is the maximum input frequency the motor controller will accept. It is set to 5 kHz so that the PWM avoids interference with the sampling frequency for the system. The input PWM signal is then amplified and made faster. The output PWM frequency of the motor controller is 53,6 kHz with a duty cycle from 10 - 90% which can not be changed in the ESCON studio. It is considered that the switching frequency of the ESCON is close to optimal when considering that the PWM frequencies is within the limit of what its datasheet specifies. The main concern of a switching frequency of 53,6 kHz on the motor would be heat dissipation. Therefore the minimum PWM frequency for the motor is calculated to see if the motor controllers PWM frequency fits the motor.

Calculating Minimum PWM Frequency

The only PWM frequency considered is the minimum switching frequency for the motor. This is done by considering the motor resistance and inductance versus the maximum amount of current ripple wanted on the motor. The values for the resistance and the inductance of the motor are calculated in appendix B.2. The formula is seen cf. 10.4 [Palle Andersen, 2016].

$$f_{\text{switch}} \geq \frac{-1}{2 \cdot \ln(1 - \frac{p}{100})} \cdot \frac{R_m}{L_m} \quad (10.4)$$

Where:

p	The maximum % current ripple in the motor.	[1]
$\frac{R_m}{L_m}$	The inverse electrical time constant of the motor.	[Hz]

Replacing with the numerical values of the resistance and the inductance and choosing a max ripple percentage of 5%, the minimum switching frequency determined to be:

$$f_{\text{switch}} \geq \frac{-1}{2 \cdot \ln(1 - \frac{5}{100})} \cdot \frac{0,82 \Omega}{156 \cdot 10^{-6} \cdot H} \approx 51,2 \text{kHz} \quad (10.5)$$

The maximum ripple in the motor is determined by making the ripple the unknown factor P_{ripple} and setting the PWM frequency to the implemented 53,6 kHz.

$$53,6 \text{kHz} = \frac{-1}{2 \cdot \ln(1 - \frac{P_{\text{ripple}}}{100})} \cdot \frac{0,82 \Omega}{156 \cdot 10^{-6} \cdot H} = P_{\text{ripple}} = 4,785\% \quad (10.6)$$

This gives that the maximum current ripple is 4,785% if considering a PWM frequency on 53,6 kHz. A general rule is that the ripple should be less than 10% of the current, so considering that is less than 5% is good considering that the system is implemented with current control.

10.1.3 Implementing Controllers

The implementing on the hardware has been described in the chapter, and therefore the implementation can proceed to the implementing the controllers on an Arduino.

10.1.4 Implementing Continuous Controller on Arduino

As the Arduino is a microprocessor the continuous controller found in Chapter 8 needs to be transformed into a discrete controller. This also means a sample time needs to be determined. The sample time needs to be faster than the settling time of the fastest subsystem i.e. the motor loop. The motor loop has a settling time of 0.0137 seconds. The sample time is selected to be 0.002 seconds as it's faster than the motor loop. This gives a sampling frequency of Equation (10.7).

$$F_s = 500 \text{ Hz} \quad (10.7)$$

With the sampling time determined the continuous controller needs to be transformed to a discrete controller. For the two P-controllers it's as simple as multiplying the sampled input with the gain to get the discrete output. For the outer loop controller it's not as simple and is done by using the Z-transform. There are a couple of different options for performing the Z-transform each with their own nuances but the differences won't be discussed and the bilinear transform will be used. For the bilinear transform s in Equation (8.15b) will be substituted with Equation (10.8).

$$s = 2F_s \frac{z - 1}{z + 1} \quad (10.8)$$

Equation (8.15b) then becomes Equation (10.9).

$$D_x = 8.8 \frac{2F_s \frac{z-1}{z+1} + 4.29}{2F_s \frac{z-1}{z+1} + 9.19} \quad (10.9a)$$

$$D_x = 8.8 \frac{2F_s(z-1) + 4.29(z+1)}{2F_s(z-1) + 9.19(z+1)} \quad (10.9b)$$

$$D_x = 8.8 \frac{(2F_s + 4.29)z + 4.29 - 2F_s}{(2F_s + 9.19)z + 9.19 - 2F_s} \quad (10.9c)$$

$$D_x = \frac{Y(z)}{X(z)} = 8.8 \frac{2F_s + 4.29 + (4.29 - 2F_s)z^{-1}}{2F_s + 9.19 + (9.19 - 2F_s)z^{-1}} \quad (10.9d)$$

$$Y(z) \left(2F_s + 9.19 + (9.19 - 2F_s)z^{-1} \right) = 8.8X(z) \left(2F_s + 4.29 + (4.29 - 2F_s)z^{-1} \right) \quad (10.9e)$$

The Z-transformed controller can then be made discrete by substituting $aY(z)z^m$ with $ay[k + m]$ and similarly for $X(z)$. This gives the discrete controller ready to be implemented in the Arduino in Equation (10.10b).

$$(2F_s + 9.19)y[k] + (9.19 - 2F_s)y[k - 1] = 8.8(2F_s + 4.29)x[k] + 8.8(4.29 - 2F_s)x[k - 1] \quad (10.10a)$$

$$y[k] = 8.8 \frac{2F_s + 4.29}{2F_s + 9.19} x[k] + 8.8 \frac{4.29 - 2F_s}{2F_s + 9.19} x[k - 1] - \frac{9.19 - 2F_s}{2F_s + 9.19} y[k - 1] \quad (10.10b)$$

Controller Software

This section describes the software implemented on the Arduino. The software can be found in the attached materials under "[Attachment/Implementation/Arduino Software/InvertedPendulumControlSoftware](#)". The structure and processes is represented with a flowchart cf. figure 10.2.

Where:

θ_a	is the angle of the arm.	[rad]
θ_s	is the angle of the stick.	[rad]
x_α	is the distance to initial upright position.	[m]
Ref_{x_α}	is the reference distance error to initial upwards position.	[m]
$x_\alpha Err$	is the distance error from initial upright position.	[m]
Ref_{θ_a}	is the reference angle of the arm.	[rad]
$\theta_a Err$	is the angle error of the arm.	[rad]
Ref_{ω_m}	is the reference velocity of the motor.	[rad s ⁻¹]
$\omega_m Err$	is the velocity error of the motor.	[rad s ⁻¹]

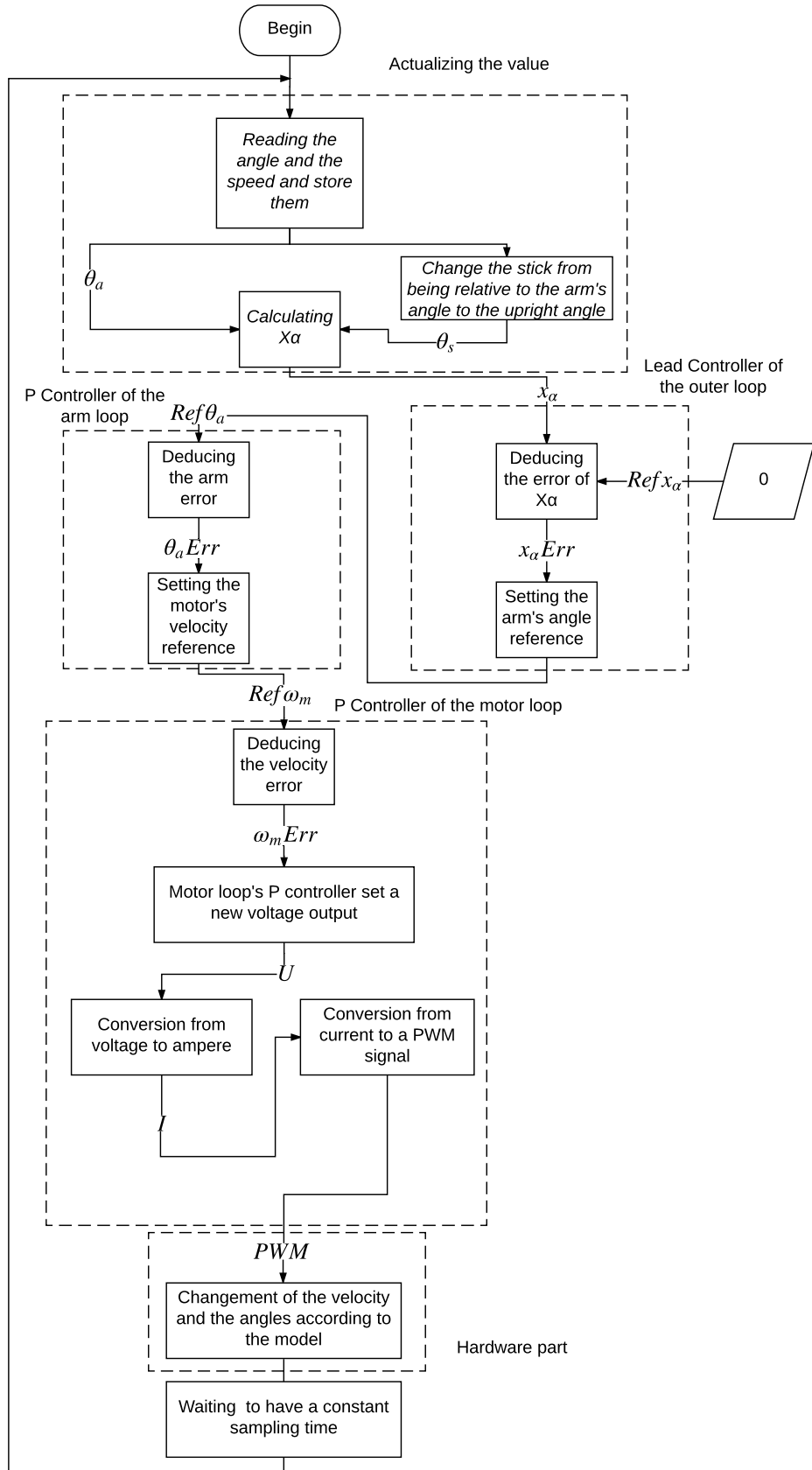


Figure 10.2: Flowchart for the implemented software on Arduino.

10.1.5 Implementation Evaluation

This following sections describes the different problems that occurred with the hardware and software trough out the implementation. They will be explained to show the progress trough out the implementation.

Filtering Sensors

During implementation of the Arm Loop it was found that a shaking occurred trough the motor, gear and out to the arm. From testing higher gains it was found that the shaking was amplified and became more unstable with the higher gains. Testing of the hardware and software was done to determine from where this shaking was sourced. To start with the sensors was checked for noise and floating. This was done to remove incorrect readings and unstable sensors. The sensors was read trough a oscilloscope and it was found that the ESCON motor controllers PWM frequency was represented in the sensor signal. This can occur from incorrect ground or wires not correctly isolated. This problem was solved by adding a capacitor to the sensors as seen cf. figure 10.1. The capacitor is connected from signal wires to ground to make a low pass filter. $1 \mu\text{F}$ is chosen, one for each signal wire and considering that it is two $10 \text{ k}\Omega$ potentiometers it will give a varying cut off frequency. The cut-off frequency is calculated to:

$$\frac{1}{2 \cdot \pi \cdot 10000 \Omega \cdot 1 \cdot 10^{-6} \text{ F}} = 15,92 \text{ Hz} \quad (10.11)$$

$$\frac{1}{2 \cdot \pi \cdot 2,97 \Omega \cdot 1 \cdot 10^{-6} \text{ F}} = 53,6 \text{ Hz} \quad (10.12)$$

Considering that the resistance changes we need to go under $\approx 2,97 \Omega$ before the cut-off frequency exceeds the frequency of the noise, and that any resistance higher will dampen with more than -3 dB. It is noticeable that the resistance values of the potentiometers is in between both limits of resistances and the noise is therefore damped. The conclusions of adding these filters removed high frequency noise that made the arm shake less. There was still a small-amplitude shaking around the setpoint when the arm was at a position and kept there. This could be down to bad range and bad optimisation of bits in the software. The software is made with scaling from analogue values down to radians, which means that reading the arm potentiometer and having a analogue value from 235 to 527 and converting it down to -0,785 to 0,785 radians will mean that that first two bits is not optimized, because they are static or close to. This gives that the 10-bit resolution of the PWM is not used optimally when two is static, but it is still better than having 8-bit with two static. This can be optimize by either changing the range of the potentiometers

to that the radian range was optimized to cover from 0-1023 and have a better bit/radians resolution. This solution could be done by having a operational amplifier with a gain of 4 and a 5 V saturation. The potentiometer should then be turned to that -0,785 is at the 0 point for the potentiometer. It can also be solved by changing the model and with the conversion **trough** out the software. Meaning that the analogue value would not be converted which would give a better resolution for the PWM output. Equally they can be combined for the best resolution. It is chosen to only implement the resolution optimization if and only if the acceptance test show that the system does not fulfil the set requirements.

PWM Frequency Problems

The stick control loop was implemented. The simulations gave gains and results that could be implemented on the system. When implemented it was found that the arm did not control correctly when the stick moved. Repetitive test gave the conclusions that the speed of the arm was to slow. Higher gains was implemented but did not give the wanted result and the gains was set back to the simulated. A oscilloscope test was made on the Arduino PWM frequency by measuring the input frequency on the motor controller. The test showed that the frequency was 100 Hz and not 5 kHz as expected. The software was revised and determined that TimerOne was used as timer twice, one for controlling PWM frequency and one for controlling the sampling time with an interrupt. The interrupt was removed and changed to a wait so that the sampling time was kept constant. The PWM frequency was then measured to be 5 kHz and the arm then behaved as wanted with the simulated gains.

I2T Limitation

Another problem observed where a run time limit on the control system. The system would slow down after around approximately a minut but it was easily observed **trough** the ESCON studio that a I2T limit was reached on the motor controller. An I2T limit is an algorithm that is described by the nominal current, the motor peak current in rms, and the motor peak current in seconds. It is used to secure the motor and driver from damage and over heating. The parameters for the algorithm was set **trough** the ESCON studio, with a nominal current on 5 A, a peak current on 11 A, and a thermal time constant on 200 seconds. When the limit is reached the motor current only goes to 5 A so the motor controller is shut off so that it cools down and can then be used again.

Controller tuning

An initial test showed that the controller designed could balance the stick however it was balanced when the arm was closer to 30° than 0° . This is likely caused by a steady state error somewhere in the system. As the motor loop controller had a steady state error the gain was increased to reduce the error. This made the stick balance closer to the upright position. The new motor loop controller becomes Equation (10.13).

$$D_{\text{motor}} = 10 \quad (10.13)$$

10.2 Rocket Implementation

10.2.1 Implementing Inertial Measurement Unit

The system consists of an Inertial measurement Unit (IMU) GY - 80. This implies that multiple integrated sensors can be used, as seen in [??](#). The PCB created and [used is seen in appendix](#). Multiple physical and software constraints have to be taken into account when implementing the system.

The rise time and settling time of the sensors are an important feature when ensuring the stability of the rocket. It cannot be too slow, otherwise the system will react to late to any angle variation. The rise time and settling time of the servomotors and rocket transfer function are [described in The](#) process of the servomotors is then considered fast enough for the system, not interfering with the angle control process.

The vibration of the rocket is a physical difficulty for the sensors as the measurements might be distorted. The placement and fixation must be carefully thought, as [described in appendix](#).

Of all the sensors available, only the gyroscope will be used in this project. This is due to the conditions of the rocket launch : the rocket will be attached to the ground, and will therefore have no use of all the potential of the IMU GY -80.

Gyroscope

The system includes a L3G4200D 3-axis gyroscope. The gyroscope is described in [appendix](#).

An example of implementing is done through a pseudo-code which converts in degree the output of the sensor in order to trace the rotation and [mouvement](#) of the system. The [angle are](#) then analyzed to measure the angle variation, and then enable the system to correct the variation.

10.2.2 Test of simulated flight

The system is connected to the servomotors. The goal is to simulate manually an angle variation of the rocket body and see the reaction of the system on the servomotors and the thruster. If the real thruster angle is equal to the desired one, then the controller is deemed acceptable and the system as fulfilling the requirements.

The experiment set up is described in appendix . An example of implementing is done through .

appendix to do

do the code/experiment to finish that part

10.2.3 Test of attached-rocket flight

The experiment set up is described in appendix .

Part IV

Test & conclusion

Chapter 11

Inverted Pendulum Acceptance Tests

In this section the tests to check whether the controllers designed for the inverted pendulum fit the requirements or not. As said in Section 7.1 the first acceptance test will not be documented as it is more an implementation requirement than a test.

11.1 Acceptance Test 2.

The goal of this test is to see if the inverted pendulum's stick and arm stay within the limits set in Requirement 2 and 3 described in Section 7.0.1. Figure 11.1 and 11.2 plots the angles of the arm and the stick over a period of 30 s the maximum and the minimum angles are put in evidence so that it is easy to compare them with the requirements.

From Figure 11.1 it can be easily seen that the arm is within the requirements by a large margin of 0.68 rad or 38.96°. This result is due to the transformation of the outer loop described in Section 8.2.1. Indeed the reference is not anymore the upright angle of the stick but the distance of a point on the stick compared with its position when both the arm and the stick are in upright position. Due to this the controller will try to keep both the arm and the stick in the upright angle which explains the very low angle variation of the arm compared to the requirement.

In Figure 11.2 the largest angle the stick takes is 0.05 rad while the Requirement 2 precise a limit of 0.9 rad. So once again the requirement is respected by a large margin.

From the results seen it can be concluded that the second acceptance test is a success.

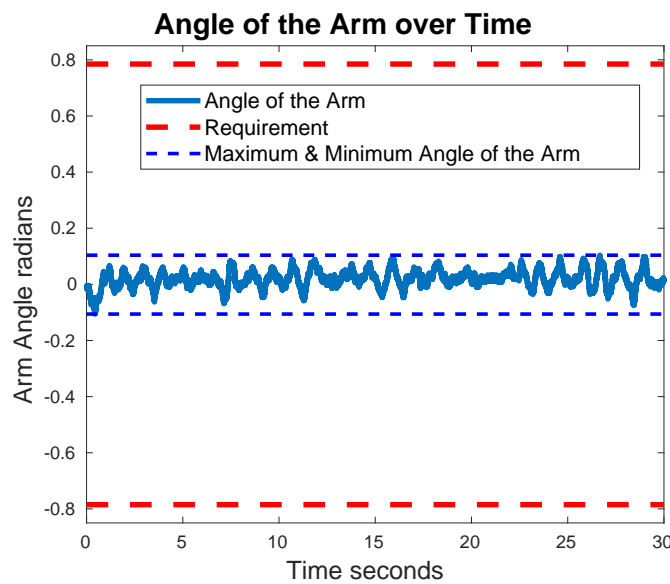


Figure 11.1: Plot of the angle of the arm over time with the limits set by the Requirement 1.

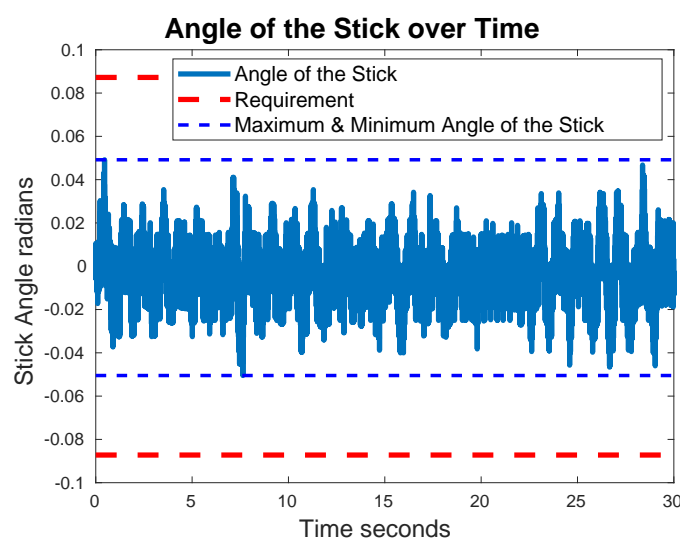


Figure 11.2: Plot of the angle of the Stick over time with the limits set by the Requirement 2.

11.2 Acceptance Test 3.

Unfortunately a method to precisely hold and release the stick was not found, as such no precise data were able to be collected for this test. However, a video was taken during the test and will be joined with the report. This video shows the reactions of the stick when different pushes are applied to it. The maximum angle for the stick set in the requirements are present and can be used as reference points. It can be noted that during the whole video the stick keeps its balance.

The results for the acceptance tests of the stick are a success.

Chapter 12

Discussion

12.1 Inverted Pendulum possible improvements

The inverted pendulum as it is does fulfill all requirements. Furthermore, the possible simple improvements such as the suppression of the shaking is already discussed in Section 10.1. So there is not much to talk about. What could have been done however, is to try other control design schemes such as space equations, bode plot and test them to see which one performs the best. Unfortunately too much time was wasted fixing the set up to be able to do so.

12.2 Rocket

12.3 Differences between the Rocket and the Inverted Pendulum

As explained in Section 6.2 the models are slightly different. First of all, opposite angles were chosen in the beginning of the modeling process. Moreover, the the pendulum is fixed to the gears and motor, while the rocket is floating in the air, and thus canceling the gravity. Regarding to root locus, the inverted pendulum has two more zeros in 0 and two real poles equidistant from zero, whereas the rocket has two poles in 0. The difference in poles is due to the absence of gravity into the rocket modeling, while the difference in zeros might be due to the fact that the arm is rigidly attached compared to the thruster.

Unfortunately even if the systems are close, an identical model could not be found. This difference might come from the setup and its extra arm, which introduce a rotational force instead of a horizontal force e.g an inverted pendulum with a cart.

Bibliography

- [1] Taylor W. Barton Kent H. Lundberg. History of inverted-pendulum systems. *IFAC*, 42:131 to 135, 2010.
- [2] NASA. Rocket structure, 2015.
- [3] Tom Benson. rocket, 2014.
- [4] 2007 Group 631. Studentthesis, 2007.
- [5] MaxonMotor. *Maxon Escon 50/5 Servocontroller*.
- [6] C. R. Nave. Moment of inertia of a rod, 2016.
- [7] C. R. Nave. Natural frequency of pendulum, 2016.
- [8] Parvex. *Axem Disc DC Servo Motor Manual*, 2003.
- [9] NIST. Standard gravitational acceleration, 2016.
- [10] GY-80 IMU. Imu gy-80, 2015.

Appendix A

Test Journal: Template

Test participants: Maxime & Robin & Bang

Date: 12/10-2016

Purpose

The purpose of the test is to calculate the internal resistance and inductance for the DC motor.

Test equipment and components

Table A.1: List of measurement equipment and components

Name	Brand	Model	AAU-number
Multimeter	Fluke	37	08181
Powersupply	Hameg triple	HM7042	33902
DC motor	Maxon	41.023.038-00.00-052	N/A

Setup

Measurement setup is seen on Figure E.1

Pictures and describing text



Figure A.1: Measurement setup.

Method

Step by step of test, maybe in enumerate

1. one
2. two

Raw data

Or maybe a plot if there's many results. (Remember to save the raw data anyway.)

Data processing

Conclusion

Appendix B

Test Journal: Gear Train System

Test participants: Maxime & Geoffroy

Date: 28/2/2017

Purpose

The objective of this test is to determine all the of the gear train system composed of the DC motor and the gear train.

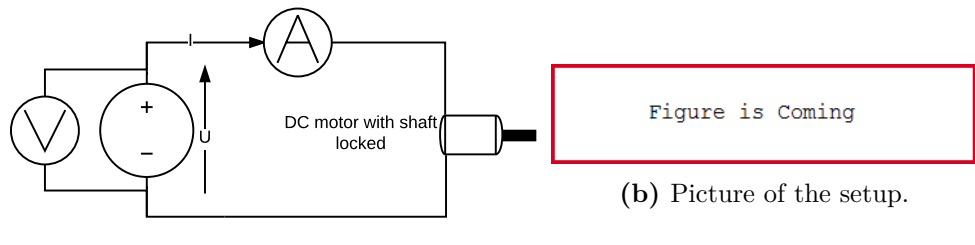
B.1 Electronics characteristics

B.1.1 Internal Resistance of the DC Motor R_m

The first parameter to be tested is the internal resistance of the motor R_m . This resistance is needed in the motor's transfer function and will be used to determine the other parameters of the motor.

Setup

Figure B.1 shows a diagram and photo of the measurement set up



(a) Diagram of the setup.

Figure B.1: The measurement setup.

Method

This test consists of having the motor shaft locked while the voltage is increased by 0.5 V between measurements.

Raw data

Figure B.2 is the plotted evolution of the voltage of the circuit according to the current.

Figure B.2: Raw data used to determine R_m

Voltage (V)	Current (A)
0.50	0.33
1.00	0.71
1.50	1.13
2.00	1.67
2.49	2.34
2.98	2.94
3.50	3.75
3.99	4.68
4.50	5.54
4.98	6.11
5.54	6.46
6.02	7.40
6.51	8.26
7.01	9.14

Data Processing

In order to find the motor's resistance R_m , the electrical equations of the motor will be used:

$$U_m = R_m \cdot i + L_m \frac{di}{dt} + K_e \omega_m \quad (\text{B.1})$$

With the motor shaft locked, $\omega_m = 0$. Moreover, the measurements are made a couple seconds after the change in voltage is made. The current is then constant, canceling its derivative.

The resulting equation is Ohm's law:

$$U_m = R_m \cdot i \quad (\text{B.2})$$

The measurement of voltage according to the current is presented in Figure B.3.

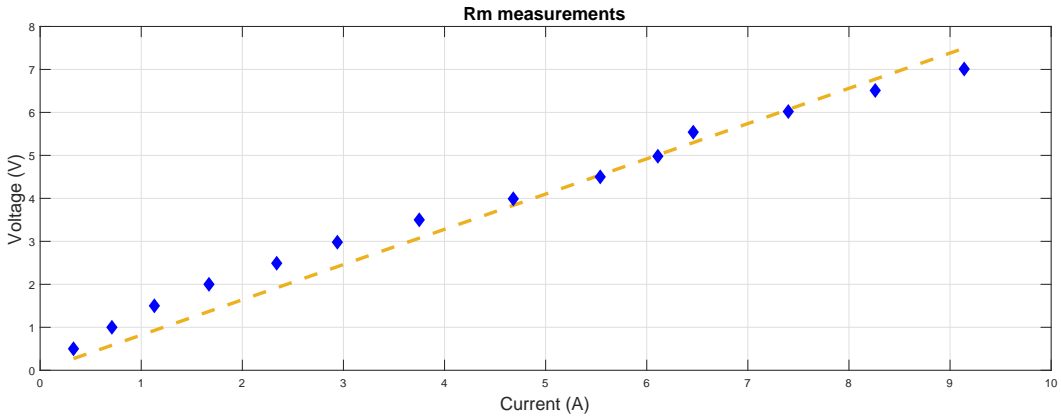


Figure B.3: Measurement of voltage according to the current

R_m is the slope of the linear approximation (in dashed yellow) of the voltage over the current:

$$U_m = R_m \cdot i \quad (\text{B.3a})$$

$$R_m \approx 0.82 \Omega \quad (\text{B.3b})$$

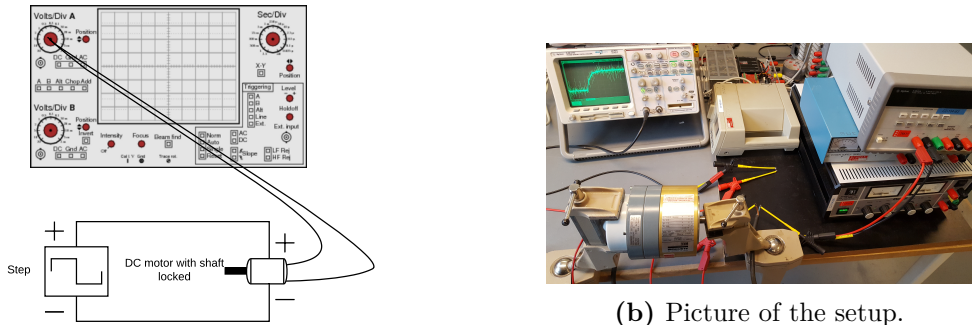
B.1.2 Internal Inductance of the DC Motor L_m

Setup

Figure B.4 shows a diagram and photo of the measurement set up.

Table B.1: List of measurement equipment and components

Name	Brand	Model	AAU-number
Oscilloscope	Agilent	54621D	33941
Powersupply	Agilent	E3631A	78577
DC motor	Alsthom BBC	F9M2	08339

**Figure B.4:** L_m measurement setup.

Method

This test consists of having the motor shaft locked while a step is applied. The current is measured through the circuit. With the current step response, the inductance of the motor can be found.

Raw data

Figure B.5 is the plotted evolution of the current of the circuit in respect to time.

Data processing

When the shaft is locked and a step is applied the DC motor's electric equation can be resumed as in Equation (B.4).

$$F(s) = \frac{I(s)}{U(s)} = \frac{\frac{1}{R_m}}{\frac{L_m}{R_m} s + 1} \quad [1] \quad (\text{B.4})$$

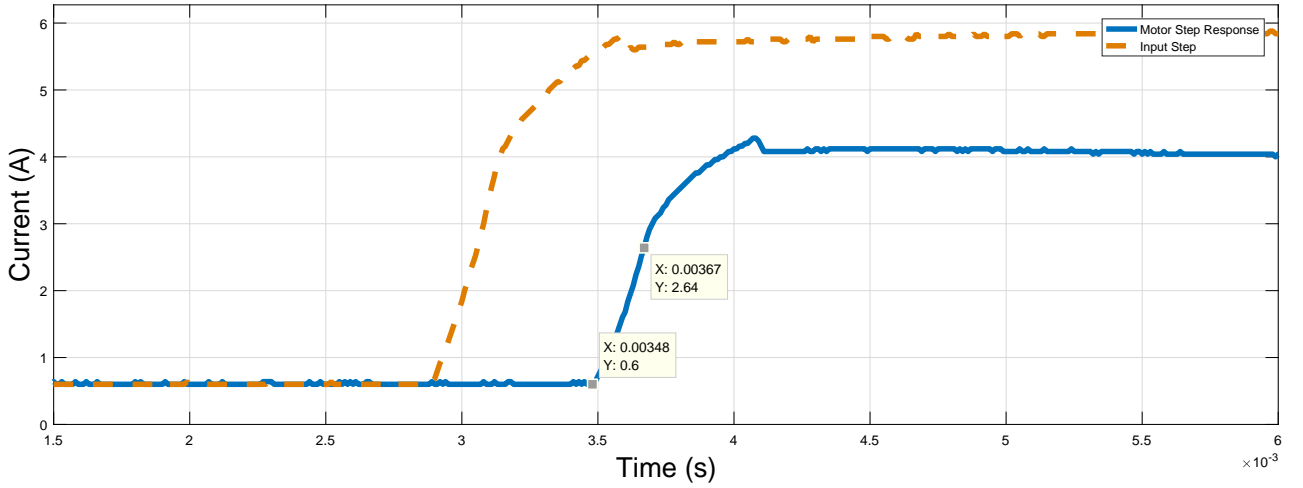


Figure B.5: Plot of the current step response in respect to time

Where:

$I(s)$ is the current in Laplace domain [1]

$U(s)$ is the body's acceleration [1]

R_m is the internal resistance of the motor [Ω]

L_m is the internal inductance of the motor [H]

When a unit step response is applied to the system ?? becomes Equation (B.5).

$$F(s) = \frac{\frac{1}{R_m}}{\frac{L_m}{R_m}s + 1} \frac{1}{s} = \frac{-\frac{1}{R_m}}{s + \frac{R_m}{L_m}} + \frac{1}{R_m s} \quad [1] \quad (\text{B.5})$$

?? is then put in the continuous time domain to get Equation (B.6).

$$f(t) = \frac{1}{R_m} \left(1 - e^{-\frac{R_m}{L_m}t} \right) \quad [1] \quad (\text{B.6})$$

Equation (B.6) means that at $t = \frac{L_m}{R_m}$ the function would give $1 - e^{-1} \approx 63.2\%$ of its settling value given that the step start at 0 seconds. Therefore, at 63.2% of the settling value $t = \frac{L_m}{R_m}$.

Since $R_m = 0.82 \Omega$ is known, finding L_m becomes trivial. Here, the step starts at 0.00348 s.

Conclusion

Since the settling value of the output current is 4.04 A. Then Equation (B.7) gives the value of L_m .

$$\frac{1}{R_m} \left(1 - e^{-\frac{R_m}{L_m} t} \right) = 4.04 \cdot 0.63212055882 \quad [s] \quad (B.7a)$$

$$t \approx 0.00367 - 0.00348 \approx 0.00019 \text{ s} \quad (B.7b)$$

$$L_m = t R_m \quad (B.7c)$$

$$L_m \approx 156 \mu\text{H} \quad (B.7d)$$

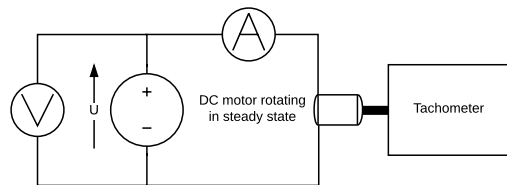
B.1.3 The DC Motor velocity constant K_e

Table B.2: List of measurement equipment and components

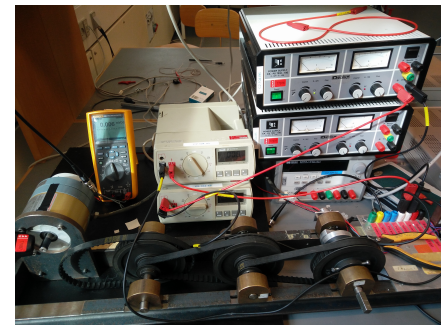
Name	Brand	Model	AAU-number
Oscilloscope	Agilent	54621D	33941
Powersupply	Agilent	E3631A	78577
DC motor	Alsthom BBC	F9M2	08339

Setup

Figure B.6 shows a diagram and photo of the measurement set up



(a) Diagram of the set up.



(b) Picture of the set up.

Figure B.6: The measurement set up for K_e .

Method

This test consists of having the motor shaft rotating in steady state while the voltage U of the generator, the angular velocity ω of the shaft and the current I are measured.

Raw data

Figure B.7 has all the measurements done.

Figure B.7: Raw data used to determine K_e

Voltage (V)	Current (A)	ω (rad/s)
3.0	0.72	52.36
3.5	0.75	67.54
4.0	0.77	83.15
4.5	0.79	98.75
5.0	0.83	113.10
5.5	0.85	126.71
6.0	0.88	140.95
6.5	0.90	156.03
7.0	0.93	170.38
7.5	0.94	185.35
8.0	0.95	198.97
8.5	0.96	214.68
9.0	0.99	229.34
9.5	1.00	244.31
10.0	1.02	258.66
10.5	1.03	274.05
11.0	1.06	289.03
11.5	1.06	304.73
12.0	1.05	321.49

Data processing

When the shaft is rotating in steady state as shown in Figure B.6a, Equation (B.8) can be derived.

$$U = K_e \omega + R_m I \quad [\text{V}] \quad (\text{B.8})$$

Where:

I is the current in the circuit	[A]
U is the generator's voltage	[V]
K_e is the velocity constant of the motor	[V rad ⁻¹ s]
R_m is the internal resistance of the motor	[Ω]

From Equation (B.8) Equation (B.9) is obtained by isolating K_e .

$$K_e = \frac{U - R_m I}{\omega} \quad [\text{V rad}^{-1} \text{ s}] \quad (\text{B.9})$$

Conclusion

Figure B.8 plot the K_e found for each measurement. The K_e used in the model is average of these points. This gives $K_e = 0.0343 \text{ V rad}^{-1} \text{ s}$

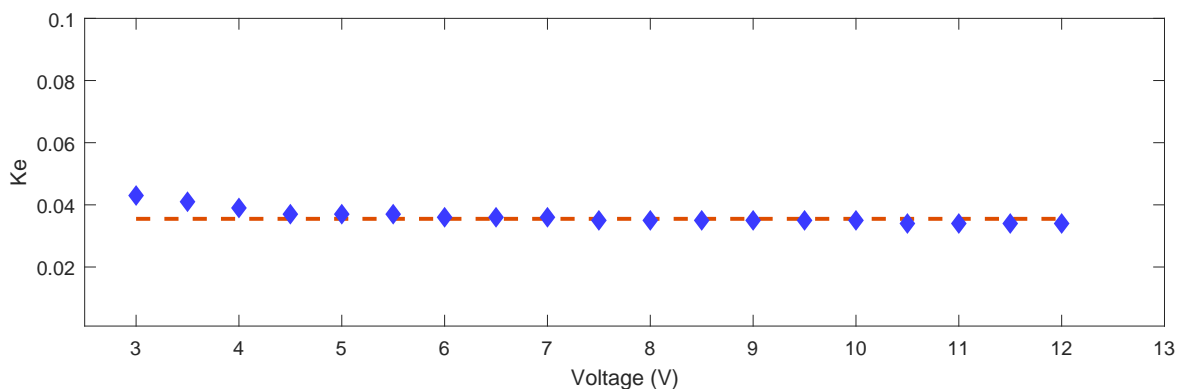


Figure B.8: Plot of K_e found for each measures

B.1.4 The DC Motor torque constant K_t

Table B.3: List of measurement equipment and components

Name	Brand	Model	AAU-number
Oscilloscope	Agilent	54621D	33941
Powersupply	Agilent	E3631A	78577
DC motor	Alsthom BBC	F9M2	08339

Setup

Figure B.9 shows a diagram and photo of the measurement set up

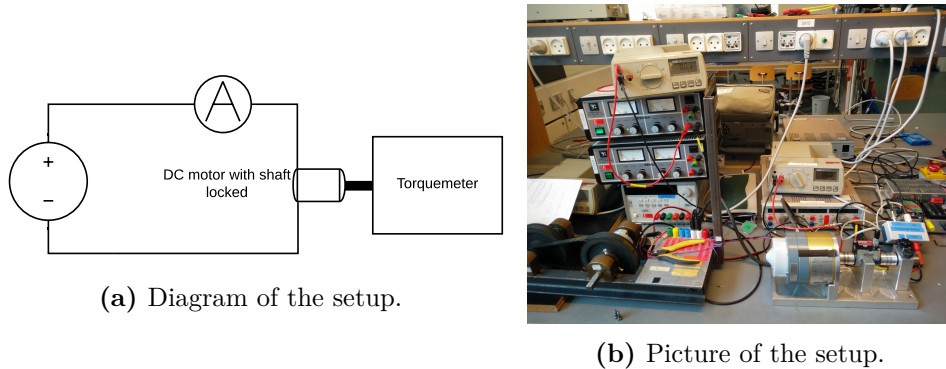


Figure B.9: The measurement setup.

Method

This test consists of having the motor shaft locked while the torque τ_m and the current I are measured.

Raw data

Figure B.10 has all the measurements done.

Figure B.10: Raw data used to determine K_t

Current (A)	τ_m
4.0	0.1164
4.5	0.1314
5.0	0.1498
5.5	0.1606
6.0	0.1824
6.5	0.1896
7.0	0.2050
7.5	0.2192
8.0	0.2332
8.5	0.2478
9.0	0.2604
9.5	0.2750
10.0	0.2900

Data processing

When the motor is in steady state and the shaft locked as shown in Figure B.9a, Equation (B.10) is found from Equation (5.32a).

$$K_t = \frac{\tau_m}{I} \quad [\text{N m A}^{-1}] \quad (\text{B.10})$$

Where:

I is the current in the circuit	[A]
τ_m is the torque of the motor	[N m]
K_t is the motor's torque constant	[N m A ⁻¹]

Conclusion

Figure B.11 plot the K_t found for each measurement. The K_t used in the model is average of these points. This gives $K_t = 0.0293 \text{ N m A}^{-1}$

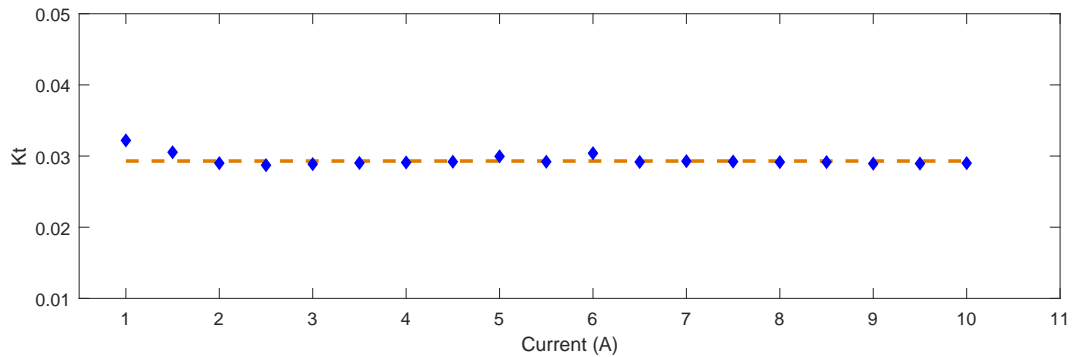


Figure B.11: Plot of K_t found for each measures

It should be noticed that K_e and K_t values are close, which comforts the results of the tests since they are theoretically equal.

B.2 Mechanical Characteristics

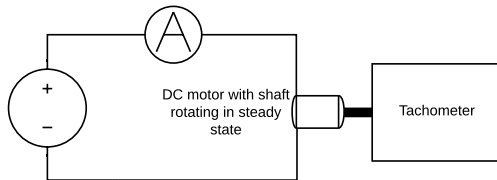
B.2.1 Frictions B_m

Setup

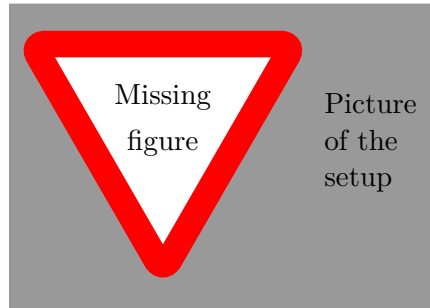
Figure B.12 shows a diagram and photo of the measurement set up.

Table B.4: List of measurement equipment and components

Name	Brand	Model	AAU-number
Oscilloscope	Agilent	54621D	33941
Powersupply	Agilent	E3631A	78577
DC motor	Alsthom BBC	F9M2	08339



(a) Diagram of the set up.



(b) Picture of the setup.

Figure B.12: The measurement set up for .

Method

This test consists of having the motor shaft running in steady state while the torque τ_m , the shaft angular velocity ω and the current I are measured.

Raw data

Figure B.13 has all the measurements done.

Data processing

The motor and the shaft are in steady state so $\tau_m = \tau_{fm}$ which combined with Equation (5.32b) gives Equation (B.11).

$$B_m = \frac{K_t I}{\omega} \quad [\text{N rad}^{-1} \text{s}] \quad (\text{B.11})$$

Where:

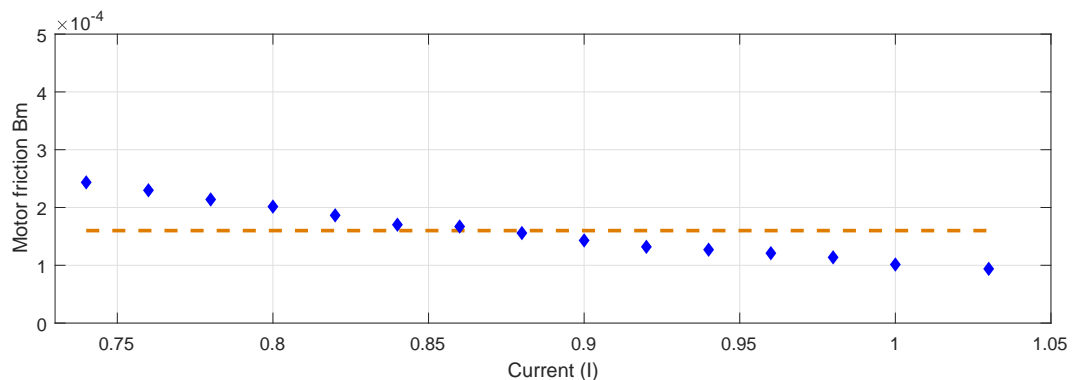
- | | |
|--|----------------------------------|
| I is the current in the circuit | [A] |
| K_t is the motor's torque constant | $[\text{N m A}^{-1}]$ |
| ω is the shaft's angular velocity | $[\text{rad s}^{-1}]$ |
| B_m is the viscous friction constant | $[\text{N m rad}^{-1} \text{s}]$ |

Figure B.13: Raw data used to determine B_m

Current (A)	ω (rad/s)
0.74	89.0
0.76	96.9
0.78	106.8
0.80	116.2
0.82	128.8
0.84	144.5
0.86	150.8
0.88	165.5
0.90	184.3
0.92	204.2
0.94	216.8
0.96	232.5
0.98	252.4
1.00	289.0
1.03	321.5

Conclusion

Figure B.14 plot the B_m found for each measurement. The B_m used in the model is average of these points. This gives $B_m = 120 \mu\text{N m rad}^{-1} \text{ s}$.

**Figure B.14:** Plot of B_m found for each measures

B.2.2 Moment of Inertia of the Gears J_{gear}

The moment of inertia of the gear train was thoroughly calculated in a previous report and will be used here.

Method

The gear train can be divided in three parts: the large wheels, the small wheels and the axles. The latter is a solid cylinder whereas the wheels are considered as multiple hollowed cylinders. The moment of inertia about a symmetry axis through the center of mass for a hollow cylinder is described in Equation (B.12) [?]:

$$J_{\text{hc}} = \frac{1}{2}M(R_1^2 + R_2^2) \quad (\text{B.12})$$

Where:

J_{hc} is the moment of inertia about a symmetry axis through the center of mass for a hollow cylinder	[kg m ²]
M is the mass of the hollowed cylinder	[kg]
R_1 is the inner radius of the hollowed cylinder	[m]
R_2 is the outer radius of the hollowed cylinder	[m]

For the axles, the inner radius R_1 is equal to zero, giving equation Equation (B.13) for the solid cylinder.

$$J_{\text{sc}} = \frac{1}{2}MR^2 \quad (\text{B.13})$$

Where:

J_{sc} is the moment of inertia about a symmetry axis through the center of mass for a solid cylinder	[kg m ²]
M is the mass of the solid cylinder	[kg]
R is the inner radius of the solid cylinder	[m]

The mass of each wheels and axles are calculated using their volumes and the density of iron.

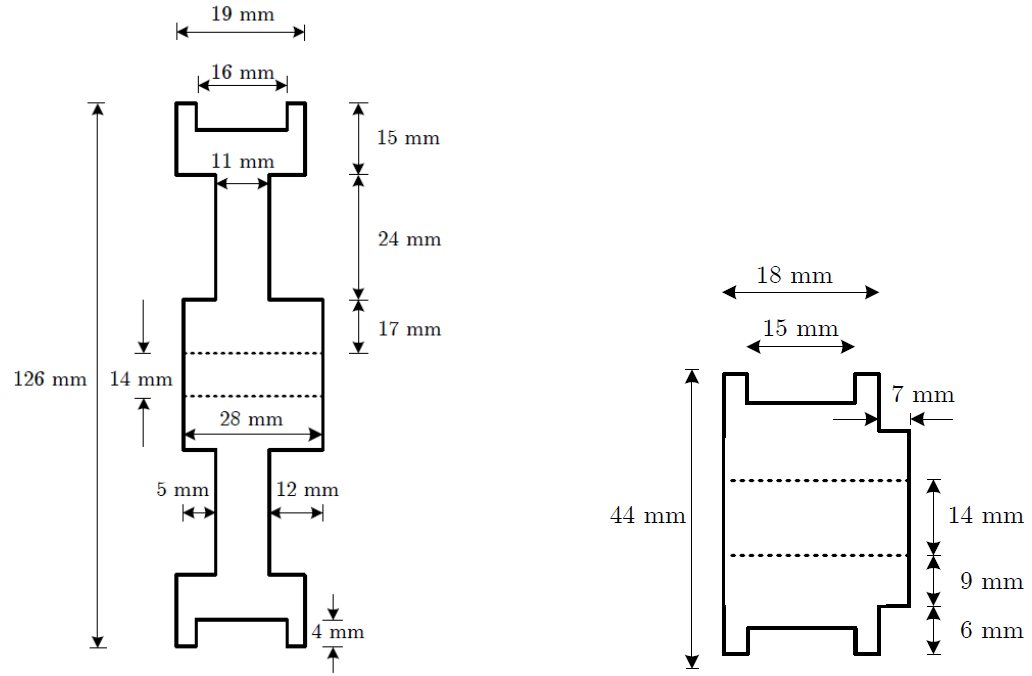


Figure B.15: Cross section of a large wheel [4].

Figure B.16: Cross section of a small wheel [4].

Conclusion

The moment of inertia for each part of the gear system [4]:

$$\text{Large Wheel: } J_{\text{Large}} = 1.433 \cdot 10^{-3} \text{ kg m}^2 \quad (\text{B.14a})$$

$$\text{Small Wheel: } J_{\text{Small}} = 0.037 \cdot 10^{-3} \text{ kg m}^2 \quad (\text{B.14b})$$

$$\text{Axe 1: } J_{A1} = 0.083 \cdot 10^{-3} \text{ kg m}^2 \quad (\text{B.14c})$$

$$\text{Axe 2: } J_{A2} = 0.078 \cdot 10^{-3} \text{ kg m}^2 \quad (\text{B.14d})$$

$$\text{Axe 3: } J_{A3} = 0.092 \cdot 10^{-3} \text{ kg m}^2 \quad (\text{B.14e})$$

The total moment of inertia of the gear system can be calculated from Equation (5.28b) in Section 5.3.

$$J_{\text{gear}} = N^2 J_1 + N^4 J_2 + N^6 J_3 \quad (\text{B.15})$$

With:

$$J_1 = J_{\text{Large}} + J_{\text{Small}} + J_{A1} = 1.553 \cdot 10^{-3} \text{ kg m}^2 \quad (\text{B.16a})$$

$$J_2 = J_{\text{Large}} + J_{\text{Small}} + J_{A2} = 1.548 \cdot 10^{-3} \text{ kg m}^2 \quad (\text{B.16b})$$

$$J_3 = J_{\text{Large}} + J_{\text{Small}} + J_{A3} = 1.562 \cdot 10^{-3} \text{ kg m}^2 \quad (\text{B.16c})$$

Finally, J_{gear} is calculated to be

$$J_{\text{gear}} = 0.153 \cdot 10^{-3} \text{ kg m}^2 \quad (\text{B.17})$$

Appendix C

Linearization of the Arm and Stick Model

This appendix will linearize Equation (C.1)

$$J_s \ddot{\theta}_s = \frac{l_s}{2} M_s \left(-l_a \ddot{\theta}_a \cos(\theta_a - \theta_s) + l_a \dot{\theta}_a^2 \sin(\theta_a - \theta_s) - \frac{l_s}{2} \ddot{\theta}_s - g \sin(\theta_s) \right) - b_{as} \dot{\theta}_{as} \quad (\text{C.1})$$

The linearization is made with a 1st order Taylor approximation. The linearization is done at the equilibrium point where the arm is in an upright position i.e. $\theta_s = 0$. In the equilibrium point the derivatives of all the inputs and outputs are 0. In this case the inputs and outputs are θ_a and θ_s and the operating point is $\bar{\theta}_a = 0$ and $\bar{\theta}_s = 0$. The nonlinear model is expressed as a function of the inputs and outputs as seen in Equation (C.2).

$$f(\theta_a, \dot{\theta}_a, \ddot{\theta}_a, \theta_s, \dot{\theta}_s) = \frac{l_s}{2} M_s \left(-l_a \ddot{\theta}_a \cos(\theta_a - \theta_s) + l_a \dot{\theta}_a^2 \sin(\theta_a - \theta_s) - \frac{l_s}{2} \ddot{\theta}_s - g \sin(\theta_s) \right) - b_{as} \dot{\theta}_{as} - J_s \ddot{\theta}_s \quad (\text{C.2})$$

Generally all equilibriums can be found by setting Equation (C.2) equal to 0 and the derivatives to 0 and solving for $\theta_a = \bar{\theta}_a$ and $\theta_s = \bar{\theta}_s$. For the pendulum it's easy to see the only two equilibriums are the stick pointing straight up and straight down.

The 1st order Taylor approximation of an equation with multiple variables is seen in Equation (C.3).

$$\begin{aligned} f(\theta_a, \dot{\theta}_a, \ddot{\theta}_a, \theta_s, \ddot{\theta}_s) &\approx f(\bar{\theta}_a, 0, 0, \bar{\theta}_s, 0) + \frac{\partial f}{\partial \theta_a}\Big|_{(\bar{\theta}_a, \bar{\theta}_s)} \hat{\theta}_a \\ &+ \frac{\partial f}{\partial \dot{\theta}_a}\Big|_{(\bar{\theta}_a, \bar{\theta}_s)} \hat{\dot{\theta}}_a + \frac{\partial f}{\partial \ddot{\theta}_a}\Big|_{(\bar{\theta}_a, \bar{\theta}_s)} \hat{\ddot{\theta}}_a \\ &+ \frac{\partial f}{\partial \theta_s}\Big|_{(\bar{\theta}_a, \bar{\theta}_s)} \hat{\theta}_s + \frac{\partial f}{\partial \dot{\theta}_s}\Big|_{(\bar{\theta}_a, \bar{\theta}_s)} \hat{\dot{\theta}}_s \end{aligned} \quad (\text{C.3})$$

Where:

$$\begin{aligned} \bar{\theta} &\text{ denotes the angle in an operating point} & [\text{rad}] \\ \hat{\theta} &\text{ denotes the angle of the small signal variances} & [\text{rad}] \end{aligned}$$

The 3 terms with sin or cos in Equation (5.7) will be approximated individually using Equation (C.3), remembering that $\bar{\theta} = \dot{\theta} = \ddot{\theta} = 0$ in the equilibrium.

$$\begin{aligned} -l_a \ddot{\theta}_a \cos(\theta_a - \theta_s) &\approx 0 + l_a \bar{\ddot{\theta}}_a \sin(\bar{\theta}_a - \bar{\theta}_s) \hat{\theta}_a \\ &- l_a \cos(\bar{\theta}_a - \bar{\theta}_s) \hat{\dot{\theta}}_a - l_a \bar{\ddot{\theta}}_a \sin(\bar{\theta}_a - \bar{\theta}_s) \hat{\theta}_s \end{aligned} \quad (\text{C.4a})$$

$$-l_a \ddot{\theta}_a \cos(\theta_a - \theta_s) \approx -l_a \hat{\dot{\theta}}_a \quad (\text{C.4b})$$

$$\begin{aligned} l_a \dot{\theta}_a^2 \sin(\theta_a - \theta_s) &\approx 0 + l_a \bar{\dot{\theta}}_a^2 \cos(\bar{\theta}_a - \bar{\theta}_s) \hat{\theta}_a \\ &+ 2l_a \bar{\dot{\theta}}_a \sin(\bar{\theta}_a - \bar{\theta}_s) \hat{\dot{\theta}}_a - l_a \bar{\dot{\theta}}_a^2 \cos(\bar{\theta}_a - \bar{\theta}_s) \hat{\theta}_s \end{aligned} \quad (\text{C.5a})$$

$$l_a \dot{\theta}_a^2 \sin(\bar{\theta}_a - \bar{\theta}_s) \approx 0 \quad (\text{C.5b})$$

$$g \sin(\theta_s) \approx g \sin(\bar{\theta}_s) + g \cos(\bar{\theta}_s) \hat{\theta}_s \quad (\text{C.6a})$$

$$g \sin(\theta_s) \approx g \hat{\theta}_s \quad (\text{C.6b})$$

The linearized model then becomes Equation (C.7).

$$J_s \hat{\dot{\theta}}_s = \frac{l_s}{2} M_s \left(-l_a \hat{\dot{\theta}}_a - \frac{l_s}{2} \hat{\dot{\theta}}_s - g \hat{\theta}_s \right) - b_{as} \hat{\dot{\theta}}_{as} \quad (\text{C.7})$$

Appendix D

Test Journal: Tachometer

Test participants: Mathias
Date: 10/04-2017

Purpose

The purpose of the test is to determine the linearity and precision of the tachometer used in the system.

Test equipment and components

Table D.1: List of measurement equipment and components

Name	Brand	Model	AAU-number
Oscilloscope	Agilent	54621D	33941
Power supply	Agilent	E3631A	78577
DC motor	Alsthom BBC	F9M2	08339
Tachometer	Compact Instruments	A2108	77087
Tachometer	Internal in motor	-	-

Setup

The powersupply is connected to the motor directly. Both tachometers is connected to the oscilloscope to read output voltages. The internal tachometer functions as a generator, and will give a voltage depending on the motors RPM.

Method

Step by step of test, maybe in enumerate

1. Connect motor directly to the power supply.
2. Connect tachometers to the oscilloscope.
3. Place a reflective tape on the motor axle.
4. Set holder for external tachometer so it lights at the motor axle.
5. Set the power supply to 2 V.
6. Note external tachometers voltage from the oscilloscope, and times the voltage with 1000 to find the number of rotations per minute.
7. Note the internal tachometers voltage from the oscilloscope, and times the voltage with 333,33 RPM/V to get numbers of rotations per minute.
8. Change the voltage with 1 V increments from 2 V - 10 V.
9. Note the Voltage and RPM with each increment.

Raw data

Table D.2: Rotations Per Minute of the both tachometers.

Motor Voltage	Internal Tachometer (RPM)	A2108 (RPM)	Difference (RPM)
2 V	204	202	2
3 V	506	502	4
4 V	763	760	3
5 V	1023	1024	1
6 V	1324	1322	2
7 V	1641	1640	1
8 V	1912	1913	1
9 V	2218	2214	4
10 V	2460	2456	4

Data processing

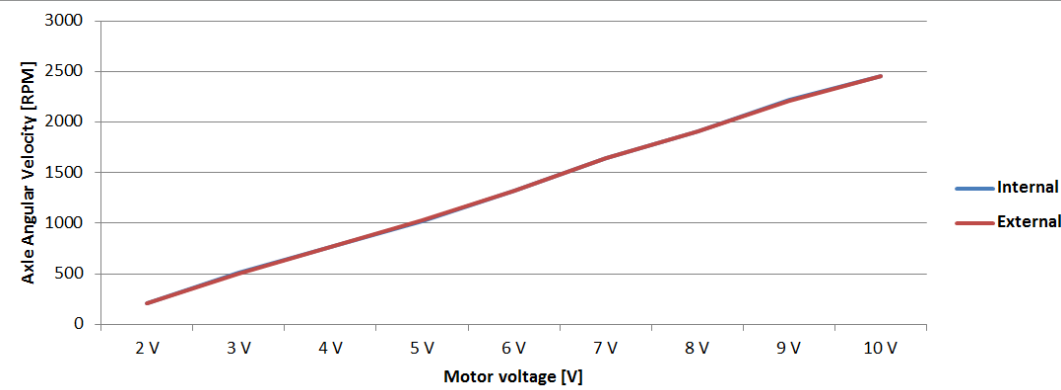


Figure D.1: Plot of RPM found for both tachometers

Which based on the know conversions gives a transfer function for the tachometer that is a relation between the tachometer voltage and motor velocity:

$$\frac{\frac{1000 \text{ RPM}}{3.130 \text{ V}} \cdot 2 \cdot \pi}{60 \text{ s}} \cdot T_{\text{Voltage}} = M_{\text{Velocity}} \text{ rad/s} \quad (\text{D.1})$$

Conclusion

It its seen cf. figure D.1 that the difference between the tachometers is so little, that the lines is on top of each other. The precision do not change with higher velocities and the internal tachometer is chosen, because it changes voltage faster because of the generator principle. The external optical tachometer needs some rotations to determine the RPM, and is not optimal when directions changes is needed.

Appendix E

Test Journal: Potentiometer

Test participants: Mathias
Date: 20/04-2017

Purpose

The purpose of the test is to find the angle which corresponds to the voltages of the potentiometers. This will be done for both the arm potentiometer and stick potentiometer.

Test equipment and components

Table E.1: List of measurement equipment and components

Name	Brand	Model	AAU-number
Multimeter	Fluke	37	08181
Oscilloscope	Agilent	54621D	33941
Power supply	Agilent	E3631A	78577
DC motor	Alsthom BBC	F9M2	08339
Potentiometer	Bourns	Linear 10 kΩ 0,5% linearity	
Potentiometer	Bourns	Linear 10 kΩ 1% linearity	
Protractor			
Spirit level			

Setup

Measurement setup is seen on Figure E.1

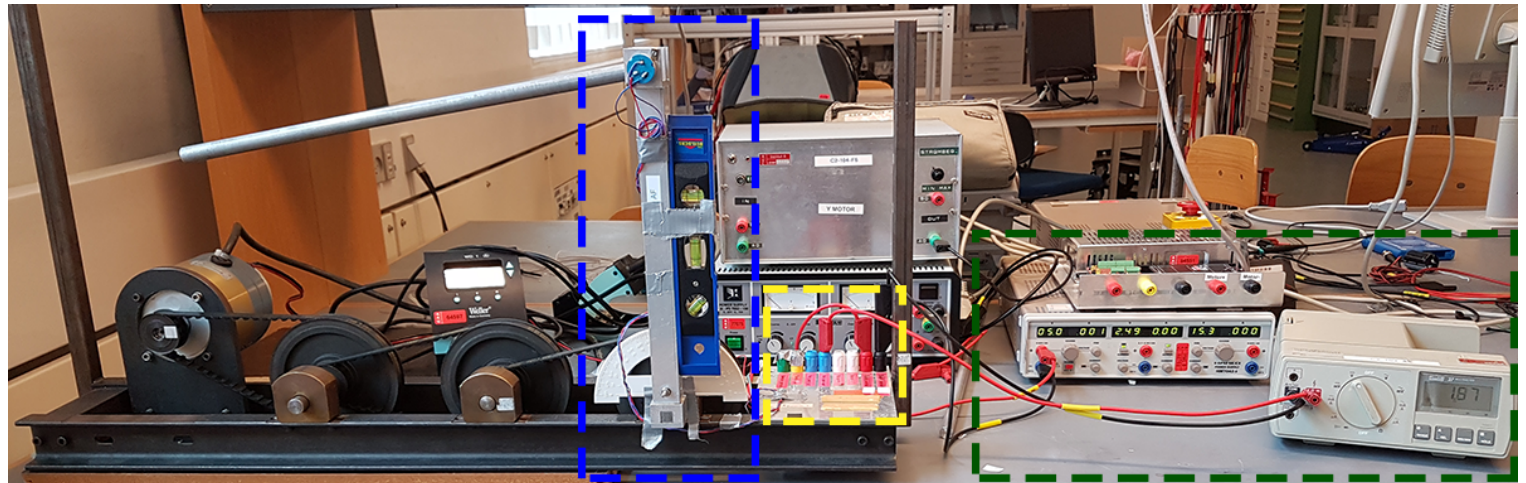


Figure E.1: Measurement setup.

Where:

Blue box contains the arm, with protractor and spirit level tool. [1]

The potentiometer is placed on the back of the opposite site of the arm axis.

Green box contains the power supply and voltmeter. [1]

Yellow box contains the power inputs and sensor outputs. [1]

Method

The procedure for the test is as following:

1. Supply the sensor with 5 V and ground through the input and output connection board in the yellow box.
2. Attach the potentiometer of the arm to the voltmeter, the stick is not considered during measurement of the arm.
3. Use the spirit level to place the arm in vertical position which is the systems 0°
4. Note the voltage.
5. Use the spirit level and protractor to place the arm in anti clockwise -45° from vertical.

6. Note the voltage, and repeat earlier with -90° , $+45^\circ$ and $+90^\circ$
7. Place the arm in 0° and lock it.
8. Change the voltmeter to read the output from the stick potentiometer.

Raw data

Voltages from each potentiometer is not expected to be the same. This is based on that the initial orientation of the potentiometers is not the same.

Position ($^\circ$)	Voltage Pot _{arm} (V)	Voltage Pot _{stick} (V)
-90°	0,437 V	1,200 V
-45°	1,146 V	1,89 V
0°	1,860 V	2,558 V
45°	2,573 V	3,23 V
90°	3,270 V	3,90 V

Table E.2: Angle position and corresponding voltage.

Data processing

The main objective to determine is outer limit and how much 1 V corresponds to in angle change. This can give the possibility to convert the analogue input on an Arduino back to the corresponding angle.

It is shown that the linearity is acceptable and the proportional angle to voltage conversion is considered linear. The conversion must be separated into two parts. This is done because the angle to voltage is different between the potentiometers. To obtain a first order function the voltages and angles are plotted and approximated for both potentiometers.

This approximation corresponds to a relation between the voltage to angle of the arm on figure E.2.

$$\theta_a = 63,64 \cdot VPot_{arm} - 117,77 \quad (\text{E.1})$$

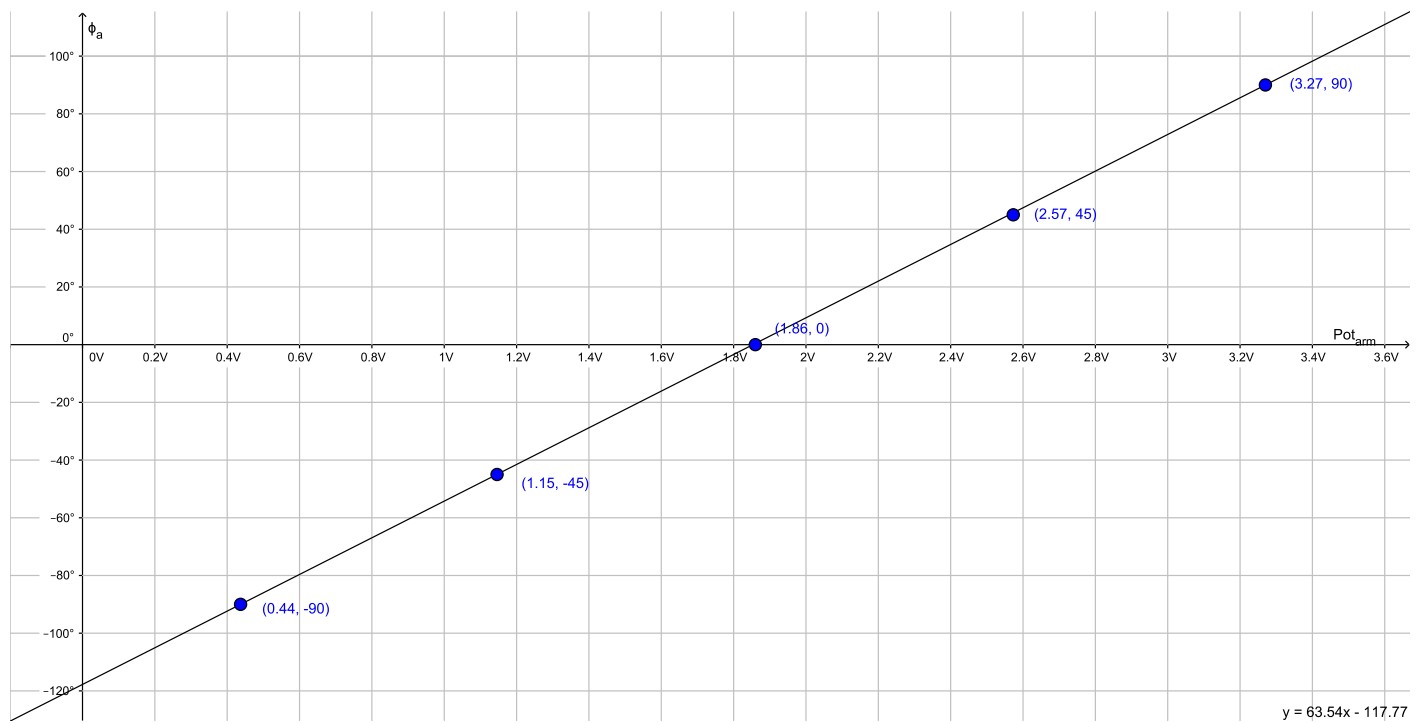


Figure E.2: First order approximation of the arm potentiometer.

The plot is repeated for the potentiometer on the stick.

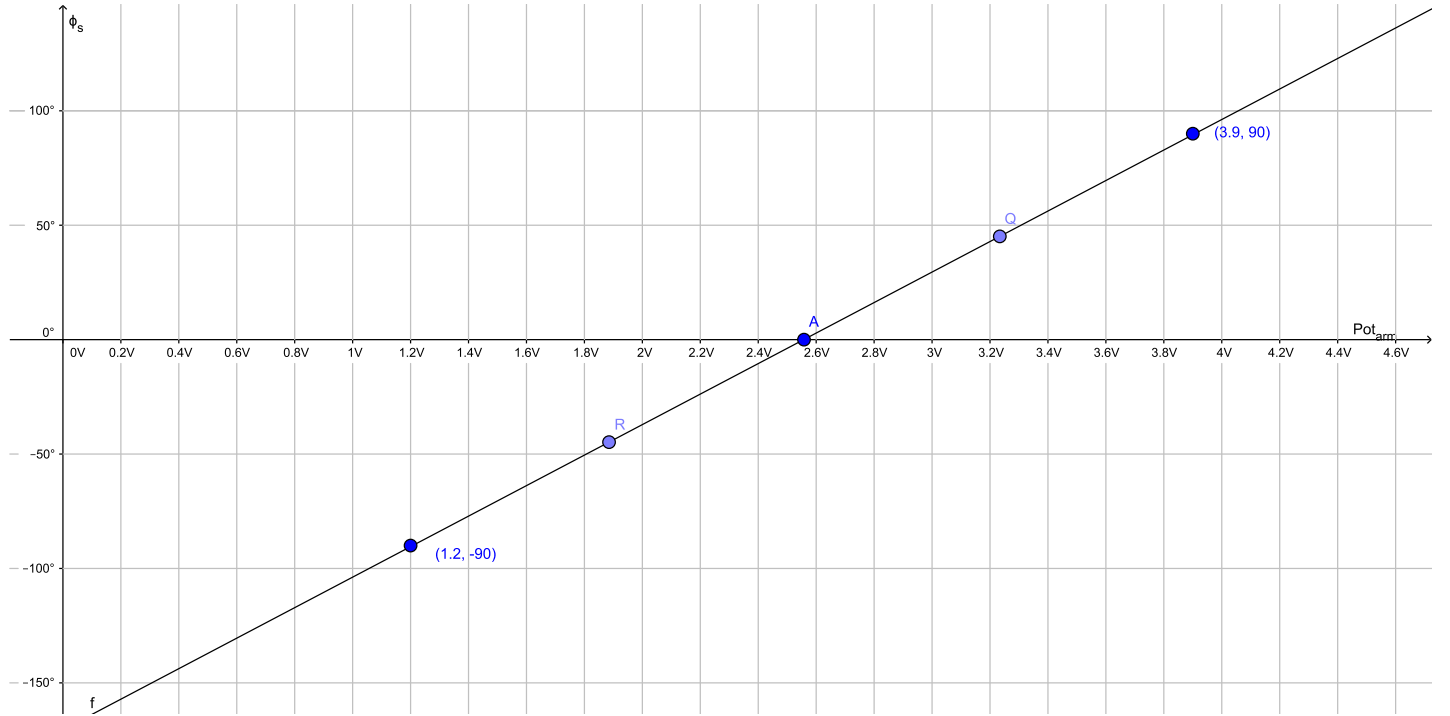


Figure E.3: First order approximation of the stick potentiometer.

This approximation that corresponds to a relation between the voltage to angle of the arm on figure E.2.

$$\theta_s = 66,66 \cdot V_{\text{Pot}_{\text{stick}}} - 170,46 \quad (\text{E.2})$$

Sampling the sensor with an Arduino will be done through reading the voltage on an input. The voltage will correspond to a proportional analog value from 0-1023, where 0 V = 0 and 5 V = 1023. Translating the voltages into angles can give us the backwards conversion. Considering that the value can take 1024 values then:

$$\frac{1024 \text{ units}}{5 \text{ V}} = 204,8 \text{ units/V} \quad (\text{E.3})$$

Considering that the precision of the measurements and using an Arduino, all values would be rounded to the nearest integer. The linear approximations might be calibrated during implementation to minimize offsets. Further implementation is processed cf. section 10.1.1.

Conclusion

The tested concludes that it is possible to convert the voltage to values that can be used with an Arduino. The test also concludes that is a use able linearity of both potentiometers when during conversions. Though the precision of the measurements shall be considered even though the measurements had similarities.

Appendix F

Test Journal: rocket motor test

Test participants: Raphaël
Date: 31/03-2017

Purpose

The purpose of the test is to characterize the thrust of the Klima D6-P rocket motor.

Test equipment and components

Table F.1: List of measurement equipment and components

Name	Brand	Model	AAU-number
Torsion scale	Made in AAU	N/A	N/A
Rocket motor	Klima	D6-P	N/A
3D printed adapter	N/A	N/A	N/A

Setup

Measurement setup is seen on Figure E.1



Figure F.1: Measurement setup.

The torsion scale was lent by Jens Frederik Dalsgaard Nielsen, and the Arduino code was improved to filter the data. This code is available in the attached files.

Method

The scale was calibrated using a known weight before the experiments.

1. The motor is placed inside the adapter, facing the ground
2. The scale is clamped strongly on the table. The clamping should be the same as during the calibration.
3. Scale turned on, a standard quick fuse and a lighter was used to start the motor.
4. After the motor had burned, the scale was shut off and the files on its SD card copied to a computer.
5. The operation was repeated with two motors from two different boxes.
6. Using Matlab, the data was plotted and put to scale according to the calibration.

Raw data

The raw data from the scale is in the attached files.

Data processing

Using the calibration weight, the data was put to scale using the Matlab code "scale_reader.m" attached. It produced the graph displayed here. The force in Newton was translated in equivalent gram of lift for easier interpretation.

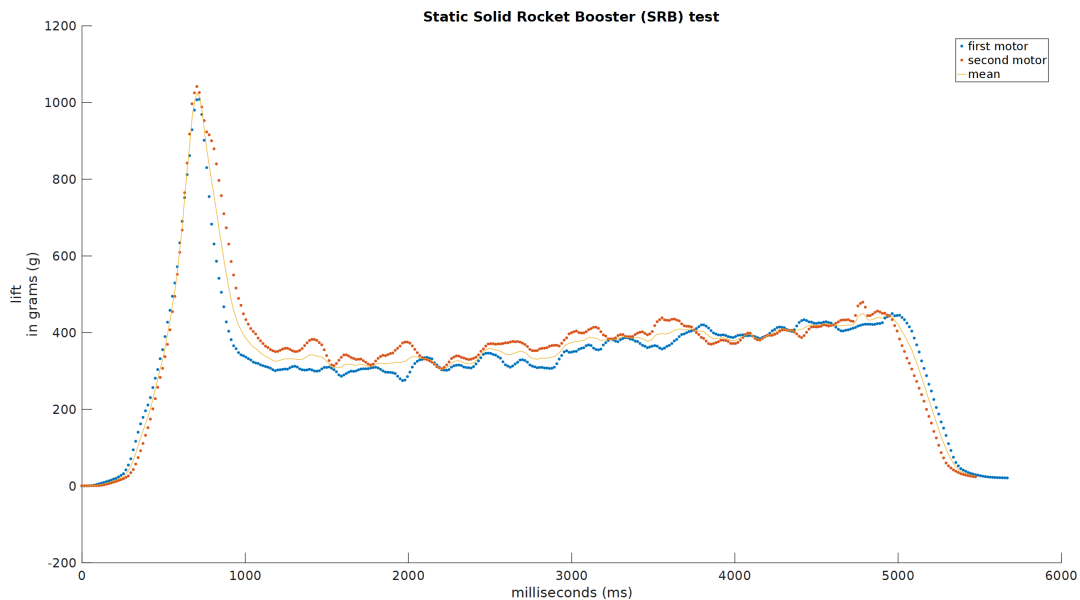


Figure F.2: Processed thrust data

Conclusion

It can be seen that the two motors are very similar. The thrust builds up quickly producing a force peak of around 10 Newtons, or 1 Kg equivalent lift, for less than 400 ms. It then goes down and stabilizes to 330 grams of lift, slowly going up to 410g (taking in account the 20g mass loss of the motor during the thrust). Since the rocket is less than 300 grams, the motor should be able to lift it.

Appendix G

Test Journal: Servomotors

Test participants: Romain & Raphael

Date: 01/05-2017

Purpose

The purpose of the test is to verify the proper functioning of the servomotors, and calculate the time constant of the servomotors' required tasks.

Test equipment and components

Table G.1: List of measurement equipment and components

Name	Brand	Model
Servomotors	SpringRc	SM-s2309s
Controller	Arduino	Arduino Nano
Camera	Samsung	0
Media Player Classic	Gabest	Home Cinema

Setup

The servomotors are controlled and powered by an Arduino Uno. Three different position of the servomotors sticks are set up by code found in the attachements. The measurement setup is seen on the photos of the three different positions.

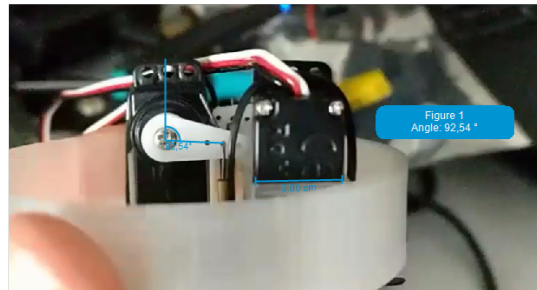


Figure G.1: Photograph of the servomotor at the medium position.

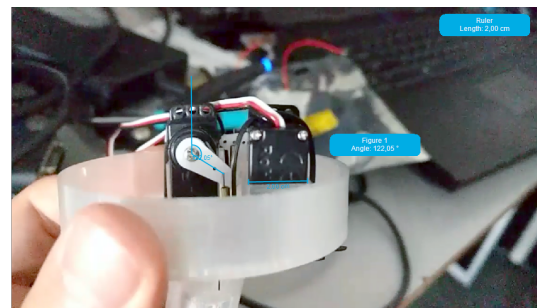


Figure G.2: Photograph of the servomotor at the lower position.

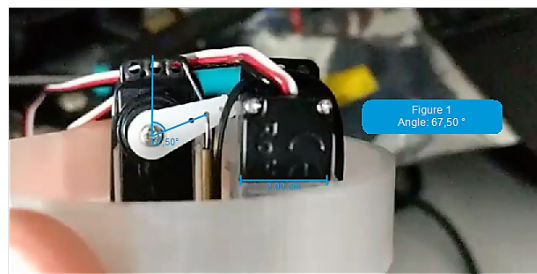


Figure G.3: Photograph of the servomotor at the higher position.

Method

The servomotors' arms are controlled to go from one position to another set one. The process is filmed in slow motion in order to analyse it. An x/y basis is used with the base set at the rotation center.

Angle variation

The angle variation is found by measuring the angle difference between the horizontal axis and the stick direction. The servomotors function properly if the angles desired correspond to the real angles.

Time constant

In order to find the time constant, the time to go from one position to another is measured using the video software. The time constant is equal to 63 per cent of the total time from one position to another.

Raw data

Angle variation

Table G.2: Measurement time of different set points.

Position	Angle(°)
Lowest	122.05
Middle	92.54
Highest	67.50

Time constant

Table G.3: Measurment time of different set points.

Test	Time of departure (s)	Time of arrival(s)	total time (s)
1	2.507	2.641	0.134
2	2.508	2.642	0.134
3	60.066	61.133	0.133
4	60.033	61.082	0.131

Data processing

Angle variation

The angle variation is found by measuring the angle difference between the horizontal axis and the stick direction. The desired angle difference between the different position is 30 °. The servomotors function properly if the angles desired correspond to the measured angles.

$$a_{mh} = 29.51^\circ \quad (G.1a)$$

$$a_{ml} = 25.04^\circ \quad (G.1b)$$

Where:

a_{mh} is the angle difference between the middle to highest position [°]
of the servomotor's arm

a_{ml} is the angle difference between the middle to lowest position [°]
of the servomotor's arm

The error comes from measure errors and to the servomotors lifting a weight.

Time constant

In order to find the time constant, the time to go from one position to another is measured using the video software. The time constant is equal to 63 per cent of the mean value of the total time from one position to another :

$$t_{constant} = \frac{63}{100} \cdot t_{mean} \quad (G.2a)$$

$$t_{constant} = \frac{63}{100} \cdot 0.133 = 0.084 \quad (G.2b)$$

Where:

$t_{constant}$ is the motor input voltage [s]

t_{mean} is the mean value of the total time from one position to [s]
another

Conclusion

The image analysis presents errors. The range of required angle movement of the servomotors is inferior to 30 degrees, meaning that the servomotors are considered

as meeting the requirements even thought errors are present. The time constant of the servomotors is 0.084 and meets the requirement of a fast reaction to a controller command.

Appendix H

Test Journal: Attached Flight

Test participants: Romain & Raphael

Date: 01/05-2017

Purpose

The purpose of the test is to experiment the hardware, software and controller of the rocker in a first attempt of a stable flight. The objective is to approve the settling time.

Test equipment and components

Table H.1: List of measurement equipment and components

Name
Rocket body
Thruster
Camera
Rope and poles

Setup

Measurement setup is seen on Figure E.1 and photo

The Rocket body is attached by two ground-fixed ropes on two opposite side position, around its center of pressure. The rocket has a maximum vertical movement of "unknown" meters.

Method

The setup of the rocket will enable a safe, for observers and the system, simulation of the rocket flight. The proper functioning of the controller is achieved if a stable movement of the ground-fixed rocket is observed.

Raw data

Photo of different positions + table of multiple test.

Table H.2: Measurement of time of different set points.

Test	Flight duration (s)	Stabilisation starting point (ms)	Percentage
1	0	0	0
2	0	0	0
3	0	0	0
4	0	0	0
5	0	0	0
6	0	0	0
7	0	0	0

Data processing

figure of mean time i guess

The rocket becomes stable after a mean time of "unknown" secondes. This corresponds to a settling time of "unknown" secondes.

Conclusion

The rocket stability comes at an acceptable period of time after take-off. The hardware, software and controller are considered as successful, and the settling time fulfills the requirement.